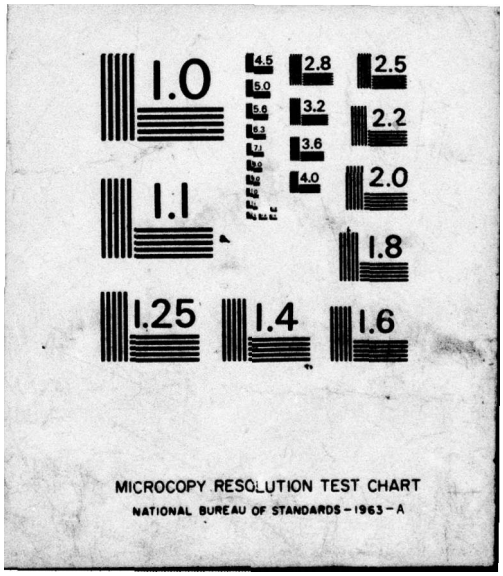
AD-A035 712 FLOW RESEARCH INC KENT WASH F/G 20/4
STABILITY AND TRANSITION IN BOUNDARY LAYERS ON REENTRY VEHICLE --ETC(U)
JUN 76 C L MERKLE F44620-74-C-0049
UNCLASSIFIED FLOW RES-71 AFOSR-TR-76-1107 NL

1 OF 2
AD A035712




1.0
1.1
1.25
1.4
1.6
1.8
2.0
2.2
2.5
2.8
3.2
3.6
4.0
4.5
5.0
5.6
6.3
7.1
MICROCOPY RESOLUTION TEST CHART
NATIONAL BUREAU OF STANDARDS - 1963 - A

AFOSR - TR - 76 - 1107

AFOSR-TR-76-1107

ADA035712

19
B.S.

FLOW RESEARCH REPORT NO. 71

STABILITY AND TRANSITION IN BOUNDARY LAYERS ON REENTRY VEHICLE NOSETIPS *

by

Charles L. Merkle

DDC
RECEIVED
FEB 16 1977
C

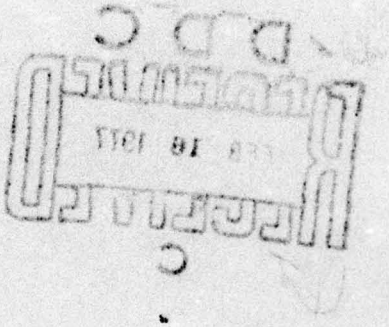
June 1976

Approved for public release;
distribution unlimited.

Flow Research, Inc.
1819 South Central Avenue
Kent, Washington 98031
(206) 854-9590, 854-1370

* This work is supported by AFOSR Contract No. F44620-74-C-0049.

AD A032 215



AIR FORCE OFFICE OF SCIENTIFIC RESEARCH (AFSC)
NOTICE OF TRANSMITTAL TO DDC
This technical report has been reviewed and is approved for public release IAW AFR 190-12 (7b).
Distribution is unlimited.
A. D. BLOSE
Technical Information Officer

UNCLASSIFIED

SECURITY CLASSIFICATION OF THIS PAGE (When Data Entered)

REPORT DOCUMENTATION PAGE	READ INSTRUCTIONS BEFORE COMPLETING FORM
1. REPORT NUMBER: AFOSR-TR-76-1107	2. GOVT ACCESSION NO.
	3. RECIPIENT'S CATALOG NUMBER
4. TITLE (and Subtitle): STABILITY AND TRANSITION IN BOUNDARY LAYERS ON REENTRY VEHICLE NOSETIPS,	5. TYPE OF REPORT & PERIOD COVERED: FINAL rept. 16 July 1975-15 July 1976
	6. PERFORMING ORG. REPORT NUMBER: Flow Research Report No 71
7. AUTHOR(s): CHARLES L. MERKLE	8. CONTRACT OR GRANT NUMBER(s): F44620-74-C-0049
9. PERFORMING ORGANIZATION NAME AND ADDRESS: FLOW RESEARCH, INC 1819 S CENTRAL AVENUE KENT, WA 98031	10. PROGRAM ELEMENT, PROJECT, TASK AREA & WORK UNIT NUMBERS: 681307 9781-02 61102F SAMSO:63311F
11. CONTROLLING OFFICE NAME AND ADDRESS: AIR FORCE OFFICE OF SCIENTIFIC RESEARCH/NA BLDG 410 BOLLING AIR FORCE BASE, D C 20332	12. REPORT DATE: June 1976 (12) 21 p.
	13. NUMBER OF PAGES: 115
14. MONITORING AGENCY NAME & ADDRESS(if different from Controlling Office): (14) Flow Res-71	15. SECURITY CLASS. (of this report): UNCLASSIFIED
	15a. DECLASSIFICATION/DOWNGRADING SCHEDULE

16. DISTRIBUTION STATEMENT (of this Report)

(16) 9781

Approved for public release; distribution unlimited.

(17) 02

17. DISTRIBUTION STATEMENT (of the abstract entered in Block 20, if different from Report)

DDC RECEIVED FEB 16 1977

18. SUPPLEMENTARY NOTES

19. KEY WORDS (Continue on reverse side if necessary and identify by block number)

BOUNDARY LAYER TRANSITION
STABILITY THEORY
NOSETIP TRANSITION
REENTRY VEHICLES

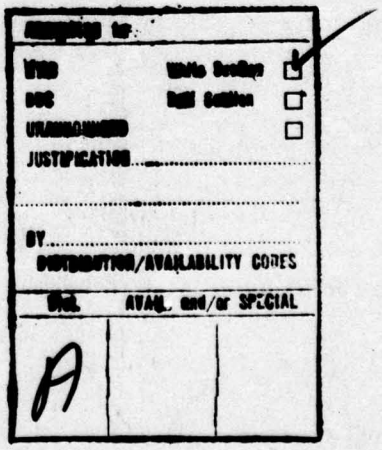
20. ABSTRACT (Continue on reverse side if necessary and identify by block number)

The stability characteristics of the boundary layer on the nosetip of a reentry vehicle have been investigated for a wide range of conditions. Results based upon classical parallel-flow stability theory indicate that boundary layers on smooth-walled nosetips are stable by a wide margin at realistic Reynolds numbers. The addition of nonparallel effects, including the axisymmetric vortex stretching that is encountered as the boundary layer is swept over the nosetip, moves the neutral stability curve to lower Reynolds numbers, but by only negligible amounts indicating that the parallel-flow analysis is more than adequate for the present

DD FORM 1473 EDITION OF 1 NOV 65 IS OBSOLETE UNCLASSIFIED

390 409

problem. The stability results for rough-surfaced nosetips, which are based on a phenomenological model for the effects of roughness on the mean flow profiles, yield completely different conclusions. The presence of roughness can produce large, strongly unstable regions on the nosetip. In particular, the interaction between roughness and other parameters is especially important. The results indicate that in the presence of roughness, wall cooling is strongly destabilizing, whereas the effects of the pressure gradient are very weak. Both of these predictions are completely different from smooth-wall stability results but are in agreement with numerous experimental transition results. The calculations also indicate that surface mass addition is destabilizing in the presence of smooth walls (but by much smaller amounts than indicated in the experiments of Demetriades), while it has very small effects in the presence of wall roughness. A general observation based on these results is that boundary layer transition on nosetips occurs because of the simultaneous effects of surface roughness, strong favorable pressure gradients, and wall cooling.



Flow Research Report No. 71
June 1976

Stability and Transition in Boundary Layers On Reentry Vehicle Nosetips*

by

Charles L. Merkle

Abstract

The stability characteristics of the boundary layer on the nosetip of a reentry vehicle have been investigated for a wide range of conditions. Results based upon classical parallel-flow stability theory indicate that boundary layers on smooth-walled nosetips are stable by a wide margin at realistic Reynolds numbers. The addition of nonparallel effects, including the axisymmetric vortex stretching that is encountered as the boundary layer is swept over the nosetip, moves the neutral stability curve to lower Reynolds numbers, but by only negligible amounts, indicating that the parallel-flow analysis is more than adequate for the present problem. The stability results for rough-surfaced nosetips, which are based on a phenomenological model for the effects of roughness on the mean flow profiles, yield completely different conclusions. The presence of roughness can produce large, strongly unstable regions on the nosetip. In particular, the interaction between roughness and other parameters is especially important. The results indicate that in the presence of roughness, wall cooling is strongly destabilizing, whereas the effects of the pressure gradient are very weak. Both of these predictions are completely different from smooth-wall stability results but are in agreement with numerous experimental transition results. The calculations also indicate that surface mass addition is destabilizing in the presence of smooth walls (but by much smaller amounts than indicated in the experiments of Demetriades), while it has very small effects in the presence of wall roughness. A general observation based on these results is that boundary layer transition on nosetips occurs because of the simultaneous effects of surface roughness, strong favorable pressure gradients, and wall cooling.

---

*This work is supported by AFOSR Contract No. F44620-74-C-0049.

Table of Contents

	Abstract	i
	Nomenclature	iv
1.	INTRODUCTION	1
2.	THE APPLICABILITY OF THE CLASSICAL STABILITY THEORY	6
	2.1 Formulation of the Nosetip Boundary Layer	6
3.	STABILITY CHARACTERISTICS OF NOSETIP BOUNDARY LAYERS	9
	3.1 The Stability Characteristics of a Nosetip Boundary Layer Using a Locally Similar Hypothesis for the Mean Flow Profiles	10
	3.2 Stability Characteristics of Nosetip Boundary Layers Based on Complete Non-Similar Analysis	16
	3.2.1 Determination of the Mean Flow	16
	3.2.2 Effects of Varying Surface Roughness in the Presence of Wall Cooling and Mass Addition: Case 1	19
	3.2.3 Effects of Varying Surface Mass Addition in the Presence of Roughness and Wall Cooling: Case 2	20
	3.2.4 Effects of Varying Wall Temperature Ratio in the Presence of Surface Roughness and Mass Addition: Case 3	21
	3.2.5 Effects of Free-Stream Noise on Transition: Case 6	22
	3.2.6 Effects of Surface Mass Addition in the Presence of Smooth Walls: Case 7	24
	3.2.7 Stability Characteristics of Laminar Stable Shapes in the Presence of Roughness, Surface Mass Addition and Heat Transfer to the Wall: Case 8	26
	3.2.8 The Effects of Roughness in the Small K/θ Range: Case 10	29
	3.2.9 Summary of Transition Test Cases	29
	3.2.10 Additional Stability Results and Comparisons	31
4.	A SUMMARY OF NOSETIP TRANSITION CHARACTERISTICS AS PREDICTED FROM STABILITY THEORY	33
	4.1 Effects of Roughness on Nosetip Transition	33
	4.2 Effects of Body Shape on Transition	36
	4.3 Effects of Wall Cooling and Surface Mass Addition	36
	4.4 Effects of Free-Stream Noise on Transition on Nosetips	36
	4.5 Effects of Free-Stream Mach Number on Nosetip Transition	37

Table of Contents (Cont'd)

		Page
5.	SUMMARY AND CONCLUSIONS	38
	References	40
	Figures	42
	APPENDIX I: Recommended Transition Test Cases (Compiled by Aerospace Corp.)	97
	APPENDIX II: Details of Mean Flow Profiles	104

Nomenclature

Symbol	Description
A^+	coefficient in roughness model, see eq. (3.2)
B'	non-dimensional blowing parameter, $\rho_o v_o/(\rho_e U_e S_t)$
C	non-dimensional viscosity-density ratio, $\rho u/\rho_e U_e$
c_p	specific heat at constant pressure
F	non-dimensional velocity, U/U_e
j	exponent to reflect differences between axisymmetric and cartesian coordinate systems; $j = 1$ refers to axisymmetric, $j = 0$ refers to cartesian coordinates
K_ε	constant in the roughness model, see eq. (3.2)
k	roughness height; also used as thermal conductivity in eqs. (3.6) and (3.7)
M_∞	free-stream Mach number
P_e	"chamber" pressure used to define the mass flux at the surface in psia (see eq. (3.16))
P_R	Prandtl number
P_{R_T}	turbulent *Prandtl number*
p	pressure
R_{e_k}	roughness Reynolds number, $U_k k/\nu_k$
R_{e_θ}	Reynolds number based on momentum thickness, $U_e\theta/\nu_e$
r	radial distance in the axisymmetric coordinate system
r_o	radial location of the body surface
T	temperature
T_e	temperature at outer edge of the boundary layer
T_w	wall temperature
t	transverse curvature term, r/r_o
U	streamwise velocity
U_e	velocity at the edge of the boundary layer
V	non-dimensional cross-stream velocity, see eq. (3.11)
v	cross-stream velocity
v_o	normal velocity at the wall (in the presence of surface mass addition)
x	independent variable for streamwise direction
y	distance normal to the wall (axisymmetric or cartesian coordinate system)

Nomenclature (Cont'd)

Symbol	Description
α	non-dimensional parameter defined in eq. (3.15)
α_i	amplification rate of disturbances
β	non-dimensional pressure gradient parameter, see eq. (3.15)
β_i	constant in roughness model, see eq. (3.1)
δ	boundary layer thickness, defined as the location at which $U/U_e = 0.999$
ε	eddy diffusivity for momentum transfer
ε_H	eddy diffusivity for enthalpy transfer
ζ	cross-stream coordinate in the Levy-Lees coordinate system, see eq. (3.10)
θ	non-dimensional temperature, T/T_e
μ	viscosity
μ_e	viscosity at the outer edge of the boundary layer
μ_T	turbulent viscosity
ν	kinematic viscosity
ν_K	kinematic viscosity evaluated at the top of the roughness elements
ξ	streamwise coordinate in the Levy-Lees coordinate system, see eq. (3.10)
ρ	density
ρ_e	density at the outer edge of the boundary layer
ρ_o	density at the wall

1. INTRODUCTION

The results of linear stability theory indicate that there is a minimum, critical Reynolds number in laminar boundary layers below which all disturbances of infinitesimal amplitude are damped, regardless of their frequency content. Above this critical Reynolds number, those components of a disturbance which lie within a certain frequency band will be amplified with time, and/or distance, as they are swept downstream. Although the precise relationship between the growth of such disturbances inside a laminar boundary layer and the onset of boundary layer transition from laminar to turbulent flow is not fully understood, there exists considerable experimental evidence that the two are intimately related.

The most well documented evidence of the connection between stability and transition occurs for the simple case of the boundary layer on a flat plate. Experimental results taken in this zero pressure gradient environment have verified that both naturally occurring and artificially induced disturbances inside a laminar boundary layer are amplified (or damped, depending on their frequency) at a rate which is in very close agreement with the predictions of linear stability theory. There is also considerable evidence which proves that the transition location moves rapidly toward the leading edge when disturbances which lie within the unstable frequency regime (as predicted by stability theory) are introduced into the free-stream, whereas the transition location is unaffected when disturbances which lie outside of the unstable regime are similarly introduced, thus indicating a direct connection between stability and transition. These results, along with numerous other experimental facts, constitute a considerable bulk of evidence, of a rather compelling nature, that boundary layer transition originates from infinitesimal disturbances inside the laminar boundary layer which grow through the linear amplification mechanism until their amplitude becomes sufficiently large that nonlinear effects (which represent the very earliest manifestation of transition) set in. In fact, if only transition data for flat plates in incompressible flow is consulted, one might reach the conclusion that stability theory can explain all the complexities of transition.

When the experimental data base is broadened to include compressible flows, such as high Mach number boundary layers with nonzero wall heat transfer, or any number of nonzero pressure gradient boundary layers, it is immediately seen that stability theory is not an absolute guide, but

that it remains an excellent indicator of transition. For numerous boundary layers of practical interest, stability theory represents our most powerful tool for understanding the transition process. Despite this extensive favorable evidence, stability theory is not unchallenged as an indicator of transition. Although the flat plate, with its meticulous documentation of experimental facts, represents a triumph of stability theory as a transition tool, certain flow fields can be found which directly contradict stability results. Perhaps the best known of such flows is Poiseuille flow in a circular pipe. Stability theory predicts that all disturbances in Poiseuille flow are damped, regardless of their frequency content, or of the local Reynolds number. In contrast to this prediction of continued stability, transition can, and does, take place in a pipe. Considerable work, both experimental and theoretical in nature, has been conducted and is currently in progress to attempt to explain this contradiction.

In the present Report, we are concerned with a second set of circumstances for which the experimental observations of transition present an embarrassment to stability theory. This present situation is the boundary layer near the stagnation region of a blunt body and, more specifically, the boundary layer on the (nearly hemispherical) nosetip of a reentry vehicle. The presence of transition in this highly favorable pressure gradient region has been referred to as the blunt-body paradox (Morkovin, 1969). The reason for this name is readily seen by reviewing the characteristics of the boundary layer in the vicinity of an axisymmetric stagnation point.

To a first approximation, the boundary layer in the stagnation region can be represented by a Falkner-Skan similarity solution with a pressure gradient parameter of $\beta = 0.5$ (corresponding to stagnation point flow on an axisymmetric body). The stability results for this highly favorable pressure gradient boundary layer indicate it is extremely stable to external disturbances. In fact, the critical Reynolds number for an incompressible, stagnation point flow is above $Re_\theta = 3000$. Stability theory would suggest that transition cannot occur at Reynolds numbers which are below the critical one (because all disturbances are damped there), and that the beginning of transition will not occur until considerably after the critical Reynolds number when the disturbances have had a sufficient time to amplify. Typical flat plate results have indicated

transition Reynolds numbers which are at least a factor of two higher than the critical value. Thus, from stability theory we would never expect transition to occur below $Re_\theta = 3000$ on a nosetip, and probably not until Re_θ reaches 5000 or 6000. By way of contrast, experimental evidence (Anderson, 1975b) indicates transition as low as $Re_\theta = 100$. Thus, despite the "stabilizing" effect of the highly favorable pressure gradient, transition on a nosetip is observed to occur earlier than on a flat plate. Stability theory, of course, predicts it would occur much later. (There is also much experimental evidence in other circumstances to indicate that favorable pressure gradients, in general, do substantially delay transition, as is suggested by the stability results.)

There are at least four plausible explanations for this failure of stability theory:

1. Stability theory is wrong for this case. Small disturbances can be amplified inside the nosetip boundary layer despite the predictions of the theory.

2. The stability predictions for the nosetip are correct; all small disturbances are damped, but there is no relationship between stability and transition in this case (and perhaps elsewhere as well). Transition takes place without regard for the stability properties of the boundary layer.

3. The stability analysis has omitted some of the important physics of the problem which, when included in the formulation, would rectify the differences between theory and experiment.

4. The stability results to which we have referred above are correct for the boundary layer for which they were calculated, but that boundary layer is not the same as the one on the nosetip.

Of these four explanations, only the first can be easily dismissed as being unlikely. There is no reason to expect that the stability results are, in themselves, incorrect. As indicated above, stability theory has been extensively verified by experiment; there is no evidence to suspect that the theory is fundamentally wrong. The remaining three items are not so easily settled, and require a more in-depth investigation. Some specific comments on these items are given below and an implicit evaluation of the items is continued throughout the Report.

The approach which we have taken in the present work is to assume, in contradiction to the suggestion in item 2, that a relationship between stability and transition does exist. We then attempt to demonstrate, through considerations along the lines suggested in items 3 and 4, that stability theory can be brought into agreement with the experimental results. An important point to note is that if justifiable reasons for modifying the stability predictions, which were alluded to above, cannot be found, this would indicate by default that stability and transition are, indeed, unrelated and that item 2 is true.

In the following sections, we first consider the effects of including additional terms (as suggested in item 3), which are omitted in classical stability analyses, in our formulation of the stability problem for the nosetip boundary layer. The outcome shows that these effects are minimal. We then take up the approach suggested in item 4 and question whether or not the mean flow profiles on a realistic nosetip can be reasonably represented by Falkner-Skan profiles. This approach is much more fruitful, and numerous stability results which ascertain the effects of surface roughness, heat transfer, ablation, pressure gradient, and compressibility on the stability properties of a nosetip boundary layer are presented. These results show that strongly unstable regions can be induced on the nosetip at Reynolds numbers substantially below a momentum thickness Reynolds number of $Re_\theta = 100$. Thus, despite the arguments noted above, we are indeed able to predict transition on nosetips using stability theory.

We hasten to point out that the predictions of unstable regions at these very low Reynolds numbers are strongly dependent upon the mean flow distortions which are induced by the surface roughness. In the present work, these distortions are simulated by a phenomenological model. Two observations on this approach are in order: First, there is insufficient experimental evidence to either justify or refute the roughness analysis. We certainly cannot claim that the analysis includes the effects of the roughness in a complete and accurate way. There is room for improvement as well as for diagnostic experimental verification. Second, we note that more preposterous than presupposing that the mean flow profiles are modified in some way by the roughness is to assume that they remain unaltered by the roughness and retain their smooth wall shapes. To bring

this comment fully into context, we note that the roughness heights with which we are concerned are of the same order as, or larger than, the momentum thickness of the boundary layer. Certainly, roughness elements of this magnitude will alter the profiles from the shape which would be expected for a mathematically smooth plate.

Finally, we note that another possible explanation for the differences between linear stability theory and experimental results is that finite, and not infinitesimal, disturbances are involved. Thus, because of their finite amplitudes, we must consider a nonlinear (as opposed to a linear) stability theory. Although differences in stability characteristics would be expected, we note that we would require the nonlinearity to change the critical Reynolds number by more than fifty-fold. Such large changes as a result of finite amplitude seem unlikely.

2. THE APPLICABILITY OF THE CLASSICAL STABILITY THEORY

2.1 Formulation of the Nosetip Boundary Layer

Classical boundary layer stability theory is based upon the assumption of parallel flow. According to this approximation, all streamwise derivatives of mean flow quantities are ignored, as are all terms which are proportional to the normal (mean) velocity component. Based upon these classical approximations, the critical Reynolds number of an incompressible boundary layer in the vicinity of an axisymmetric stagnation point is $R_\theta = 3340$ (Wazzan, Okamura and Smith, 1968). Experimental observations of nosetip boundary layers frequently note transition as early as $R_\theta = 100$. As indicated in the introduction, this discrepancy between theory and experiment could be the result of terms (or effects) which are neglected in the classical parallel flow theory, but which are important in the nosetip boundary layer. The effects of some of these additional factors are considered in this section.

It is well known that the effects of compressibility reduce the critical Reynolds number on flat plates by a small amount (Mack, 1975), and it is likewise well known that favorable pressure gradients cause the critical Reynolds number to increase slowly; however, few computations which indicate the effects of compressibility on stability characteristics in the presence of nonzero pressure gradients have been reported. For this reason, we performed a series of such calculations, the results of which were given in a previous report (Merkle, et al., 1975). These results showed that for a boundary layer corresponding to an axisymmetric stagnation point, the critical Reynolds number was lower for compressible flows than for incompressible flows, but that the reduction was not substantial. The reduction in the critical Reynolds number at a Mach number of unity was only a few percent. Since nosetip transition is generally observed to occur within the subsonic region (near the stagnation point) of the boundary layer, these Mach-one calculations should span the compressibility range of interest. Additional computation of the effects of cold walls on the stability characteristics of stagnation-point boundary layers showed that wall cooling was stabilizing (just as it is for flat plates) and caused the critical Reynolds number to increase. Finally, computation of the stability characteristics

of boundary layers subjected to a realistic nosetip pressure gradient also showed no decrease in the critical Reynolds number.

The conclusions of these investigations are obvious; the inclusion of the effects of Mach number, cold wall temperatures, and actual nosetip pressure gradients separately or in combination fails to change the critical Reynolds number substantially from its incompressible, axisymmetric-stagnation point value. (Also note that these calculations took into account the effects of temperature-dependent properties, including both viscosity and thermal conductivity.) In fact, most of these effects make the boundary layer more stable. Consequently, classical parallel-flow linear stability theory cannot explain the existence of transition on the nosetip.

Note, however, that this conclusion is only for parallel-flow stability theory. In particular, note that the strong streamwise velocity gradients (du/dx) which are experienced near the stagnation point have been ignored. Computations of these nonparallel effects by Saric and Nayfeh (1975), Bouthier (1973), and Gaster (1974) have shown that such effects are destabilizing. Besides these nonparallel effects, the present problem possesses an additional nonparallel quantity which was not present in any of the above-mentioned analyses. This additional effect is one which enters because of the axisymmetric (as opposed to planar) geometry of the problem. In classical stability theory, the stability equations for an axisymmetric body are taken as being identical to those on a planar body; the axisymmetric effects enter only through the profiles for the mean quantities. The justification for this approximation was first given by Battin and Lin (1950), and has been reviewed by Merkle, Ko, and Kubota (1974). The application of order of magnitude arguments in the present problem would likewise indicate the insignificance of the axisymmetric effects here, but the possibility of axisymmetric vortex sketching as a destabilizing mechanism seems heuristically attractive. In view of the disagreement between theory and experiment, these nonparallel effects were included in the stability formulation, so that we could explicitly evaluate their effect. The results of the complete nonparallel theory have been given in detail in a separate report (Grabowski and Merkle, 1975), and are only summarized here.

The analysis of Grabowski and Merkle includes the nonparallel effects corresponding to both the streamwise velocity gradient terms, and the axisymmetric terms. Their results show that, although both of these terms are destabilizing, they are also both quite weak (see comparison of neutral stability curves in Fig. 1). In fact, the two effects taken together decrease the critical Reynolds number by less than two percent. From these results, we draw the following three conclusions: (1) the axisymmetric vortex stretching which occurs as the Tollmein-Schlichting waves are forced over the sphere is very weak; (2) the effects of the streamwise velocity gradient corresponding to the expansion away from the stagnation point are similarly small; and, (3) as a result of these first two observations, we see that parallel flow stability theory is quite adequate for the nosetip boundary layer.

Thus, we see that the stability analysis as classically formulated continues to predict critical Reynolds numbers which are a factor of 30 above the observed transition Reynolds numbers (and transition Reynolds numbers predicted from stability theory would have to be substantially larger than the critical Reynolds numbers). Further, we have seen that the effects of compressibility and wall heat transfer do not substantially alter the stability results. Finally, we have showed that the omission of nonparallel and axisymmetric effects in the stability formulation is certainly justifiable. Consequently, we conclude that item 3 in the Introduction is not the reason for the failure of stability theory in nosetip boundary layer transition.

Having verified that nonparallel effects can be appropriately neglected, our emphasis in the remainder of the Report is concerned with evaluating the stability properties of the nosetip boundary layer under the assumption that the surface roughness modifies the mean flow profiles. For this situation, the inclusion of compressibility and heat transfer characteristics proves to be highly significant, and numerous results describing their effects are included.

3. STABILITY CHARACTERISTICS OF NOSETIP BOUNDARY LAYERS

In this section, we present a number of numerical solutions for the stability characteristics of nosetip boundary layers. In these results, the phenomenological roughness model which was mentioned in the introduction has been used to simulate the effects of roughness on the stability properties of the boundary layer. Details of this roughness model are presented by Merkle, Kubota, and Ko (1974) and Merkle, Grabowski, Kubota, and Ko (1975), and will not be repeated here. For completeness, we note that the roughness model postulates a transverse momentum transfer in the region near the roughness which arises from unsteadiness that is introduced by the roughness elements. The effects of this additional momentum transfer are expressed in terms of an eddy viscosity and an eddy conductivity which are given by

$$\frac{\varepsilon}{\nu} = K_\varepsilon \frac{u_k}{\nu} Re_k \left\{ 1 - e^{-Re_k/A^+} \right\} e^{-\beta_1 (y/k)^2} \tag{3.1}$$

$$\frac{\varepsilon_H}{\nu} = \left(\frac{P_R}{P_{R_T}} - 1 \right) + \frac{P_R}{P_{R_T}} \frac{\varepsilon}{\nu} \tag{3.2}$$

where ε is the eddy diffusivity for momentum transfer and ε_H is the corresponding eddy diffusivity for enthalpy transfer. The values which have been used for the constants in the equations are the same as those used previously. In particular, we have used:

$$\begin{aligned} K &= 0.1 \qquad & \beta_1 &= 1.0 \\ A^+ &= 40.0 \qquad & P_{R_T} &= 1.0 \end{aligned} \tag{3.3}$$

The present results are divided into two categories and are presented separately. The first group of results has been obtained by using a local similarity hypothesis for the boundary layer and finding the stability properties of these locally similar profiles. For these results, both stability maps and total amplification ratios are presented. For the second case, a complete (non-similar) numerical solution of the laminar boundary

layer has been computed (including the effects of the roughness model). Using these non-similar profiles, a series of stability maps has been compiled for a variety of parametric conditions. These particular results have been selected to coincide with the Transition Test Cases selected by the Aerospace Corporation (Baker, 1976).

3.1 The Stability Characteristics of a Nosetip Boundary Layer Using a Locally Similar Hypothesis for the Mean Flow Profiles

The stability characteristics of a nosetip boundary layer in a realistic environment have been computed and are presented in Figs. 2 through 11. These computations are for a reentry vehicle at an altitude of 59,000 feet, a free-stream stagnation pressure of 50.7 atmospheres and a free-stream Mach number, $M_\infty = 22.6$. The nosetip is nominally hemispherical in shape with a radius of 1.5 inches. The variation of boundary layer edge conditions around the nosetip is shown in Fig. 2. As indicated in the figure, the wall temperature ratio, T_w/T_e is nominally 0.53, corresponding to the cold wall conditions which are representative of reentry vehicles. Note also that the momentum thickness Reynolds number, Re_θ, remains below 200 until the sonic point is reached. The pressure distribution, expressed in terms of the Falkner-Skan similarity parameter, β, is shown in Fig. 3. The pressure gradient parameter starts from a value of $\beta = 0.5$ at the stagnation point and increases slightly. Values of β which are this high represent strongly favorable pressure gradients, an effect which, as indicated in Section 1, is normally considered to be highly stabilizing.

Mean flow profiles for the conditions corresponding to those described in the previous paragraph were computed by using a local-similarity hypothesis. At each angular position on the nosetip, the momentum thickness was chosen to match that obtained by a numerical solution of the corresponding boundary layer which was supplied to us by Anderson (1975a). Our similar flow profiles differed from those computed by Anderson in that we included the effects of wall roughness using the roughness model mentioned above.

The stability characteristics of these rough-wall, laminar, mean flow profiles were computed and the results are shown in Figs. 4 and 5 for a roughness height, $k = 0.55$ mils. As can be seen from Fig. 4, the nosetip boundary layer is strongly unstable. The critical Reynolds number occurs

about 7° from the stagnation point, while the peak amplification rate occurs around 20°. At this peak point, the non-dimensional amplification rate, α_i, is about 0.36. Since α_i is non-dimensionalized by the boundary-layer thickness, δ (the point where $u/u_e = 0.999$), this indicates a growth rate in the peak region of one e-fold in a distance of just less than three boundary-layer thicknesses. The total available amplification is quite large, as is pointed out later.

The companion curve to the amplification rate is the wave number distribution of these unstable waves. These results are shown in Fig. 5. As an example of the typical wavelength, note that the wave-number of the most unstable disturbance is about 2.0, corresponding to a wavelength of about three times the boundary-layer thickness. Longer wavelengths are noted for the lower frequencies and shorter ones for the higher frequencies.

The amplification rates for this case are shown again in Fig. 6, this time with the loci of lines of constant physical frequency superimposed. This curve, then, shows the particular path on the stability maps that a disturbance of a given physical frequency would follow as it is swept downstream in the boundary layer. As can be seen, the physical frequencies tend to follow the contour islands on the map quite closely. Because of this, those individual frequencies which pass through the center of the map tend to be amplified very strongly. A corresponding growth curve, showing the cumulative growth for each of a number of individual frequencies, is given in Fig. 7. Two of the important features of this curve are the magnitude of the total available amplification and the bandwidth of frequencies which are strongly amplified. For example, note that amplifications of as much as e^{30} are realized, and that a number of frequencies reach this magnitude at about the same time. This stability map does not generate a nice smooth envelope corresponding to a maximum growth curve as is obtained for flat plate or Falkner-Skan profiles.

If we use these rough-wall stability results along with a transition criterion based on an amplification of e^9, we see that transition would be predicted to occur some 14° from the stagnation point. For comparison, the Aerotherm transition correlation (Anderson, 1975a) indicates transition will occur at about 26°. Two observations comparing the stability results and the Aerotherm correlation should be noted. First, the Aerotherm correlation is basically an end-of-transition correlation, so that the beginning of transition would occur somewhere before the 26° position. Second, the total

amplification which is available, and the position where the amplification ratio first reaches e^9, is strongly dependent on the height of the surface roughness. Some indications of this sensitivity are presented later. It is in this spirit that we quote the e^9 amplification, namely as an indication of transition, but an indication which is more sensitive to roughness height than to the specific transition criterion used. In other words, (almost) as soon as the roughness becomes large enough to generate an unstable region on the nosetip, we can anticipate sufficiently vigorous growth that transition will occur soon after.

In an effort to determine the sensitivity of the stability predictions to the various parameters on the nosetip, and to determine which variables are responsible for the existence of the unstable region, we have varied several of them independently and observed their individual effects on the stability characteristics. For these parametric variations, we chose a position on the hemisphere corresponding to 19^o from the stagnation point (which is very near the most highly unstable region of the map), and held all other parameters constant except the one which was being varied. For each variation, the mean flow profiles were first recomputed, and then the changes in the stability characteristics were determined. The specific parameters which were varied include the wall temperature, the roughness height, the Reynolds number, and the pressure gradient parameter. The results of these parametric variations are given in Figs. 8 and 9, which show the amplification rate as a function of the frequency for the 19^o location. Figure 8 presents the effects of varying the wall temperature. The most unstable curve (largest value of $-\alpha_i$) is the one corresponding to the case, $T_w/T_e = 0.53$. As the wall temperature is increased, the boundary layer becomes noticeably more stable. For example, the peak amplification rate at $T_w/T_e = 0.53$ is $\alpha_i = 0.356$. As T_w/T_e is increased, the peak rapidly falls until at $T_w/T_e = 0.9$ the peak α_i is only -0.07. Although further calculations were not made, it is easy to see that the boundary layer could soon be stabilized completely by continuing to increase the wall temperature.

One important point to note regarding these parametric wall temperature results is that classical stability theory predicts that cooling the wall stabilizes a compressible boundary layer (except in certain special cases; Mack, 1969). The results of cooling the wall in the presence of surface

roughness has a strong destabilizing effect. This effect, which has also been noted in experimental transition results, can be attributed to the interaction between the roughness and the boundary layer. The most important fluid dynamic characterization of surface roughness is in terms of a Reynolds number which can be defined as the Reynolds number which exists locally at the top of a roughness element. We define this Reynolds number as

$$Re_k = \frac{u_k k}{\nu_k}$$

where the subscript, k, implies the variable is to be evaluated at the top of the roughness element. As the wall temperature is decreased, the boundary layer becomes thinner so that the velocity at the top of the roughness increases while, simultaneously, the viscosity decreases, making the roughness more "effective" in boundary layers over cooled walls as compared to adiabatic walls. In other words, the ratio of the roughness height, k, to some measure of the boundary layer thickness, δ, increases as the wall temperature is decreased.

The second parametric variation is for the roughness beight. These results are shown in Fig. 9. As before, the base case (k = 0.55 mils) yields a peak $\alpha_i = -0.365$. When the roughness is reduced to 4.7 mils, the peak amplification rate decreases to $\alpha_i = -0.240$; at 3.9 mils it is -0.080; while for a roughness height of 1.9 mils, the boundary layer at this particular location on the nosetip is stable to disturbances of all frequencies (and all disturbances are damped at a rate which exceeds $\alpha_i = +0.200$). These results demonstrate the drastic effects surface roughness has on the stability characteristics of the boundary layer.

The effects of changing the local pressure gradient, β, as well as the local Reynolds number, Re_θ, were also tested, but are not shown because the results were so insensitive to these variables. Changes in the pressure gradient from $\beta = 0.65$ to $\beta = 0.50$ caused almost no change in the stability results. This indicates that for these computations we are operating in a "roughness-dominated" regime in which pressure gradient has little effect (see related comments by Merkle, Kubota, and Ko, 1974). Similarly, artificial changes in Re_θ, which were achieved by increasing the boundary layer thickness while maintaining the shapes of the profiles, had little effect on the

stability characteristics. The alternative exercise of increasing the boundary layer thickness while holding the roughness height fixed (allowing the shapes of the profiles to change) would have a substantial effect on stability, but this effect is nearly the same as varying the roughness height.

In summary, we see that the most dominant cause of the instability region on the nosetip is the effects of the surface roughness. The roughness enters in a direct way, but also in an indirect way, through its effects on other parameters. For instance, wall cooling is strongly destabilizing in the presence of roughness, whereas on a smooth wall, it is stabilizing. The importance of cooling is easily seen from Fig. 8, which indicates that if this boundary layer were adiabatic, no unstable region would exist, even with the roughness present. This interaction between roughness and the other parameters in the boundary layer is a very important one. Additional examples of this are shown in the next subsection.

One final, and very interesting, result was obtained by extending the previously described stability calculations to nosetip locations further away from the stagnation point. The results of this computation are summarized in Fig. 10. This figure shows the same stability results which were presented in Fig. 4, but, in addition, it shows solutions as far away from the stagnation point as 50^{o} (note that the sonic point occurs at about 38^{o}). The unique characteristic of this nosetip stability map is that the neutral stability curve closes completely at the high Reynolds number end. Thus, there is an unstable region which starts at low angles and expands in size as as we move around the nosetip, but after a time it begins decreasing in size and finally shrinks to zero. The reason for the return to stability is the ever-decreasing value of the ratio, k/δ, which occurs as the boundary layer gradually thickens. The location where the unstable region shrinks to zero is about 47^{o}, and the local Mach number is about 1.5 at that location. Consequently, we see that the boundary layer becomes increasingly stable as we enter the supersonic regime.

If we continued the stability calculation over an entire sphere-cone reentry vehicle, we would expect to find a second unstable region somewhere back on the vehicle frustrum. We anticipate that this second unstable region would occur at (or near) classical Reynolds numbers for cones (flat plates) in the appropriate Mach number regime. A schematic diagram of these two

separate unstable regions is shown in Fig. 11. The anticipated form of these stability characteristics suggests that as the reentry vehicle descends, the transition location would initially move gradually forward on the frustrum and would be generated by the second unstable region (the first unstable region would probably not be present at very high altitudes). During this time, the growth of disturbances on the nosetip would reach larger and larger amplitudes (as the vehicle descends), but would not get sufficiently large to trigger the nonlinear interactions which are required for transition. The important point to note is that disturbances on the nosetip could grow for a time and then emerge from the unstable region and decay rapidly (so as to be of no consequence) without triggering transition. As soon as the vehicle reached a certain critical altitude, the peak amplitude of disturbances in the unstable region on the nosetip would surpass the level at which significant nonlinear interactions begin, and transition would jump discontinuously from the frustrum to the nosetip. Thus, this stability map with two unstable regions would not predict a continuous movement of the transition location from the free-stream to the nosetip, but would predict the discontinuous jump because the transition on the nosetip is caused by different instabilities (the first unstable region) than is the one on the frustrum (the second unstable region).

For comparison, we note that experimental results of nosetip transition have been interpreted in two ways. The PANT correlation is based on the assumption that the transition movement is discontinuous (as suggested above), while Demetriades and Laderman (1975) have interpreted their experiments as showing a rapid, but continuous, movement of the transition location to the nosetip.

Finally, it should be pointed out that these stability results are for laminar boundary layers only. The existence of a second stable region, or even the closing of the first unstable region, becomes meaningless if transition to turbulence occurs. Similarly, no observations concerning the probability of re-laminarization in the supersonic regions of the boundary layer can be obtained from the present analysis.

3.2 Stability Characteristics of Nosetip Boundary Layers Based on Complete Non-Similar Analysis

The previous subsection has presented some stability predictions for nosetip boundary layers that have been obtained from mean flow profiles which are based on a local similarity hypothesis. The present subsection presents a series of stability maps for various nosetip environments which have been computed using mean flow profiles obtained from a numerical, finite difference solution of the complete, non-similar boundary layer equations. Most of the computations in this section have been chosen to coincide with the Transition Test Cases which have been suggested by Baker (1976). For reference, a copy of these test cases is included as Appendix I.

3.2.1 Determination of the Mean Flow

The boundary layer code which was used for the present calculations is the one developed by Price and Harris (1972). Minor modifications have been included to adapt the code for our particular requirements. The most significant of these changes is the incorporation of the roughness model which was described above. The Price-Harris code operates in the transformed Levy-Lees plane, a formulation which is identical to the one we used for the similar flow analysis except that the non-similar terms are retained. Starting from the original equations of motion and incorporating the effects of roughness, we obtain the following equations:

continuity

$$\frac{\partial}{\partial x}\left(r^j \rho u\right) + \frac{\partial}{\partial y}\left(r^j \rho v\right) = 0 \tag{3.4}$$

momentum

$$\rho\left(u\frac{\partial u}{\partial x} + v\frac{\partial u}{\partial y}\right) = -\frac{\partial p}{\partial x} + \frac{1}{r^j}\frac{\partial}{\partial y}\left[r^j(\rho\varepsilon+\mu)\frac{\partial u}{\partial y}\right] \tag{3.5}$$

energy

$$\rho c_p\left(u\frac{\partial T}{\partial x} + v\frac{\partial T}{\partial y}\right) = u\frac{\partial p}{\partial x} + (\rho\varepsilon+\mu)\left(\frac{\partial u}{\partial x}\right)^2 + \frac{1}{r^j}\frac{\partial}{\partial y}\left[r^j\left(k + \frac{k\varepsilon_H}{v}\right)\frac{\partial T}{\partial y}\right] \tag{3.6}$$

where x and y represent a cartesian or an axisymmetric coordinate system in the usual sense. For the cartesian system, the exponent j is set to zero, so that $r^j = 1.0$, whereas for axisymmetric coordinates, $j = 1$, so that r^j is identical with y. The corresponding velocity components are denoted by u and v, and the pressure by p. The molecular viscosity and the thermal conductivity are denoted by μ and k, respectively. The effective viscosity is given by the sum of the molecular and eddy viscosities, and similarly for the thermal conductivity:

$$\begin{aligned} \mu_T &= \mu + \rho\varepsilon \\ k_T &= k + \frac{k\varepsilon_H}{\nu} \quad . \end{aligned} \tag{3.7}$$

We define a turbulent Prandtl number, Pr_T, as

$$P_{R_T} = \frac{\mu_T c_\rho}{k_T} = P_R \left(\frac{1+\varepsilon/\nu}{1+\varepsilon_H/\nu} \right) . \tag{3.8}$$

Using these definitions, the diffusion terms in the momentum and energy equations can be written in their classical laminar form,

$$\frac{1}{r_j} \frac{\partial}{\partial y} \left(r^j \mu_T \frac{\partial u}{\partial y} \right) \quad \text{and} \quad \frac{c_p}{r_j} \frac{\partial}{\partial y} \left(\frac{r^j \mu_T}{P_{R_T}} \frac{\partial T}{\partial y} \right) , \tag{3.9}$$

where c_p has been taken as constant.

We now introduce the Levy-Lees transformation,

$$\xi(x) = \int_0^x \rho_e u_e \mu_e r_0^{2j} dx$$

$$\eta(x,y) = \frac{\rho_e u_e r_0}{\sqrt{2\xi}} \int_0^x t^j \left(\frac{\rho}{\rho_e} \right) dy \tag{3.10}$$

where ξ and η are the transformed coordinates, and t represents the transverse curvature term ($t = r/r_0$). The subscripts e and 0 refer to conditions at the edge of the boundary layer and on the surface of the body. Introducing the non-dimensional dependent variables F, θ, and V as:

$$F = u/u_e, \qquad \theta = T/T_e \ ,$$

and

$$V = \frac{2\xi}{\rho_e u_e \mu_e r_0^{2j}} \left[F \frac{\partial \eta}{\partial x} + \frac{\rho v r_0^j t^j}{\sqrt{2\xi}} \right] \ , \tag{3.11}$$

and combining with the equations of motion, we obtain,

continuity

$$\frac{\partial v}{\partial \eta} + 2\xi \frac{\partial F}{\partial \xi} + F = 0 \tag{3.12}$$

momentum

$$2\xi F \frac{\partial F}{\partial \xi} + v \frac{\partial F}{\partial \xi} - \frac{\partial}{\partial \eta} \left[t^{2j} C \left(1 + \frac{\varepsilon}{\nu} \right) \frac{\partial F}{\partial \eta} \right] + \beta \left[F^2 - \theta \right] = 0. \tag{3.13}$$

energy

$$2\xi F \frac{\partial \theta}{\partial \xi} + v \frac{\partial \theta}{\partial \eta} - \frac{\partial}{\partial \eta} \left[t^{2j} \frac{C}{P_{R_T}} \left(1 + \frac{\varepsilon}{\nu} \right) \frac{\partial \theta}{\partial \eta} \right] - \alpha C t^{2j} \left(1 + \frac{\varepsilon}{\nu} \right) \left(\frac{\partial F}{\partial \eta} \right)^2 = 0 \tag{3.14}$$

where the parameters,

$$\beta = \frac{2\xi}{u_e} \frac{du_e}{d\xi}$$

$$\alpha = u_e^2 / C_p T_e \tag{3.15}$$

and

$$C = \frac{\rho \mu}{\rho_e \mu_e} \ ,$$

have been defined. Equations (3.12) to (3.14), which include the roughness model, have been solved numerically to obtain the mean flow profiles for the velocity and temperature that are used in the following stability results. Details of the mean flow profiles are given in Appendix II.

3.3.2 Effects of Varying Surface Roughness in the Presence of Wall Cooling and Mass Addition: Case 1

The parameters which were used for the first three test cases differed slightly from those described in the Transition Test Cases (Appendix I). The differences are as follows: The free-stream stagnation pressure was taken as 280 psia instead of 220 psia, and the mass addition was chosen to be similar to that reported by Demetriades and Laderman (1975), rather than specifying $B' = 0.6$. The differences are only slight and are not expected to affect the results materially. They were introduced because portions of these calculations had been completed before the Transition Test Cases were received. The specific mass flux which was specified at the wall is

$$\rho_o v_o = \frac{P_c^2 - 8.56}{9.63} \left\{ .00675 \cos 2\theta + .00875 \right\} \frac{\text{lb.-sec.}}{\text{ft}^3} \qquad (3.16)$$

where P_c represents the chamber pressure (in psia) which was used to inject the mass at the surface. A plot showing the mass flux at the wall for several values of P_c is given in Fig. 12.

Cases 1, 2, and 3 are for a 7-inch sphere. The stability results for the base case with $k = 6.0$ mils, $T_w/T_e = 0.6$, and $P_c = 30$ psia, are given in Figs. 13 and 14. Figure 13 shows the amplification rates in the unstable regime. As can be seen, the unstable region is quite extensive. The critical Reynolds number occurs about 5 degrees from the stagnation point. The unstable region extends to beyond the sonic point, and although the computations were not carried further, it appears, as for the nosetip described in the previous subsection, that the stability region is beginning to decrease in size and that this neutral stability curve would also close on itself. For this case, peak amplification rates are about $\alpha_i = -0.51$. The corresponding wave numbers are shown in Fig. 14. The degree of instability exhibited in this map would certainly suggest that transition would occur at these conditions.

The stability maps for the parametric variation in roughness height are shown in Figs. 15 through 20. The amplification rates for $k = 4.0$, 3.0, and

2.0 mils are given in Figs. 15, 17 and 19, respectively; the wave numbers are given in Figs. 16, 18 and 20. With the successive reductions in roughness height, the unstable region gradually decreases in size and the peak amplification rates also decrease. As indicated above the peak amplification rate for the 5.0 mil case is $\alpha_i = -0.51$. As k is decreased, the peak drops to $\alpha_i = -0.505$ for k = 4.0 mils, to $\alpha_i = -0.45$ for k = 3.0 mils, and to $\alpha_i = -0.30$ for k = 2.0 mils. When the roughness was decreased to k = 1.0 mils, the boundary layer became completely stable.

The critical Reynolds number also increases slowly as the roughness is decreased. Starting from its low value of about 5 degrees for k = 5.0 mils, the critical Reynolds number increased to 5.5, 7.0 and 10.5 degrees as the roughness height was varied from 4.0 to 3.0 and, finally, 2.0 mils. A composite curve which compares the neutral stability curves for these four cases is shown in Fig. 21. Again, recall that a roughness of k = 1.0 mil allowed the boundary layer to be completely stable.

Since the total available amplification has not been computed for these curves (nor for the others in this series), it is difficult to determine a predicted transition location from these stability results; however, based upon our previous results, we estimate that transition would occur on the nosetip for all four of these cases (with roughness height equal to 2, 3, 4, and 5 mils). Since the boundary layer becomes completely stable for k = 1.0 mil, transition would definitely not be observed (according to the stability predictions) for roughnesses of one mil or less. Thus, we would expect transition to appear on the nosetip when the roughness is between 1.0 and 2.0 mils. (Along with these comments, we wish to point out that the principle use that these stability maps are intended to serve is as an aid to understanding nosetip transition and the movement of transition in response to changes in the various parameters. The principle emphasis is not to be placed on obtaining quantitative predictions of transition locations.)

3.2.3 Effects of Varying Surface Mass Addition in the Presence of Roughness and Wall Cooling: Case 2

The second set of stability maps in this series of calculations shows the variations in the stability characteristics as the surface mass addition is varied. Again, the base case for effects of changes in mass addition is

the stability map shown in Figs. 13 and 14. For this base case, the roughness is 5.0 mils, the wall temperature ratio is 0.6, and the chamber pressure (which controls mass addition) is 30 psia. If all parameters except the mass addition are held fixed, and the mass addition is set to zero, the resulting stability characteristics are as shown in Figs. 22 and 23. The amplification rates with no mass addition, which are shown in Fig. 22, are almost identical to the base case where the chamber pressure was 30 psia. The wave numbers are similarly alike. A back-to-back comparison of the neutral stability results in Fig. 24 verifies the closeness of these two cases. For example, the lower neutral stability curve for the case with mass addition extends to marginally lower frequencies than does the one without, whereas the opposite is true for the upper neutral stability curve. If the peak amplification rates are compared, the case with mass addition appears to be slightly more unstable ($\alpha_i = -0.51$) than the case without mass addition ($\alpha_i = -0.45$).

The conclusion which is to be drawn from these stability results is that surface mass addition, in the presence of surface roughness, has essentially no effect (or a very slightly destabilizing effect) on the stability characteristics of a nosetip boundary layer. Consequently, we would expect transition on a rough wall to be relatively insensitive to surface mass addition. Stability results which demonstrate the effects of mass addition on a smooth wall are considerably different, as is described later.

The physical reason for the insensitivity to surface mass addition is apparent. Surface mass addition tends to distort the velocity profile and make it more unstable, but at the same time, it reduces the velocity at the tops of the roughness elements, thereby lowering the roughness Reynolds number and making the roughness less effective. The net impact of these two opposite effects on boundary layer stability is very small. A comparison between the roughness Reynolds numbers for the mass addition and no mass addition cases is shown in Fig. 25.

3.2.4 Effects of Varying Wall Temperature Ratio in the Presence of Surface Roughness and Mass Addition: Case 3

The third example in this series is concerned with determining the effects of the wall temperature ratio, T_w/T_e, on the stability characteristics of a nosetip boundary layer. As indicated in Subsection 3.1, the classical smooth wall results show that cooling the wall makes the boundary layer more stable,

whereas rough wall results indicate that wall cooling is destabilizing. The present rough wall results likewise show that cold wall cases are substantially more unstable than adiabatic wall cases. The results for these wall temperature ratios are shown in Figs. 13 and 14 ($T_w/T_e = 0.6$), Figs. 26 and 27 ($T_w/T_e = 0.8$), and Figs. 28 and 29 ($T_w/T_e = 1.0$). For all three of these stability maps, the roughness is taken as 5.0 mils, and the surface mass addition is that induced by a chamber pressure of 30 psia in eq. (3.16). A comparison of the peak amplification rates as the wall temperature is increased shows that the peak α_i changes from -0.51 to -0.42 and -0.32 as the wall temperature is changed from $T_w/T_e = 0.6$, to 0.8 and 1.0. The area enclosed by the neutral stability curves also decreases rapidly as the wall temperature is raised; this comparison is shown in Fig. 30. Note that the critical Reynolds number is only slightly changed as the wall temperature is varied, but that the width of the frequency spectrum which is unstable to small disturbances decreases rapidly, particularly near the lower neutral stability line. This pattern is similar to that observed for roughness also (see Fig. 21): The unstable region on the nosetip seems to diminish (with decreasing roughness or with increasing wall temperature) by a rapid rise in the lower neutral stability curve while the upper neutral stability curve and the critical Reynolds numbers remain almost fixed. Thus, with decreased wall temperature or increased surface roughness, the boundary layer is unstable to a wider spectrum of disturbances, but the unstable region occurs at essentially the same angular positions on the sphere. As the wall temperature is increased, the transition location would be expected to move further from the stagnation point and eventually to jump to the trailing cone frustrum. Increased cooling would not only cause disturbances to be amplified by larger amounts, but would cause the boundary layer to be susceptible to a wider range of disturbances. The effects of wall temperature on the roughness Reynolds are given in Fig. 31.

3.2.5 Effects of Free-Stream Noise on Transition: Case 6

The stability map for a nosetip boundary layer on a sphere in the presence of conditions identical to those specified in Case 6 (except that the stagnation pressure was again taken as 280, instead of 260, psia) is shown in Figs. 32 and 33. These stability results show that for this case (wall roughness, $k = 5.0$ mils, no surface mass addition, $T_w/T_e = 1.0$), a moderately large unstable region (whose peak amplification rate is

$\alpha_i = -0.34$) exists. Although this stability region is considerably smaller than that shown in Fig. 13, it still appears large enough to cause transition.

The application of stability theory to the prediction or understanding of transition implies that transition is dependent on the amplitude of the unsteady disturbances inside the laminar boundary layer. This amplitude, in turn, is dependent on two separate factors: the initial amplitude of the disturbances before they are amplified by the boundary layer, and the total amplification ratio which is available between the critical Reynolds number and the location at which transition begins. Both of these factors are frequency dependent, and their interaction becomes important when the initial disturbance environment has significant amounts of energy concentrated in the unstable frequency regime. From this viewpoint, the most important factor to consider when attempting to determine how the external acoustic environment affects transition (as is requested in Case 6) is to determine how the frequency content of the external disturbance field compares with the unstable frequency regime which is predicted by the stability theory. In order to facilitate such a comparison, we have replotted the stability map in Fig. 32 in terms of the dimensional frequency spectrum. These dimensional results are shown in Fig. 34. As seen from the figure, the unstable frequency domain lies between 10,000 and 1,000,000 cps. Transition would be expected to be particularly sensitive to external disturbances in this frequency regime. A second observation which can be made in regards to Fig. 34 is that lines of constant physical frequency are the paths which are followed by individual disturbance components as they are swept around the nosetip. In this regard, Fig. 34 shows the same information for this situation as was shown in Fig. 6.

The comments above refer to the mechanism by which external disturbances are expected to interact with the boundary layer; however, it should be pointed out that a small change in the amplification ratio (such as can be effected by a small change in surface roughness) can overwhelm the effects of a large change in the external environment. The reason for this is simply due to the exponential growth which is experienced in the unstable region. Further, the amount of growth in the unstable region is so large and so rapid that changes in the initial amplitude (assumed here to be related to the free-stream disturbance level) will have little effect on the location

at which a specific amplitude (if this is used as a transition criterion) is reached downstream. Finally, the initial disturbance level will almost certainly arise from, not one, but two sources: the external environment plus disturbances generated by the roughness elements themselves. Thus, doubling the free-stream disturbance level will have a lesser effect on the disturbance level in the boundary layer, even upstream of the critical point. As a result of these factors, we anticipate that the location of transition in the presence of such large wall roughnesses would be scarcely affected by free-stream disturbances. More precise predictions can be made after the total growth curves have been computed for this case.

3.2.6 Effects of Surface Mass Addition in the Presence of Smooth Walls: Case 7

Case 7 in the Transition Test Cases is concerned with the effects of mass addition into an adiabatic boundary layer on a smooth spherical surface. As in the previous cases, the stagnation pressure was chosen as 280 psia (as compared to the 220 psia called out in Case 7). The surface mass addition was also specified from Eq. (3.16) instead of from the parameter, $B' = 0.6$. Again, these differences are expected to have no qualitative effects on the predicted stability results, and only minor quantitative effects.

For this smooth wall configuration, stability maps have been computed for each of three chamber pressures (*i.e.*, three mass addition rates), $P_c = 30$, $P_c = 45$, and $P_c = 60$ psia. The corresponding non-dimensional mass fluxes have been given in Fig. 12. The stability calculations for a boundary layer with surface mass addition corresponding to 30 psia showed that for these conditions, the boundary layer is stable to all disturbances. When the chamber pressure is increased to 45 psia, a small unstable region appears. The details of this region are shown in Fig. 35. The unstable region begins quite near the stagnation point (8 degrees), but closes on itself (similar to the results in Subsection 3.2) considerably before the edge Mach number reaches the sonic value. The reason for this closure of the region is, of course, readily traced to the $\cos 2\theta$ behavior which is specified for the surface mass flux (see eq. 3.16). As we go farther from the stagnation point, the mass flux decreases so that the boundary layer begins to approach a non-blown state. The corresponding wave number distributions for the 45 psia case are given in Fig. 36.

When the chamber pressure is raised to 60 psia, the unstable region increases again to a size which is substantially larger than the 45 psia case. These results are shown in Figs. 37 and 38. Notice from Fig. 37 that, although the neutral stability curve for this case is now quite large and extends over a substantial part of the nosetip, the peak amplification rate is still quite small ($\alpha_i = 0.05$). Because of this relatively weak amplification, we would still not expect transition to occur on the nosetip even for this relatively large blowing rate. A comparison between the neutral stability curves for these two mass addition rates is given in Fig. 39.

A few comments are in order with regard to these smooth wall stability calculations. First of all, we note that since the wall is assumed to be smooth, the effects of the roughness model are not included in this calculation. Consequently, these results (Figs. 35 through 39) correspond to classical stability results which must stand on their own merit. (By contrast, the predictions which are based on the roughness model can be validated or invalidated, in whole or part, by adequate experimental verification of the manner in which roughness affects transition. Such information is currently not available.) Thus, these results are similar to the stability results for incompressible flow in the presence of a $\beta = 0.5$ pressure gradient parameter; if the stability results indicate the boundary layer is stable in the presence of mass addition, there is no reason to suspect them to be wrong so long as the classical assumptions (such as the parallel flow approximation and the treatment of an axisymmetric stability problem as if it were planar) hold. As noted in Section 2, these assumptions appear to be more than adequate.

If we compare these stability results with the experimental results of Demetriades and Laderman (1975), we observe a contradiction. The experimental results indicate transition occurring on the nosetip for bleed chamber pressures as low as 20 psia. Our results indicate complete stability at $P_c = 30$ psia, and suggest transition would not occur until P_c was raised to 60 psia, or higher. One possible reason for this discrepancy is that the porous wall model used by Demetriades and Laderman did not generate the same mean flow profile as was used in these calculations because the mass flux at the surface was not sufficiently evenly distributed, but the "graininess" induced by the mass addition through the porous surface affected the profiles.

Finally, we should also contrast these smooth-wall, surface mass addition results with the rough-wall, mass addition results discussed in Subsection 3.2.3. For the rough-wall case, the effects of surface mass addition were very slightly destabilizing whereas for the present smooth-wall results, the effects of mass addition exhibit a substantial destabilizing effect. This represents another example of the manner in which the effects of various parameters on boundary layer stability are altered in the presence of roughness, as compared to their effects in the presence of smooth walls.

3.2.7 Stability Characteristics of Laminar Stable Shapes in the Presence of Roughness, Surface Mass Addition and Heat Transfer to the Wall: Case 8

The above results have all been for the boundary layer on a sphere of 7-inch radius in a Mach 6 stream whose total pressure is 280 psia. We now consider the effect of body shape on the stability characteristics of such boundary layers by looking at a so-called laminar stable shape. The coordinates for this body have been given by Baker (1976) and are tabulated in Appendix I. Before presenting our results, we note that the predominant effect of the change in the body shape is expected to occur through the changes in the external pressure field which is impressed on the boundary layer. The pressure distribution for this laminar stable shape as well as the previous ones for the sphere have been obtained from a Newtonian flow approximation. Since the area of prime interest in these calculations is the subsonic region before the external flow passes through the sonic point, this restriction to Newtonian theory should give a relatively accurate pressure distribution.

A comparison of the local pressure gradients on the present laminar, stable shape and on the spherical nosetip which was used for the previous calculations is given in Fig. 40. These results are presented in terms of the distance in feet from the stagnation point for each of the two bodies. The pressure gradient is presented in terms of the pressure gradient parameter, β, which is defined as

$$\beta = \frac{2\xi}{u_e} \frac{du_e}{d\xi} \tag{3.17}$$

where ξ is the transformed streamwise coordinate. Although this pressure gradient parameter is identically the same as the Falkner-Skan parameter, there is no restriction here to a similarity analysis; this parameter is chosen only as a convenient non-dimensional measure of the pressure variation. As can be seen from Fig. 40, the laminar stable shape experiences pressure gradients which are considerably more favorable than those on the spherical body. Also note that the arc-length distance along the two surfaces is not a very realistic parameter against which these two bodies can be compared. As a means of partially compensating for this shortcoming, the Mach number distributions along the two bodies are given in Fig. 41. As can be seen from this figure, the sonic point occurs considerably farther from the stagnation point on the laminar stable shape body than on the sphere. This effect is important in stability theory, where the total amplification is dependent on the distance over which the disturbance is amplified. For this reason, the stability maps for the laminar stable shape are presented in terms of arc-length rather than in terms of an angular variable.

The stability maps for the laminar stable shape are presented in Figs. 42 through 49, with a composite of the neutral stability curves for the various cases given in Fig. 50. The parametric variation in this series is in the height of the surface roughness. Figures 42 and 43 show the stability map for a roughness corresponding to 5.0 mils, with a wall temperature ratio, $T_w/T_e = 0.6$ and a surface mass addition specified by $B' = 0.6$. (For these laminar stable shape results, the specified value of $B' = \rho_o v_o/\rho_e u_e S_t$ has been used instead of the result in Eq. 3.16.) Figure 42 immediately shows that the boundary layer for this laminar stable shape is strongly unstable and certainly indicates that transition would be encountered for this roughness level. The corresponding stability map for $k = 3.0$ mils is given in Figs. 44 and 45. Again, the unstable region is substantial and the peak amplification rate is quite large ($\alpha_i = 0.53$). A further decrease in the roughness height to $k = 2.0$ mils, results in a smaller unstable region with the peak amplification rate decreased to $\alpha_i = -0.40$. These results are given in Figs. 46 and 47. When the surface roughness height is specified as $k = 1.5$ mils, a much smaller unstable region with the peak α_i being -0.20 is obtained as indicated in Figs. 48 and 49. Computations with a roughness level of 1.0 mil showed a completely stable boundary layer.

Reviewing these stability results, we see that the boundary layer on the laminar stable shape is slightly more unstable than the one on the sphere for a roughness of 5.0 mils. As the roughness is decreased, this trend persists and even at a roughness of 2.0 mils, the boundary layer for the laminar stable shape appears to be more unstable than that for the sphere (compare Figs. 46 and 19). More exact comparisons between the two can be made once the total amplification ratios have been computed.

A number of comments are in order regarding the stability comparisons between the sphere and the laminar stable shape. First of all, the boundary layer on the laminar stable shape seems to be more unstable despite its higher pressure gradient. This is in part due to the fact that the unstable region is spread out over a longer distance so that disturbances have a longer interval in which to amplify. This is, of course, a scaling argument; the same could be said of two spheres of different diameters. An effect which is perhaps more pertinent is that the boundary layer becomes slightly more unstable (α_i becomes more negative) when the pressure gradient becomes more favorable. This interaction between roughness and pressure gradient is similar to those previously noted for wall temperature variations and surface mass addition changes. In the presence of roughness, the effects of pressure gradient are drastically different than in the presence of a smooth wall. Increasing the pressure gradient for the case of a boundary layer on a smooth wall is decidedly stabilizing; a similar increase in the presence of wall roughness makes little change in the stability characteristics and may even make the boundary layer more unstable. These changes can, again, be attributed to the interaction between the thinning effect of a favorable pressure gradient on the boundary layer, in conjunction with a fixed roughness height. Thus, as the pressure gradient is increased, the boundary layer becomes thinner (δ becomes smaller) so that k/δ increases (for fixed k) and the effects of roughness become more predominant. Cooling the wall likewise thins the boundary layer making k/δ larger, while mass addition at the surface tends to thicken the boundary layer making k/δ smaller. These competing effects are the source of the very different behaviors of these various parameters in the presence of a rough wall as compared to a smooth wall.

In conjunction with these comments, some observations should be made on the relative stability of the boundary layer on the laminar stable shape as compared to the one on the sphere as the roughness is decreased from this "roughness-dominated" regime to a regime in which the roughness has little effect. As noted before, when the smooth-wall limit is reached, the boundary layer on the laminar stable shape must be more stable, so there must be a cross-over in behavior when the roughness is decreased from very large to very small values. The interesting question of how the stability of the two boundary layers compares in the intermediate regime between smooth wall values and roughness-dominated characteristics cannot be answered conclusively at the present time since not enough computations are available in this regime (which would be the interval between k = 1.0 and k = 2.0 mils). Based on the information which has been presented here, it appears that, as the roughness is decreased, the boundary layer on the sphere would become stable slightly earlier than the one on the laminar stable body.

3.2.8 The Effects of Roughness in the Small K/θ Range: Case 10.

Mean flow profiles for the nosetip boundary layer corresponding to the conditions in Case 10 have been computed. For these flow conditions (20 micron roughness, Tw/Te = 0.75, a nose radius, Rn = 4.0" and no surface mass addition) the mean flow calculations showed a peak roughness Reynolds number of $Re_K = 0.7$. Previous experience suggests that for instability to occur on the nosetip at these Reynolds numbers, the roughness Reynolds number has to be about 20 to 30. No stability results were run to verify the required increase, but it is estimated that the roughness would have to be increased by about a factor of six to generate an unstable region on the nosetip. (In this region, the roughness Reynolds number is nearly proportional to the square of the roughness height). No explanation for the differences between these estimates and the experimental results which were observed for a case similar to this (Bugliarello, 1957; Hall, Speegle, and Piland, 1957) is known (although the difference could be due to any of a number of procedures which were followed in the experimental program, rather than to a limitation of the predictions).

3.2.9 Summary of Transition Test Cases

A brief summary of the ten transition test cases is given below in order to condense the important results in a single place.

Case I. The stability predictions indicate that transition will occur on the nosetip for roughness of k = 2.0 mils or larger. Transition will not occur for roughnesses of less than 1.0 mil.

Case II. The stability characteristics of rough-wall boundary layers in the presence of modest amounts of surface mass addition are essentially identical to those for zero mass addition. If mass addition in the presence of surface roughness has any net effect on transition, it appears that it will cause transition to occur marginally sooner.

Case III. The effects of wall temperature are very important in the presence of roughness. Increasing the wall temperature to about Tw/Te = 1.2 or 1.3 would probably stabilize the present boundary layer (even in the presence of 5-mil roughness) and prevent transition. Cooling the wall in the presence of roughness is strongly destabilizing.

Case IV. Due to a lack of time, no computations were done for this case.

Case V. Again, no computations were done for this case; however our present theory has no mechanism for accounting for the shape of the roughness elements. Consequently, the present theory would predict identical results for Cases IV and V.

Case VI. The boundary layer under the present conditions is unstable. Consequently, if the free-stream disturbance level is increased, the transition location should move toward the stagnation point, as long as these disturbances contain energy in the unstable frequency range; however, the movement is expected to be very small for these high roughness conditions.

Case VII. The effects of surface mass addition in the presence of smooth walls is destabilizing, and sufficient mass addition will cause transition to occur on the nosetip. The mass addition must be increased above B' = 1.2 to observe nosetip transition.

Case VIII. In the presence of roughness, the boundary layer on a laminar stable shape is slightly more unstable than that on a spherical nosetip (despite the more favorable presence gradient).

It is even estimated that the laminar shape will remain unstable to lower surface roughnesses than the sphere.

Case IX. No computations were made for this case, but it is anticipated that the boundary layer with a 10-micron roughness would be stable to all disturbances. The roughness would have to be increased by at least a factor of 10 to observe transition on the nosetip.

Case X. Only mean flow profiles were computed for this case, and from these, it is estimated that the roughness height would have to be increased by at least a factor of 6 to obtain transition on the nosetip.

3.2.10 Additional Stability Results and Comparisons

A few additional stability calculations have been completed based on the non-similar mean-flow profiles. These are described in this section.

Figures 51 and 52 show the stability map for the laminar stable shape (Section 3.2.8) for the case of no surface mass addition, a roughness height of 5.0 mils, and a wall temperature ratio, Tw/Te = 1.0. By comparing these results with those on Fig. 42 (k = 5.0 mils, Tw/Te = 0.6, and B' = 0.6), we see that the effect of heat transfer to the wall in the boundary layer on the laminar stable shape is about the same as it was for the sphere (if we again assume the surface mass addition has little effect on boundary layer stability). These two neutral curves are compared on Fig. 53 (the similar comparison for the sphere is given on Fig. 31).

A second comparison of neutral stability curves is given on Fig. 54. This figure shows the effects of blowing in an adiabatic wall environment. The two neutral stability curves compared here are for boundary layers in which the roughness is 5.0 mils, the wall temperature ratio is unity, and the surface mass addition is that corresponding to a chamber pressure of 30 psia in one case, and to zero mass addition in the other. Again, these results indicate the surface mass addition in the presence of surface roughness has only a very small effect. The complete stability maps for these two cases is given in Figs. 29 and 30 and Figs. 32 and 33. A corresponding comparison of the effects of surface mass addition on a cold wall is given in Fig. 24.

A final comparison is given on Fig. 55. This figure compares the neutral stability curves for rough wall conditions (k = 5.0 mils) in the absence of surface mass addition for two wall temperature ratios, and, again, indicates the strong destabilizing effects of wall cooling.

4. A SUMMARY OF NOSETIP TRANSITION CHARACTERISTICS AS PREDICTED FROM STABILITY THEORY

In addition to the transition test cases, the document in Appendix I raises a number of questions concerning boundary layer transition on reentry vehicle nosetips. This section presents a general discussion of these and related topics. This discussion is based upon information obtained from our previous stability calculations and experience, and reflects the physics of boundary layer transition as interpreted from a linear stability viewpoint.

4.1 Effects of Roughness on Nosetip Transition

As indicated by the stability calculations in the previous section and by extensive experimental observations (see, for example, Anderson, 1975b, 1974, 1973; and Powars, 1973), surface roughness has a dominating influence on boundary layer transition on nosetip. Two intrinsic characteristics of nosetip boundary layers combine to make them exceptionally sensitive to the height and the character of roughness elements on the surface. These two characteristics are the highly favorable pressure gradient and the cold wall environment to which nosetip boundary layers are subjected. The favorable pressure gradient serves to keep the boundary layer thin in comparison with its zero pressure-gradient counterpart (at similar free-stream Reynolds numbers), thus making the roughness much more effective in promoting transition. The cold wall-temperature likewise tends to reduce the boundary layer thickness and cause a similar enhancement of the interaction between the roughness and the boundary layer.

According to the present analysis, the effects of roughness on the stability characteristics of the boundary layer, and on the transition location are dependent upon the roughness height alone. No additional characteristics of the roughness such as the number of roughness elements, their shape, or the distribution of roughness heights, are included, although these must certainly play a role. The dimensional length which is used to characterize the roughness enters the analysis through two different non-dimensional parameters, the roughness Reynolds number, Re_k, and the ratio of the roughness height to the boundary layer thickness, k/δ. It seems reasonable to expect that these two parameters are also important in

actual experimental situations. The role of the roughness height in the Reynolds number is particularly crucial, especially for small or intermediate roughness heights, because Re_k is essentially proportional to the square of the roughness height. (The roughness Reynolds number, $U_k k/\nu_k$, depends on k directly, and also through u_k which, for small values of k, is nearly proportional to k). Thus, small changes in k result in considerably larger changes in Re_k. Because of this effect, one characteristic of surface roughness which seems particularly important is the distribution of roughness heights. For example, a surface whose roughness is characterized by elements which are completely identical in height (maximum, minimum and RMS heights all the same) would probably behave quite differently from one having an identical RMS roughness, but a substantial spread in the heights of the individual elements so that some were considerably larger than the RMS value. Because of the approximate dependence of the Reynolds number, Re_K, on the square of k, the larger elements would have an unproportionately large effect on transition. By contrast, the number of elements, or their shape would be expected to have a smaller effect on transition. Some experimental evidence to support this point of view has been obtained for the case in which only a few roughness elements are present on the surface (VanDriest and McCauley, 1960).

Since our roughness model was originally developed (Merkle, Kubota, and Ko, 1974), some similar models which do have the capability of incorporating more of the characteristics of the roughness have been proposed. Notable among these are the drag models suggested by Finson (1975) and Chen (1976). Both of these models deduce the effect of the roughness elements from the drag of the elements. Finson's model emphasizes the disturbances produced by the element, while Chen's analysis is primarily concerned with changes in the mean flow profiles. Either of these models would allow the height distribution as well as the number of elements and element shape to be included in the analysis. We have made some preliminary mean flow computations using a roughness model which is similar to Chen's, but no comparison between this model and our original results is available as yet. Although the development of improved models for the description of the effects of roughness on nosetip boundary layers is to be encouraged, a word of caution is in order. It is noted, as mentioned earlier, that

essentially no experimental evidence which describes how or why roughness affects transition is available (although countless experiments have sought to determine the magnitude of the effect of roughness on transition). Without this knowledge, attempts to predict the effects of roughness on transition are severely hampered. We strongly feel that improvements in the prediction and control of nosetip transition are closely dependent upon improved analytical and experimental understanding of the mechanisms by which surface roughness affects transition.

Some further points of interest concerning the effects of roughness on nosetip boundary layers can be seen by considering very small, and very large roughnesses. Some calculations concerning the effects of very small roughnesses on boundary layer transition were discussed in Section 3.2.8. As noted there, our analysis indicates that once the surface roughness decreases below a certain fraction of the boundary layer thickness (so that the roughness Reynolds number decreases below a value of about 20), the effect of the roughness becomes negligible, and the boundary layer behaves as though it were smooth. The experimental evidence by Hall, Speegle and Piland (1957) and Buglia (1957), which was also noted there, suggests that roughness continues to have an effect on the transition location when the roughness Reynolds numbers are (apparently) less than unity. The fact that nosetip transition was observed in the presence of 10-micron surface roughnesses is, in itself, highly surprising (when considered from a stability point of view). Our present analysis will not predict transition for roughnesses of this magnitude, and it is difficult to imagine a mechanism which could lead to transition in such an environment. (Two possible explanations are that the surface roughness characteristics could have been changed during flight, or that the sustainer engine which continued to burn during the test interval could have generated vibrations which caused the boundary layer to become turbulent).

The opposite extreme of very large roughness is also unique. When the roughness elements become larger than the boundary layer and protrude out of it, the meaning of transition becomes clouded. In this extreme, the wakes behind the individual roughness elements and their interaction with each other would probably become important and the definition of a mean velocity profile would begin to lose its meaning. For this extremely

large roughness case, our analysis can no longer be expected to remain valid because the "sub-layer" near the wall where the eddy viscosity is defined extends across the entire boundary layer thickness. In this limit, the rough-wall boundary layer becomes identical to a smooth-wall boundary layer except for the augmented viscosity.

4.2 Effects of Body Shape on Transition

As indicated in Section 3.2.7, the effects of body shape on transition enter primarily through the pressure gradient. Other potential effects of body shape are the generation of unstable flow fields outside of the boundary layer, or changes in the shock shape which affect the boundary layer through entropy swallowing. Our results have indicated that, for the roughness levels which are encountered on typical nosetips, the stability characteristics of the boundary layer are only slightly sensitive to pressure gradient, and that favorable pressure gradients might even be destabilizing; consequently, we anticipate that body shape would have little effect on the transition location

4.3 Effects of Wall Cooling and Surface Mass Addition

Our results have clearly shown that wall cooling in the presence of roughness is destabilizing, while classical stability results (and some flat plate transition results) show that cooling is (generally) stabilizing. These predictions are in agreement with numerous experimental results. The effects of surface mass addition in the presence of rough walls has almost no effect on stability and transition for either cold or adiabatic walls.

The effects of surface mass addition in the presence of smooth walls is destabilizing, and can lead to unstable nosetip boundary layers; however the sensitivity to mass addition is smaller than that to roughness or to wall temperature in the presence of roughness. The amount of mass which must be added at the surface of a perfectly smooth sphere in order to generate instability is considerably larger than the mass addition which is added to the boundary layer on a typical ablating nosetip.

4.4 Effects of Free-Stream Noise on Transition on Nosetips

Because of the strong amplification which is encountered in boundary layers on a rough surface, and because the roughness can also serve to generate disturbances which are amplified by the boundary layer, it is anticipated that free-stream disturbances will have a minimal effect on the location of transition. Even for smooth-walled nosetips, the stability

predictions would indicate an insensitivity to free-stream disturbances, because the boundary layer is stable to all disturbances, and energy from the free stream is quickly damped by the boundary layer (barring non-linear effects). In the intermediate cases where the roughness height is just sufficient to cause the boundary layer on the nosetip to be marginally unstable, disturbances from the free-stream could, if in the proper frequency regime, cause transition to occur on the nosetip, when in a clean environment it would not occur until behind the nosetip. However, since the boundary layer is so sensitive to roughness, minute changes in the roughness characteristics would easily mask this effect.

4.5 Effects of Free-Stream Mach Number on Nosetip Transition

A complete parametric study of the effects of Mach number on nosetip transition has not yet been made, but these effects are expected to be small. Stability characteristics generally have a relatively strong dependence on Mach number, but for the nosetip transition problem, these effects do not enter directly since we are generally concerned with the subsonic portions of the boundary layer near the stagnation point.

5. SUMMARY AND CONCLUSIONS

Linear stability theory has been used as an aid in understanding the mechanisms of boundary layer transition on reentry vehicle nosetips. Some of the significant conclusions which can be drawn from the present work include:

(1) Classical, parallel-flow linear stability theory based on mean flow profiles which ignore the presence of surface roughness predicts that all disturbances inside the boundary layer will be damped even at Reynolds numbers which are 30 times larger than the observed transition Reynolds numbers.

(2) The nonparallel effects which are traditionally ignored in stability analyses have been evaluated, and it has been shown that they are indeed negligible. Specifically, the nonparallel effects associated with the acceleration of the free-stream flow away from the stagnation point, and those that derive from the vortex stretching which arises as the boundary expands around the axisymmetric nosetip are small and can be ignored.

(3) When our previously developed phenomenological model for incorporating the effects of the roughness into the mean flow is included in the analysis, the resulting nosetip profiles are highly unstable to small disturbances. Transition predictions based on these profiles are in qualitative agreement with experiment. Some specific results of the stability calculations are:

(a) The effects of most parameters are radically different in the presence of rough walls as compared to smooth walls as noted below;

(b) The effect of cooling the wall, which is weakly stabilizing in the presence of smooth walls, becomes strongly destabilizing in the presence of roughness. This appears to be in general agreement with experiment.

(c) The effects of favorable pressure gradients are strongly stabilizing on smooth walls but have very weak effects (or even slightly destabilizing effects) in the presence of roughness. This also appears to be in general agreement with experiment.

(d) Surface mass addition has a moderate destabilizing effect in boundary layers on smooth walls, but has essentially no effect in the presence of wall roughness. There is essentially no experimental evidence available to verify or refute this prediction.

(4) Smooth-wall boundary layers on nosetips can be sufficiently destabilized by surface mass addition to cause them to be unstable in the subsonic regime, so that stability theory will predict transition on the nosetip; but, the amount of mass addition which is required is several times that realized in typical reentry vehicle ablation environments.

REFERENCES

Anderson, A. D. (1973) "Analysis of PANT Series A Rough Wall Calorimeter Data, Part II: Surface Roughness Effects on Boundary Layer Transition," Aerotherm Report 73-81, Aerotherm Corp., Mountain View, CA.

Anderson, A. D. (1974) "Passive Nosetip Technology (PANT) Interim Report, Vol. III, Surface Roughness Effects, Part III, Transition Data Correlation and Analysis," Aerotherm Report 74-90, Aerotherm Corp., Mountain View, CA (Confidential).

Anderson, A. D. (1975a) Aerotherm/Acurex, Inc., personal communication.

Anderson, A. D. (1975b) "Boundary Layer Transition on Nosetips With Rough Surfaces, Appendix A," Aerotherm Corp., Mountain View, CA.

Baker, R. L. (1976), Aerospace Corp., personal communication.

Battin, R. H. and Lin, C. C. (1950) "On the Stability of the Boundary Layer Over a Cone," J. Aero. Sci., 17, 453.

Bouthier, M. (1973) "Stabilite Lineaire des Ecoulements Presque Paralleles. II. LaCouche Limits de Blasius," J. Mechanique, 12, 75.

Buglia, J. J. (1957) "Heat Transfer and Boundary Layer Transition on a Highly Polished Hemisphere-Cone in Free Flight," NASA TN D-955.

Chen, K. (1976) Presentation given at "Street A IV Summary Meeting," by Aoco Systems Division, Space and Missile Organization, Los Angeles, CA, January 29, 1976.

Demetriades, A. and Laderman, A. J. (1975) "Advanced Penetration Problems Program Final Report, Volume II," SAMSO TR No. 75-51, Space and Missile Systems Organization, Air Force Systems Command, Los Angeles, CA.

Finson, M. L. (1975) "A Reynolds Number Stress Model For Boundary Layer Transition With Application to Rough Surfaces," PSI TR-34, Physical Sciences, Inc., Wakefield, MA.

Gaster, M. (1974) "On the Effects of Boundary-Layer Growth on Flow Stability," J. Fluid Mech., 66, 465.

Grabowski, W. J. and Merkle, C. L. (1975) "Nonparallel Stability of Axisymmetric Stagnation Point Boundary-Layer Flow," Flow Research Note No. 86.

Hall, J. R., Speegle, K. C., and Piland, R. O. (1957) "Preliminary Results From Free-Flight Investigations of Boundary Layer Transition and Heat Transfer on a Highly Polished Hemisphere-Cylinder in Free-Flight," NACA RM L57D18c.

Mack, L. M. (1969) "Boundary Layer Stability Theory," Report 900-277, Rev. A, Jet Propulsion Laboratory, Pasadena, CA.

Mack, L. M. (1975) "On the Application of Linear Stability Theory to the Problem of Supersonic Boundary Layer Transistion," AIAA J., 13, no. 3, 278.

Merkle, C. L., Grabowski, W. J., Kubota, T., and Ko, D. R. S. (1975) "Analysis of Nosetip Boundary Layer Transition Mechanisms," AFOSR-TR-75-1462; see also Flow Research Report No. 60.

Merkle, C. L., Ko, D. R. S., and Kubota, T. (1974) "The Effect of Axisymmetric Geometry on Boundary Layer Transition As Predicted by Linear Stability Theory," AFOSR-TR-75-0192; see also, Flow Research Report No. 39.

Merkle, C. L., Kubota, T., and Ko, D. R. S. (1974) "An Analytical Study of the Effects of Surface Roughness on Boundary Layer Transition," AFOSR-TR-75-0190; see also, Flow Research Report No. 40.

Morkovin, M. V. (1969) "Critical Evaluation of Transition From Laminar to Turbulent Shear Layers With Emphasis on Hypersonically Traveling Bodies," AFFDL-TR-68-149, Wright-Patterson Air Force Base, OH.

Price, J. M. and Harris, J. E. (1972) "Computer Program For Solving Compressible Nonsimilar-Boundary-Layer Equations For Laminar, Transitional, or Turbulent Flows of a Perfect Gas," NASA TM X-2458, NASA, Langley Research Center, Hampton, VA.

Powars, C. A. (1973) "Analysis of PANT Series A Rough Wall Calorimeter Data, Part I: Surface Roughness Effects on Heat Transfer," Report 73-80, Aerotherm Corp., Mountain View, CA.

Saric, W. S. and Nayfeh, A. H. (1975) "Non-Parallel Stability of Boundary Layer Flows," Phys. Fluids, 18, 945.

VanDriest, E. R. and McCauley, W. D. (1960) "The Effect of Controlled Three-Dimensional Roughness on Boundary-Layer Transition at Supersonic Speeds," J. Aero. Sciences, 28, 261.

Wazzan, A. R., Okamura, T. T., and Smith, A. M. O. (1968) "Spatial and Temporal Stability Charts For the Falkner-Skan Boundary Layer Profile," Report No. DAC-67-086, Douglas Aircraft Company, Long Beach, CA.

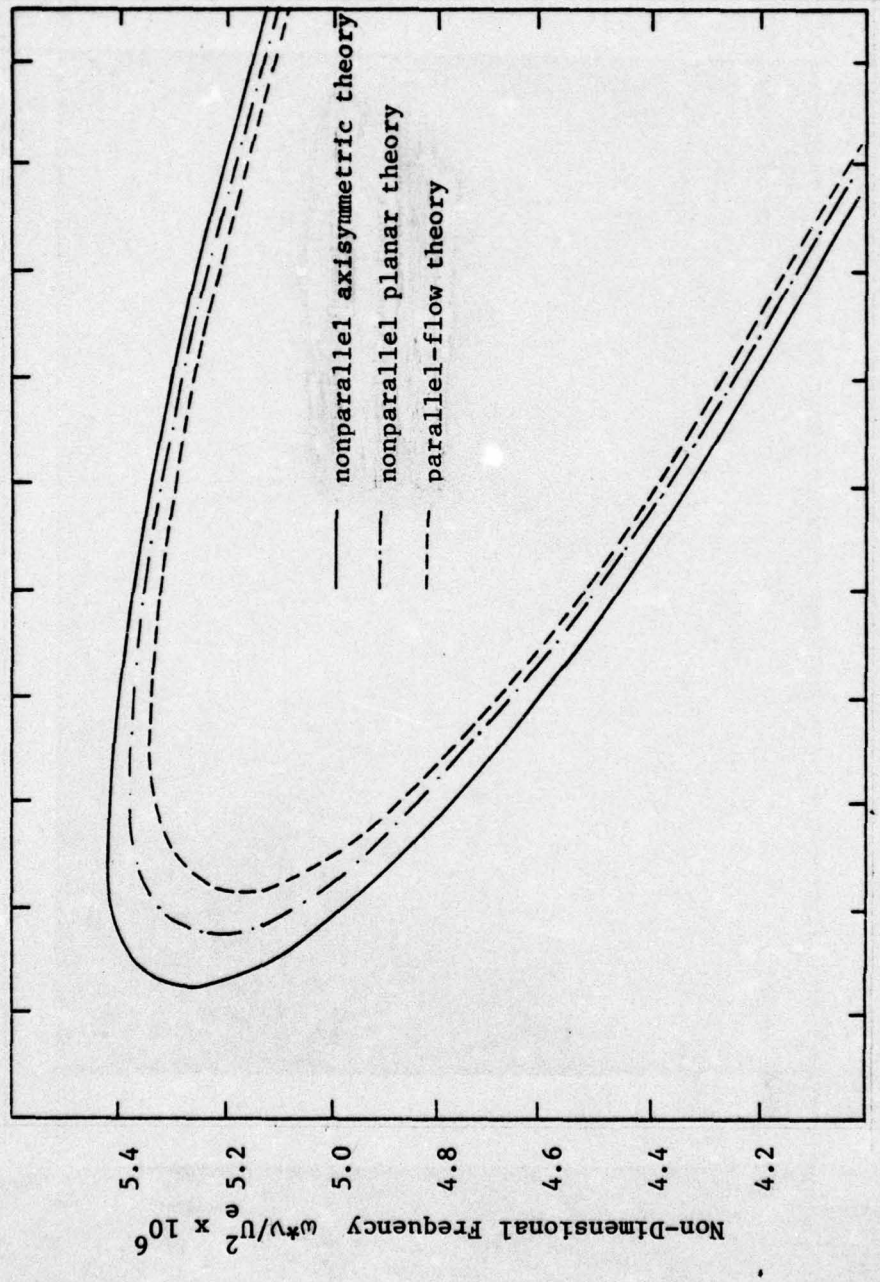


Figure 1 Effects of Axisymmetric Nonparallel Flow Terms on the Stability Characteristics of a Blunt-Body Boundary Layer

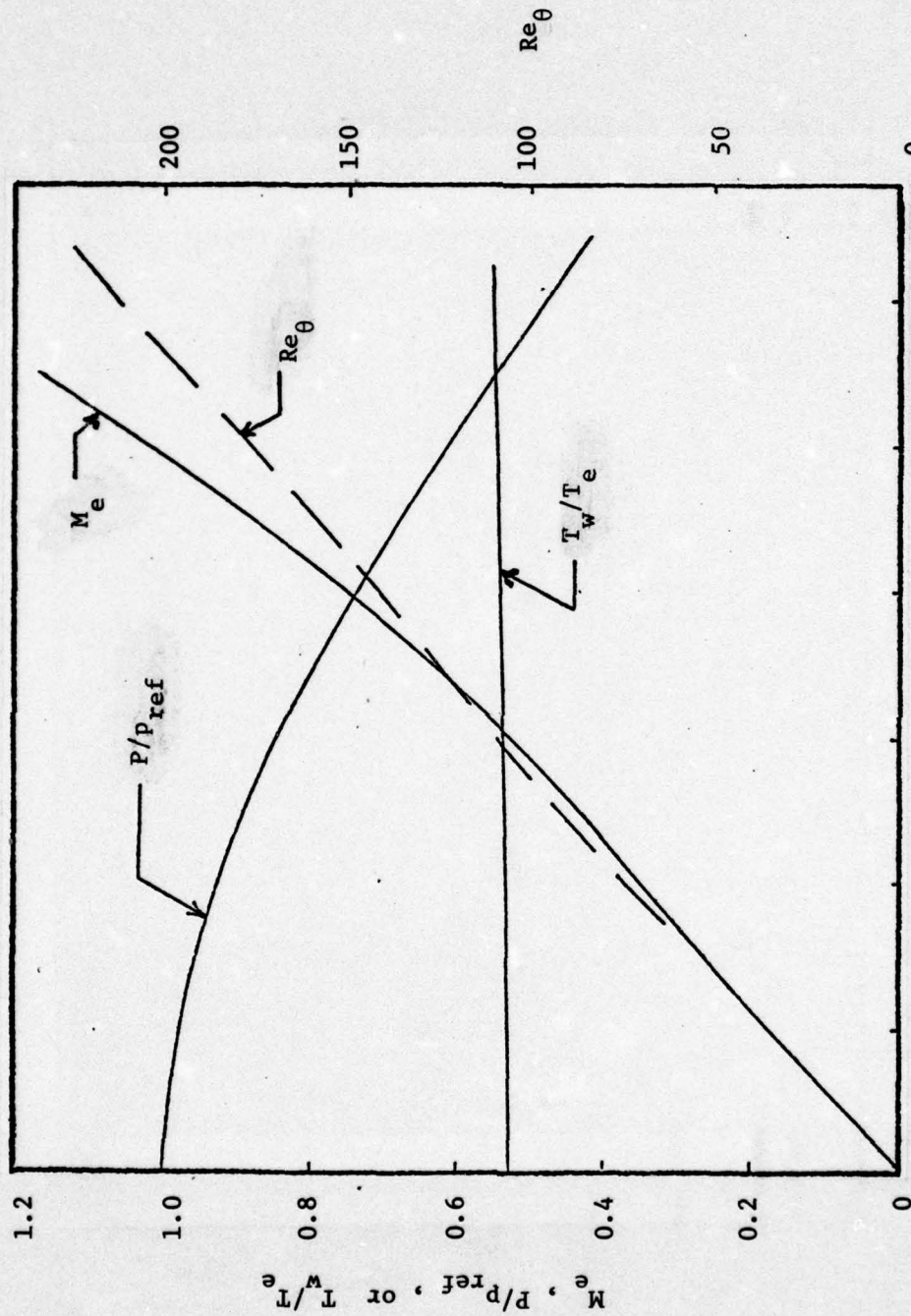


Figure 2 Nosetip Boundary-Layer Edge Conditions

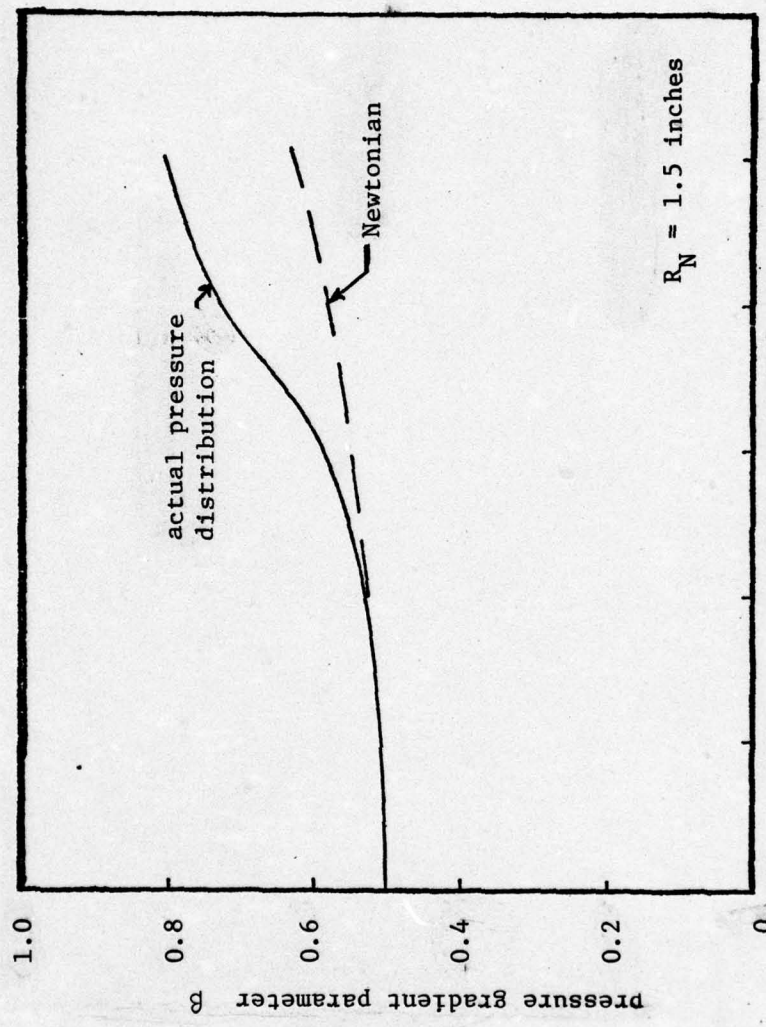


Figure 3 Variation of the Pressure Gradient Parameter on the Nosetip

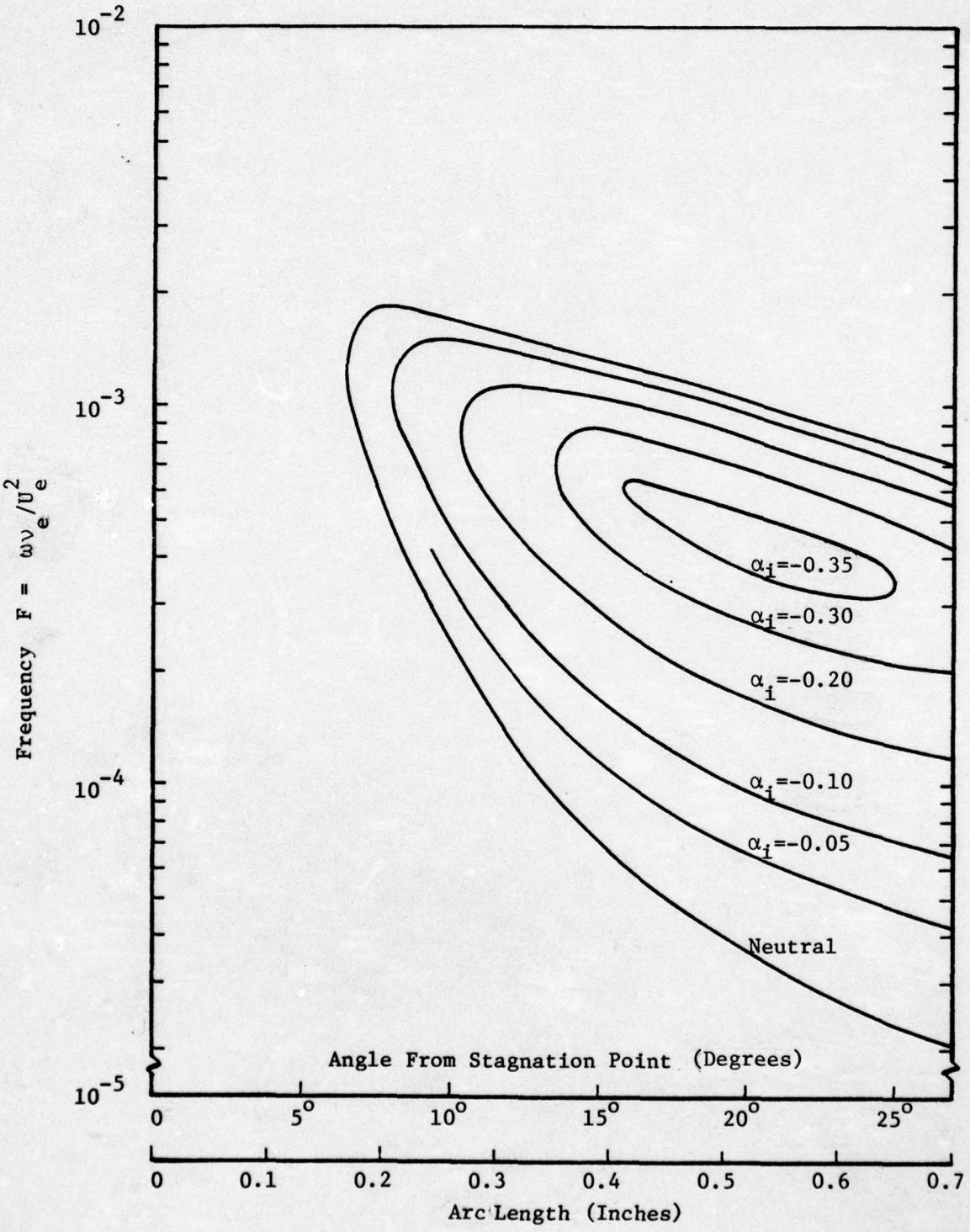


Figure 4 Stability Map for Nosetip Boundary Layer--Amplification Rate

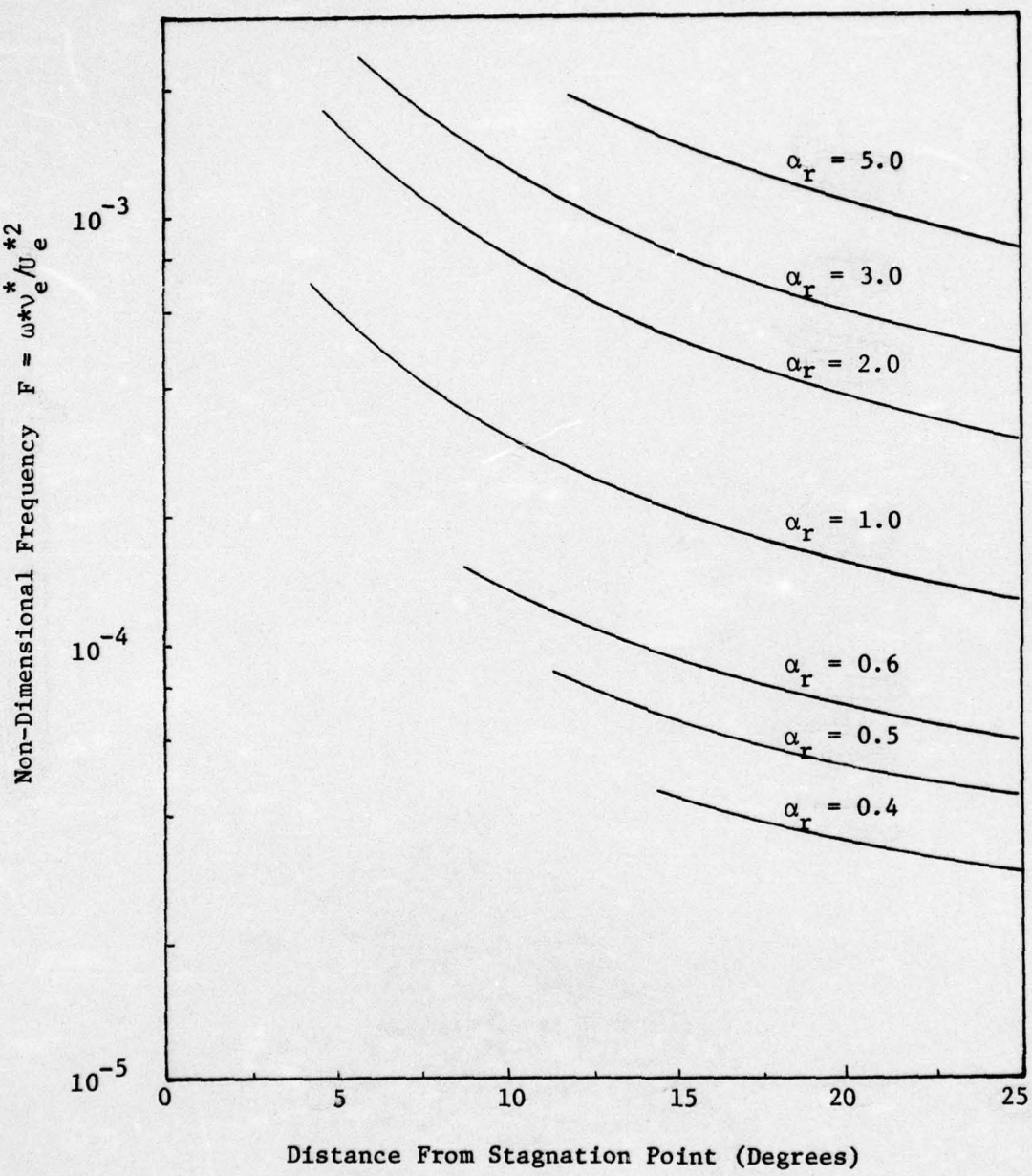


Figure 5 Stability Map For Nosetip Boundary--Wave Number

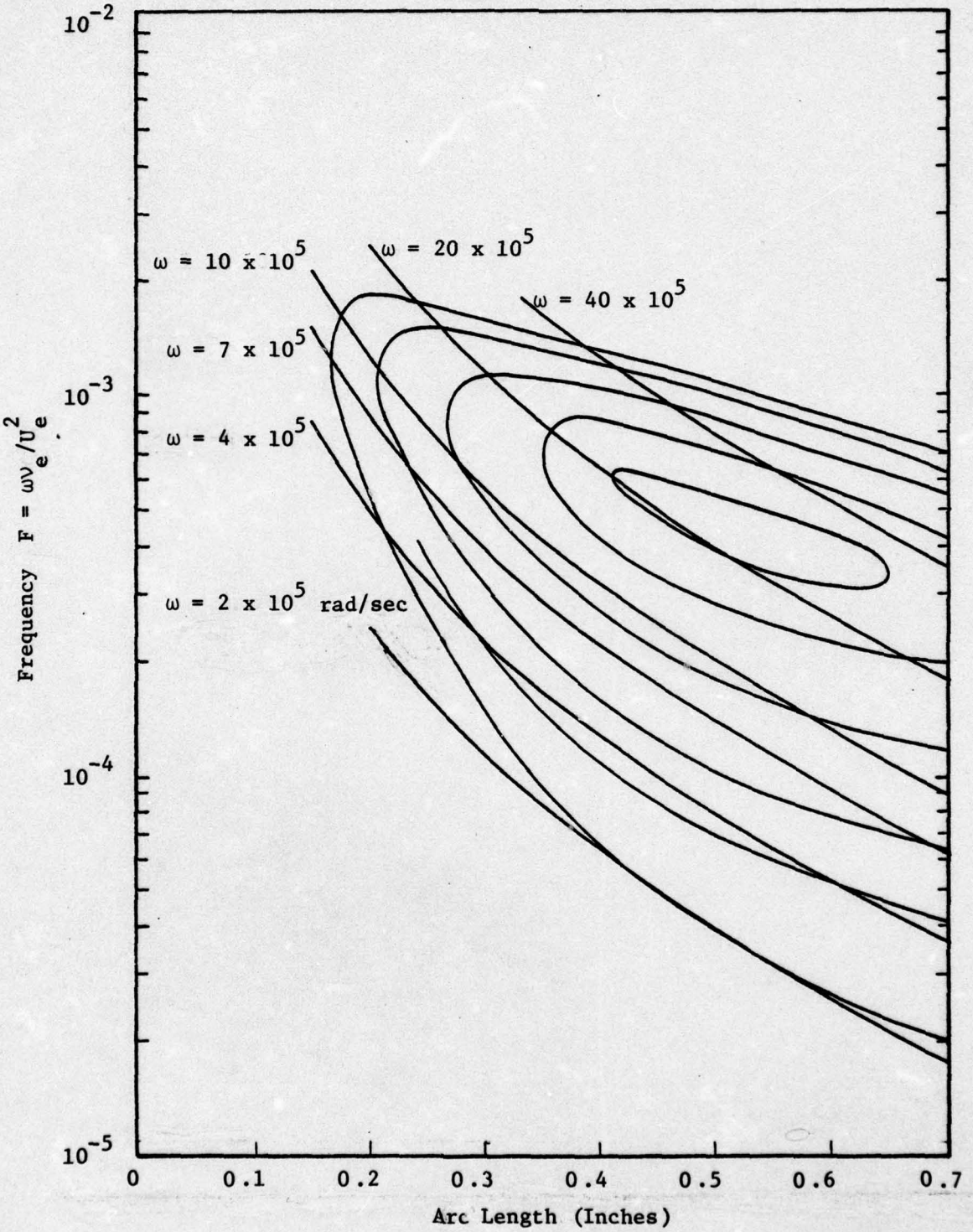


Figure 6 Stability Number Map For Nosetip Boundary Layer Showing Lines of Constant Physical Frequency

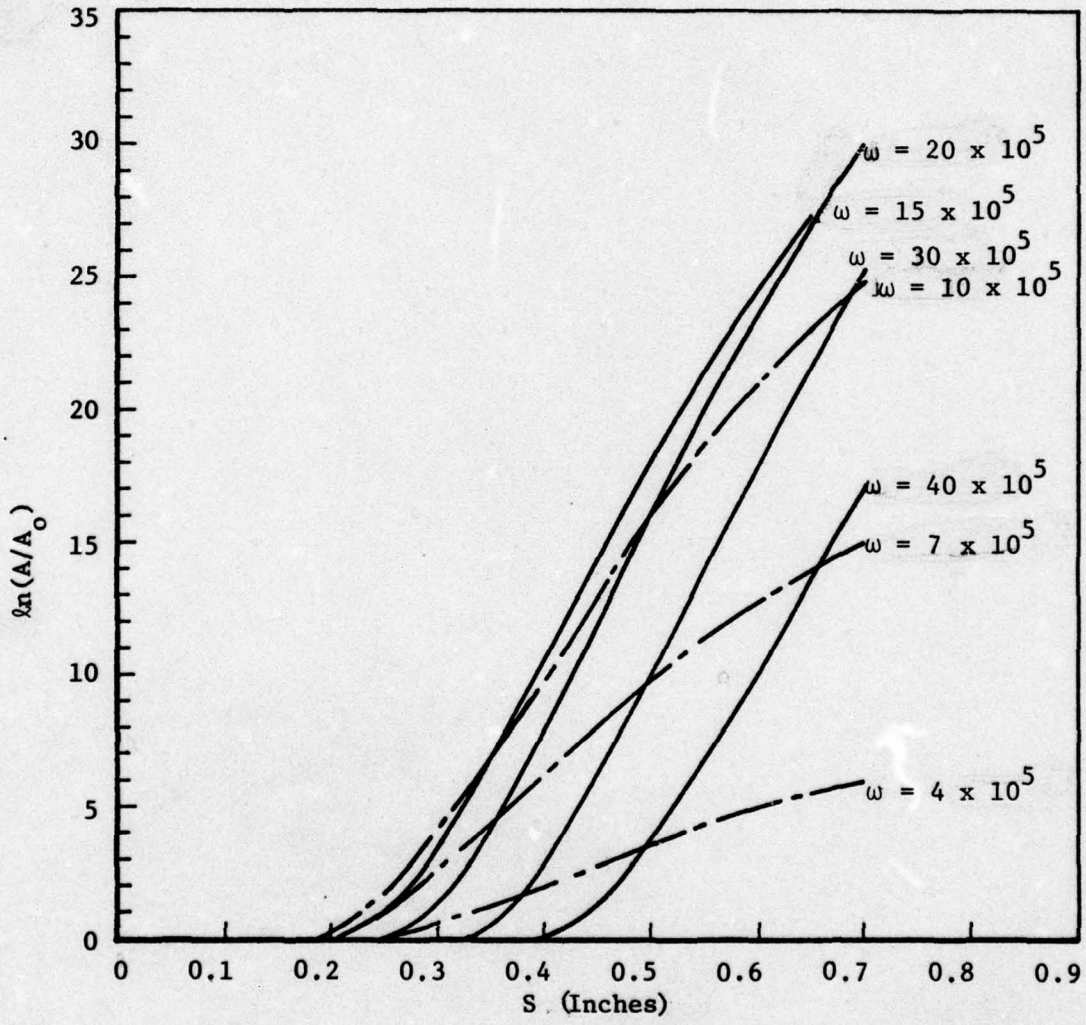


Figure 7 Growth of Disturbances in a Nosetip Boundary Layer

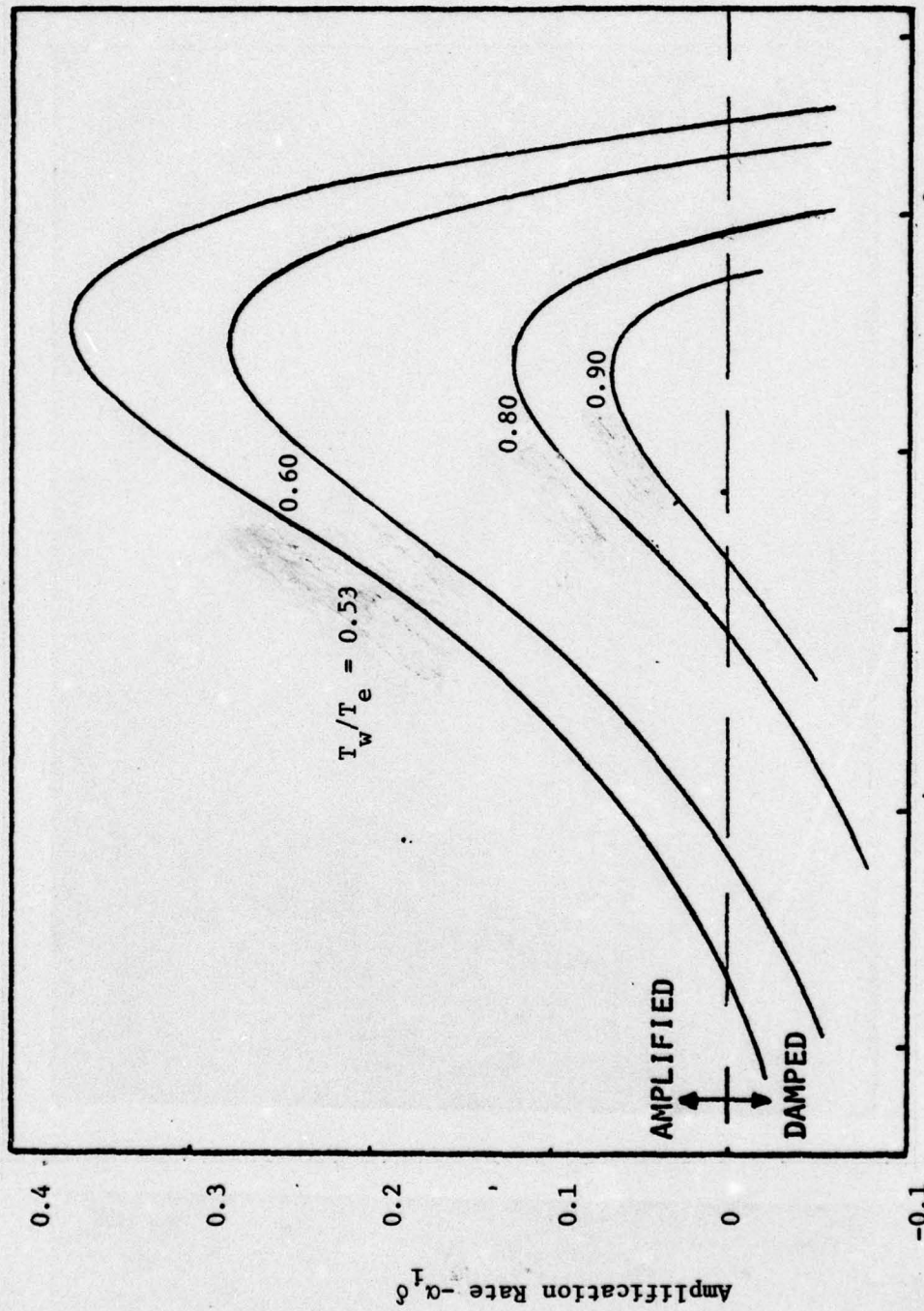


Figure 8 Effects of Wall Temperature on the Stability Characteristics of a Nosetip Boundary Layer

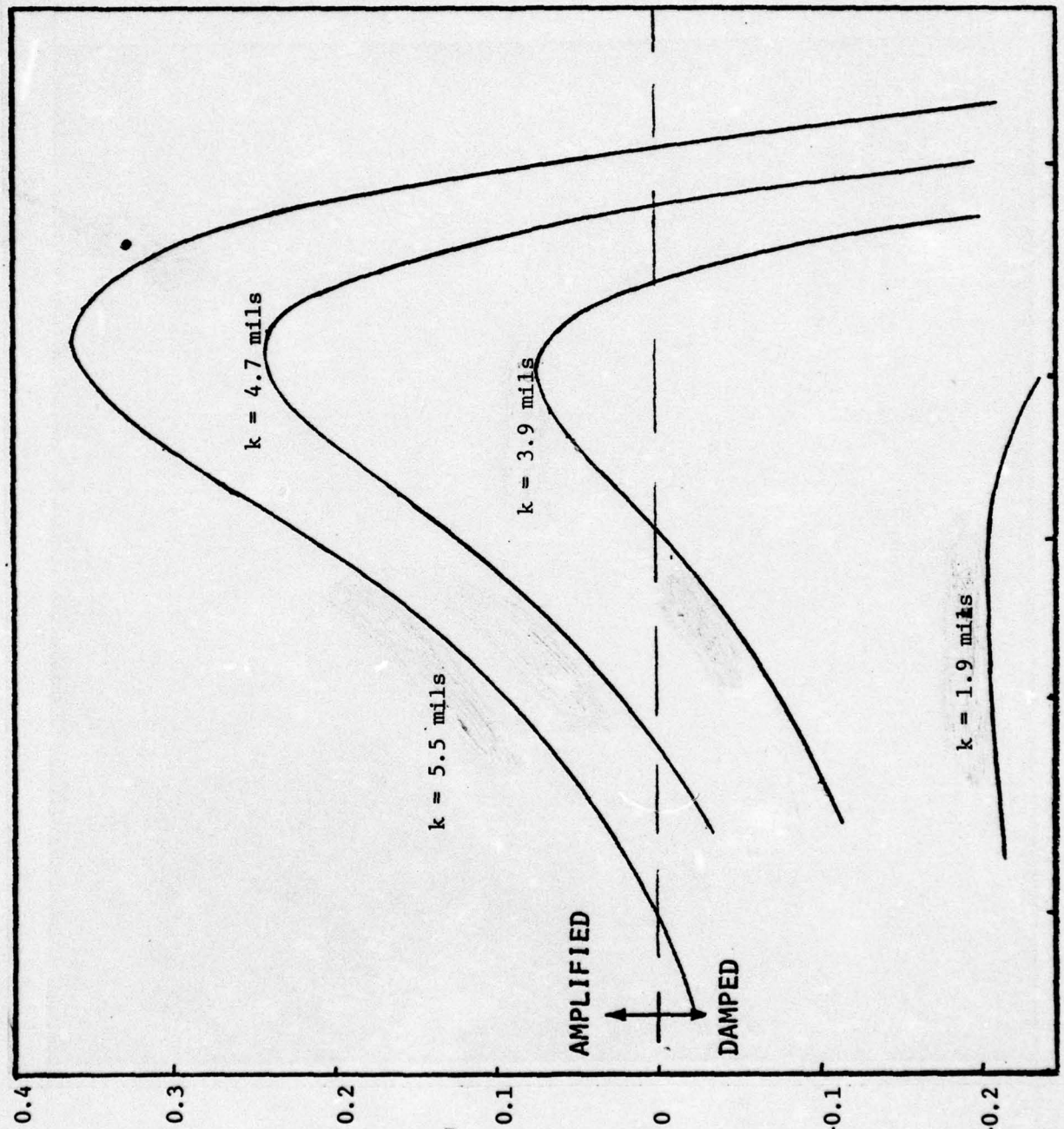


Figure 9 Effects of Roughness Height on the Stability Characteristics of a Nosetip Boundary Layer

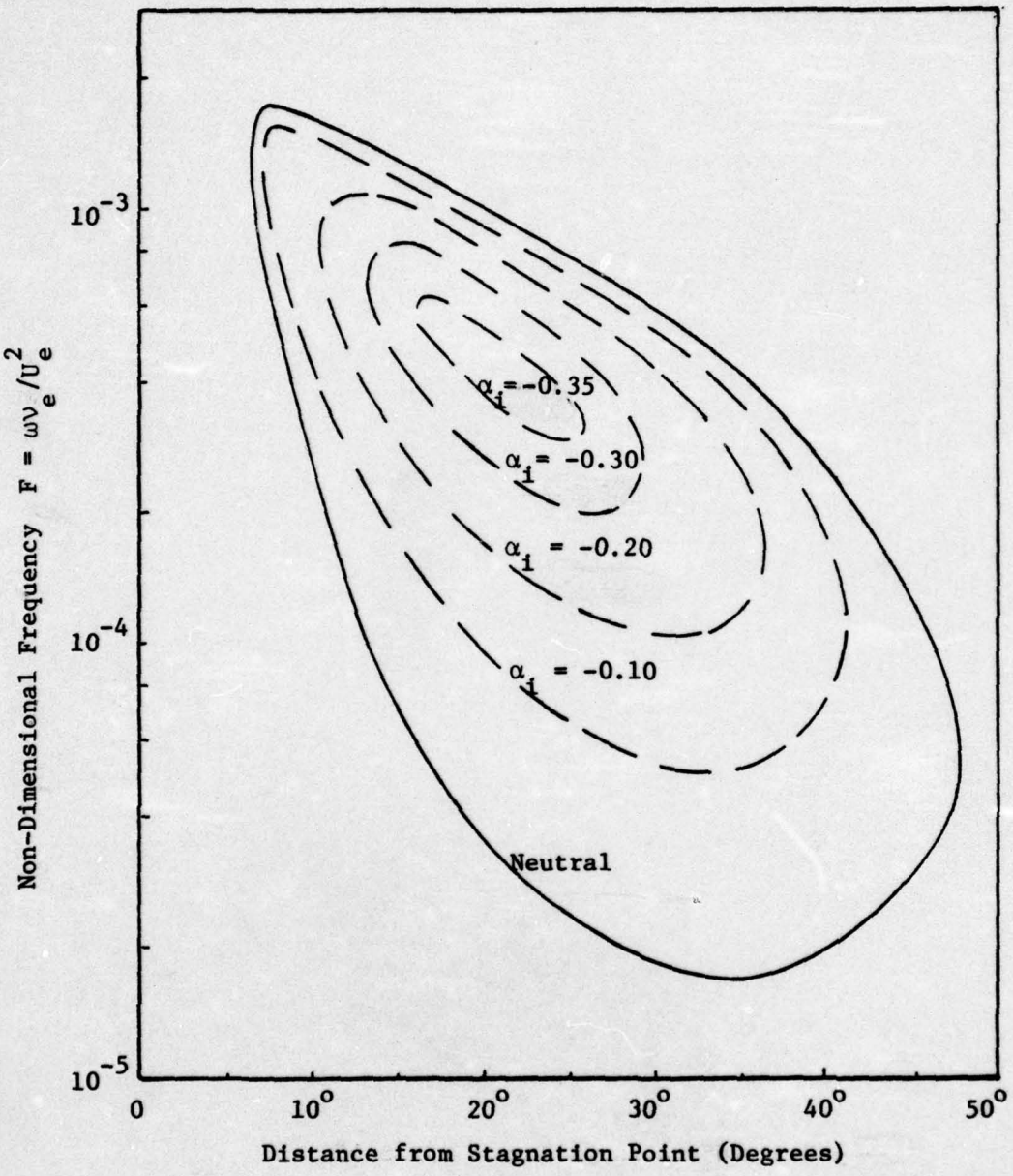


Figure 10 Stability Map For Nosetip Boundary Layer--Extended Region

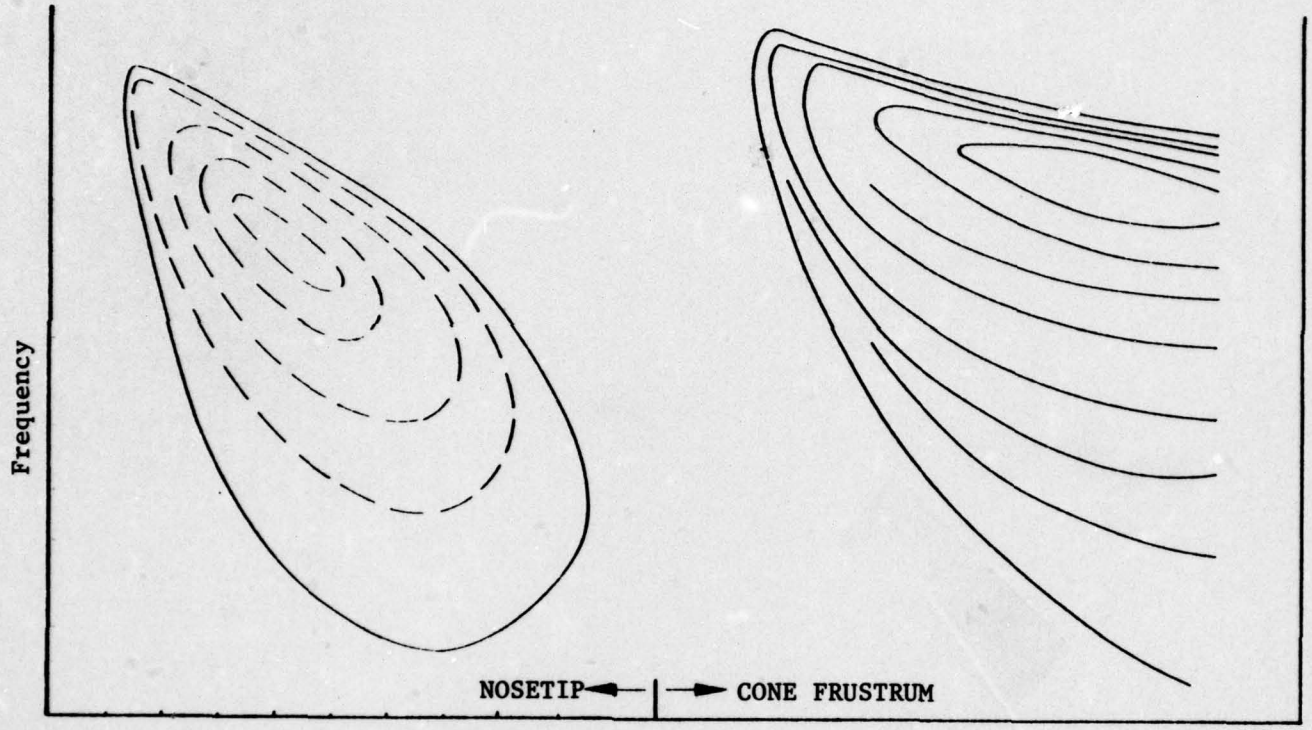


Figure 11 Anticipated Stability Characteristics of Reentry Vehicles

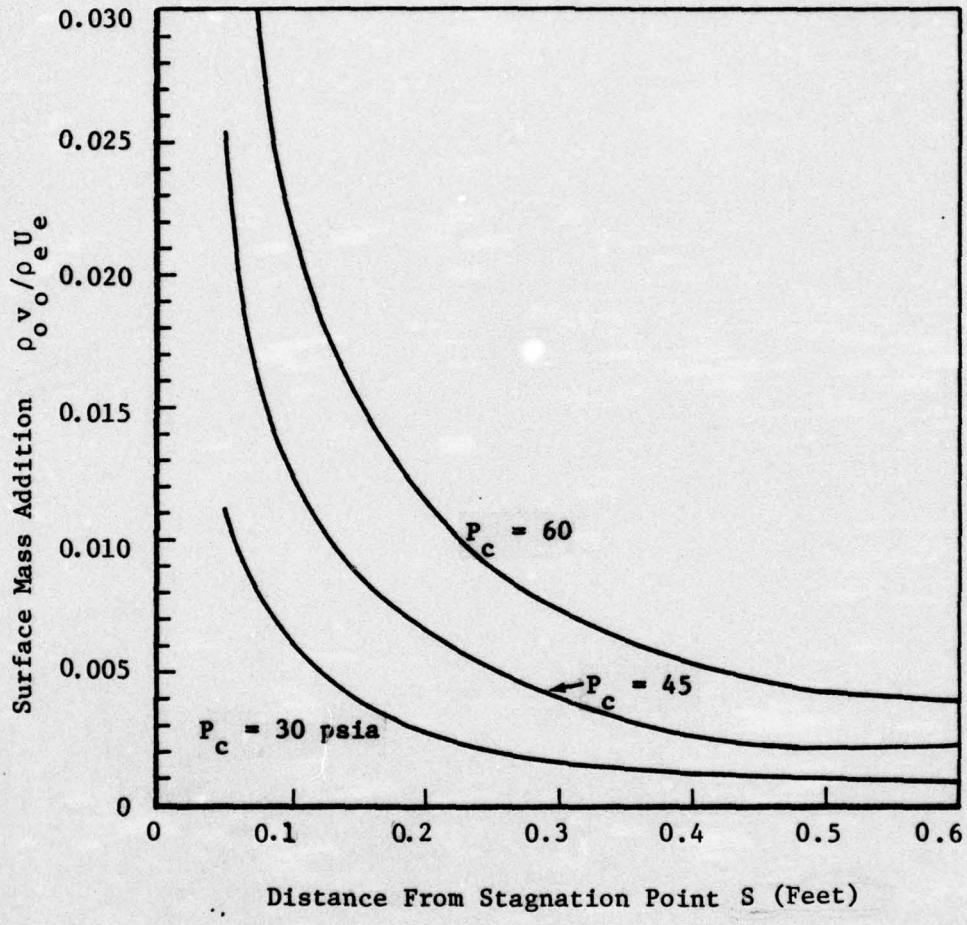


Figure 12 Non-Dimensional Mass Flux at the Wall

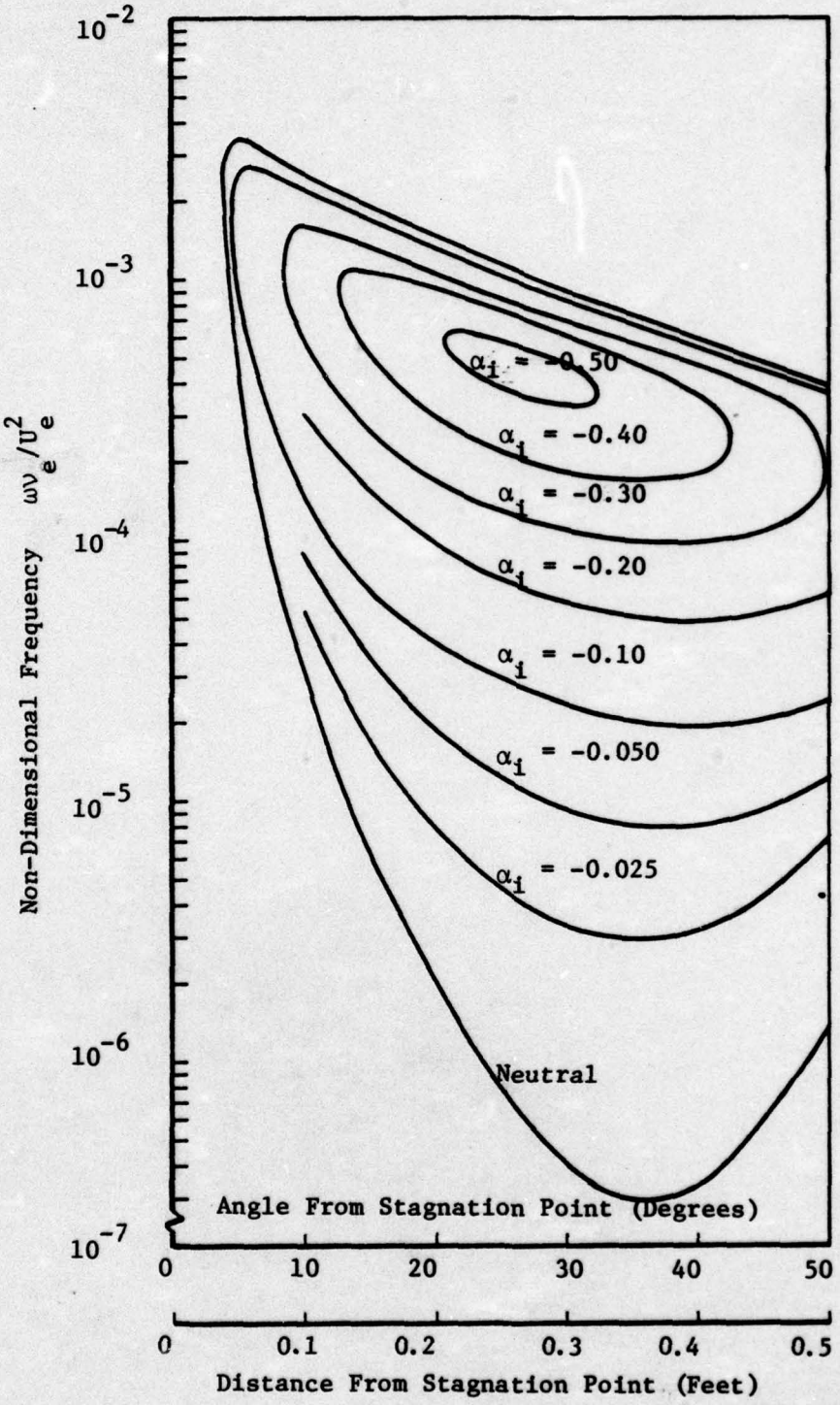


Figure 13 Stability Characteristics of a 7-Inch Sphere; T_w/T_e = 0.6 , k =5.0 mils , P_c = 30 psia -- Amplification Rates

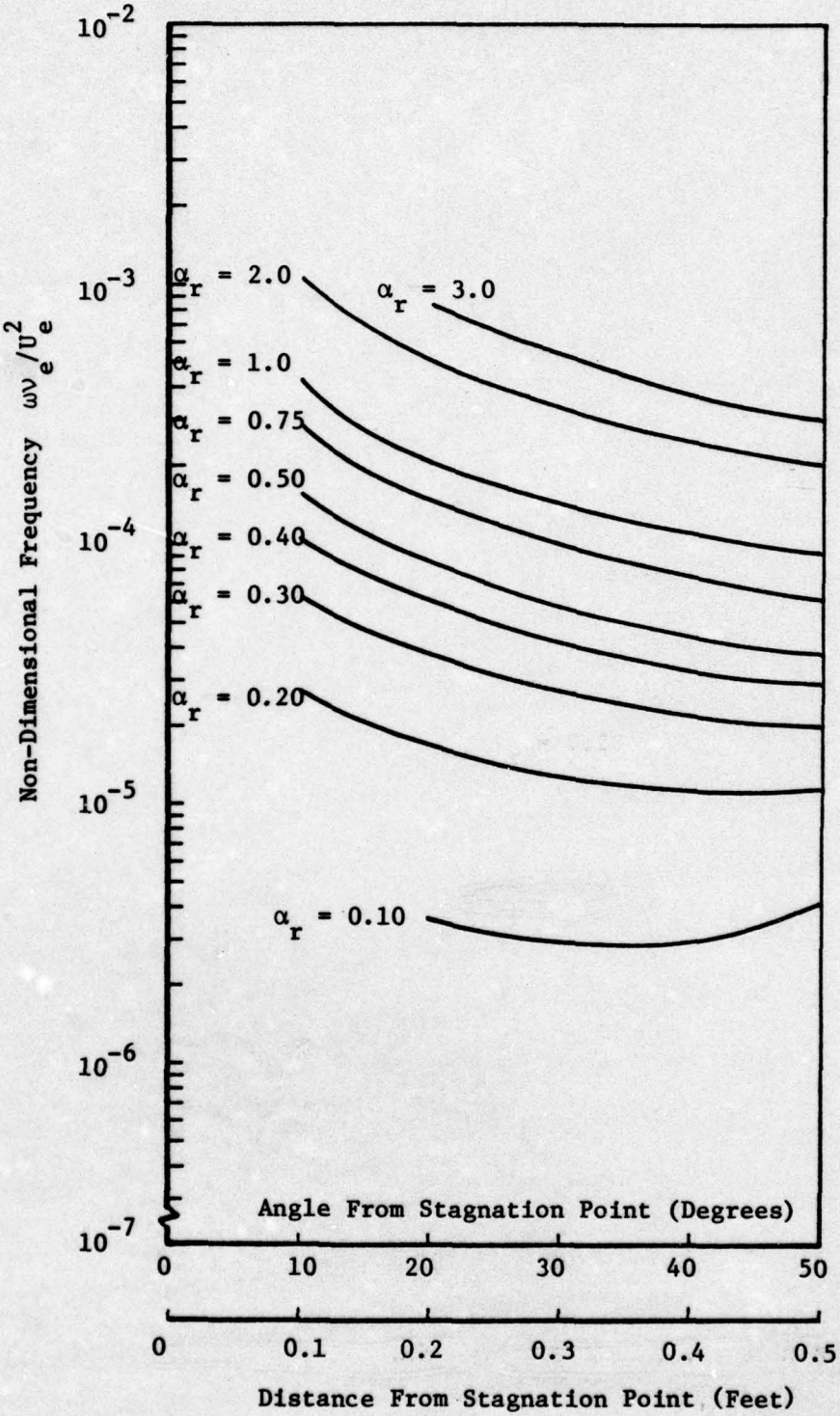


Figure 14 Stability Characteristics of a 7-Inch Sphere; T_w/T_e = 0.6 , k = 5.0 mils , P_c = 30 psia -- Wave Numbers

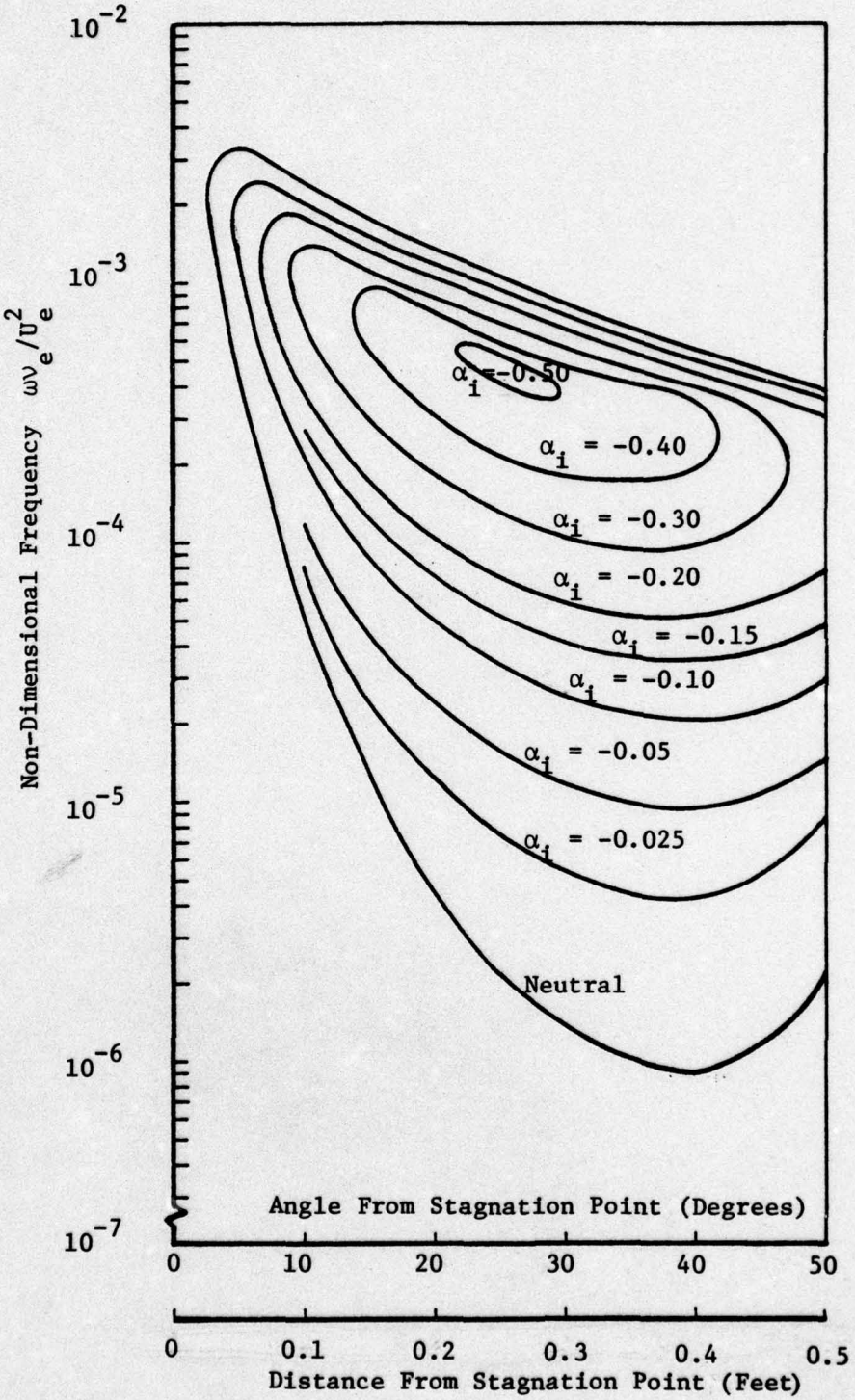


Figure 15 Stability Characteristics of a 7-Inch Sphere; T_w/T_e = 0.6 , k = 4.0 mils , P_c = 30 psia -- Amplification Rates

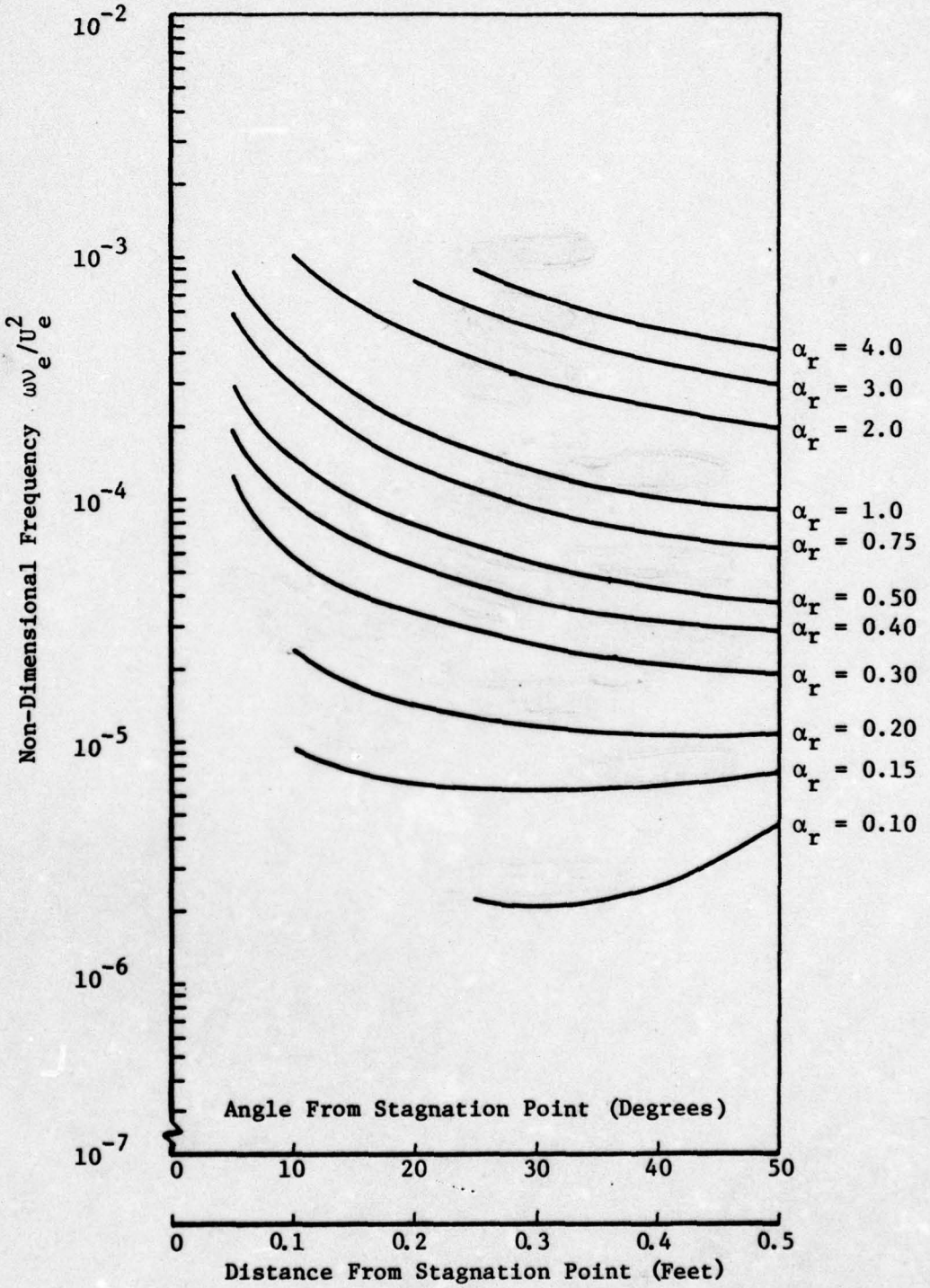


Figure 16 Stability Characteristics of a 7-Inch Sphere; T_w/T_e = 0.6 , k = 4.0 mils, P_c = 30 psia -- Wave Numbers

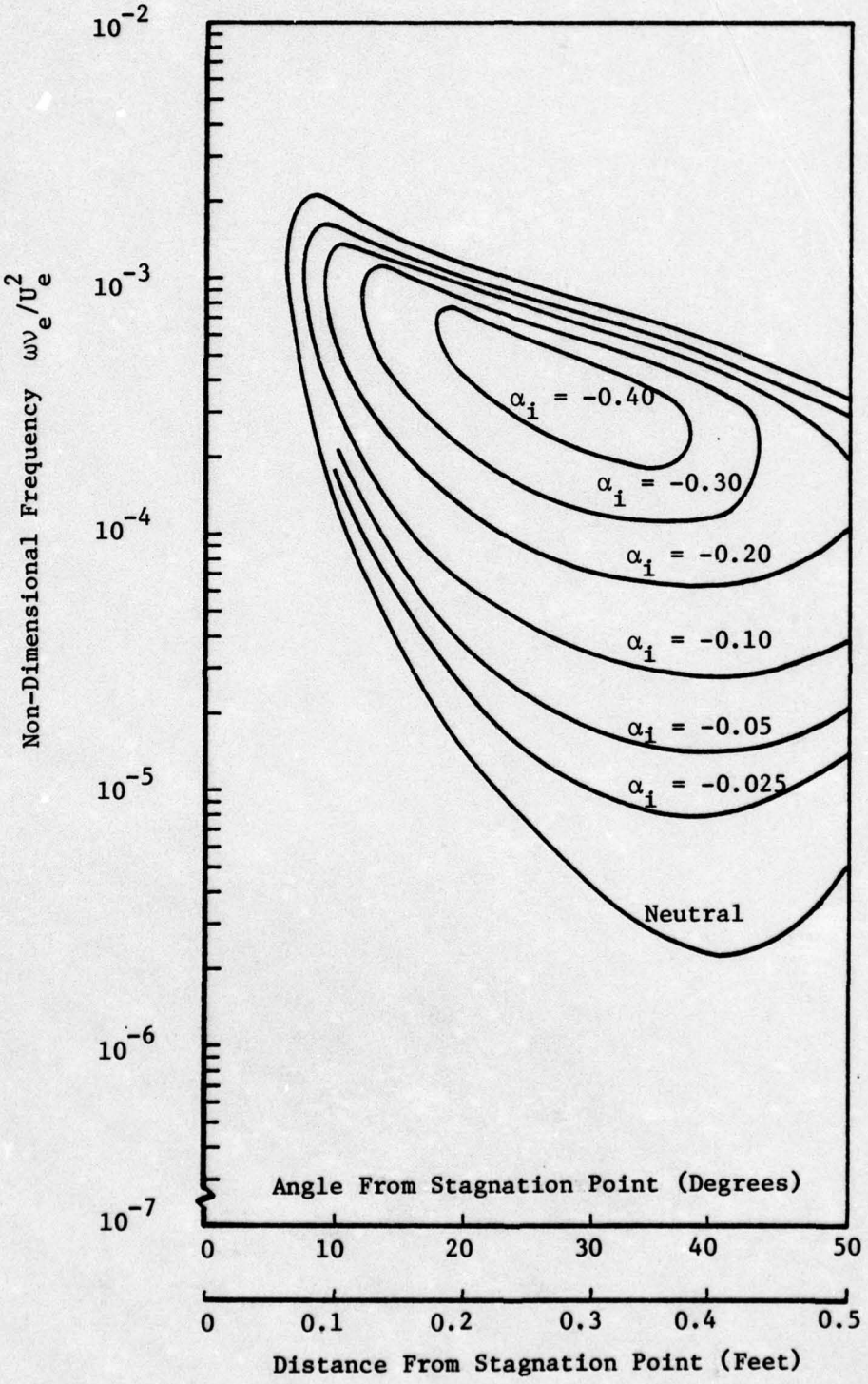


Figure 17 Stability Characteristics of a 7-Inch Sphere; T_w/T_e = 0.6 , k = 3.0 mils , P_c = 30 psia -- Amplification Rates

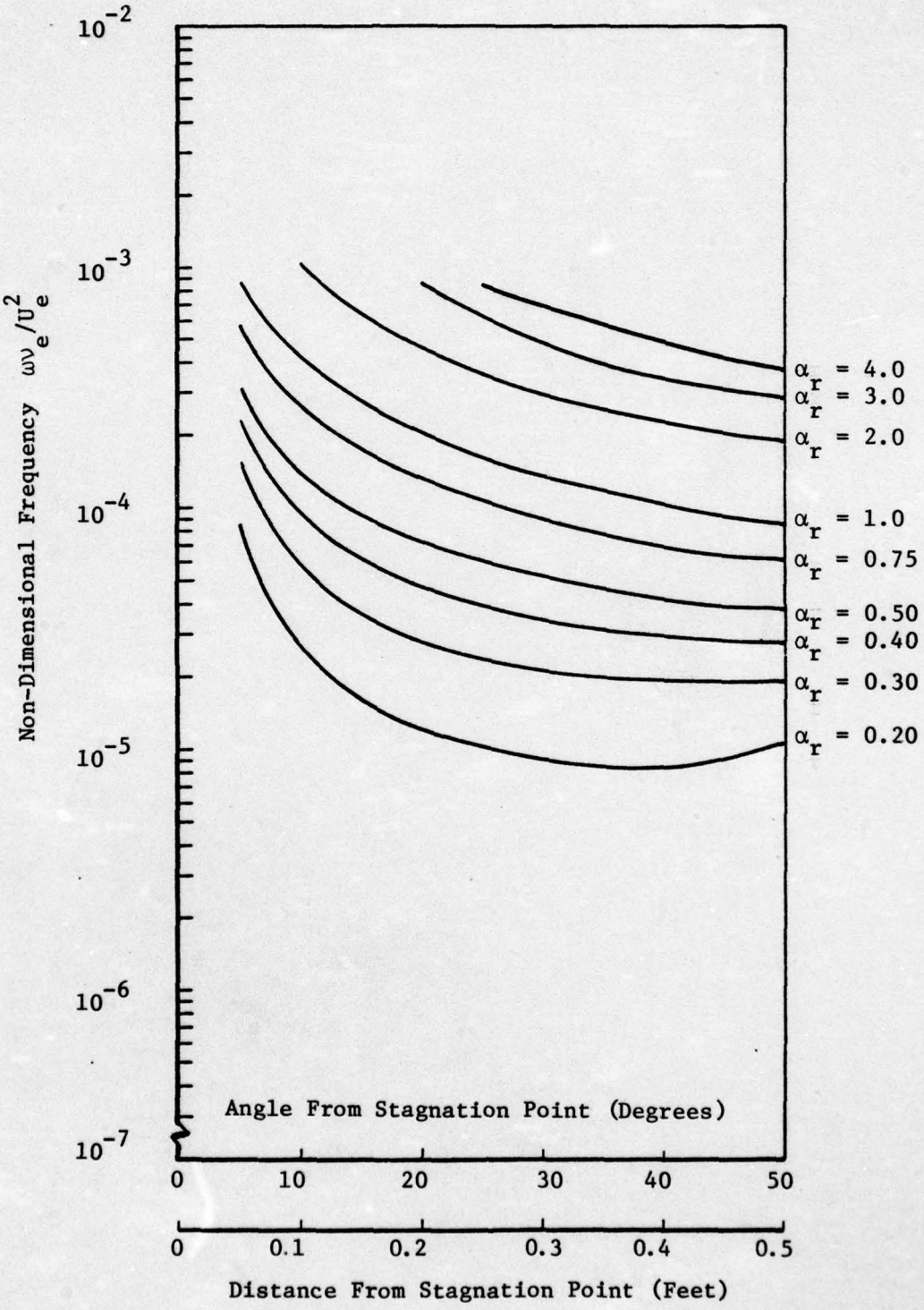


Figure 18 Stability Characteristics of a 7-Inch Sphere; T_w/T_e = 0.6 , k = 3.0 mils , P_c = 30 psia -- Wave Numbers

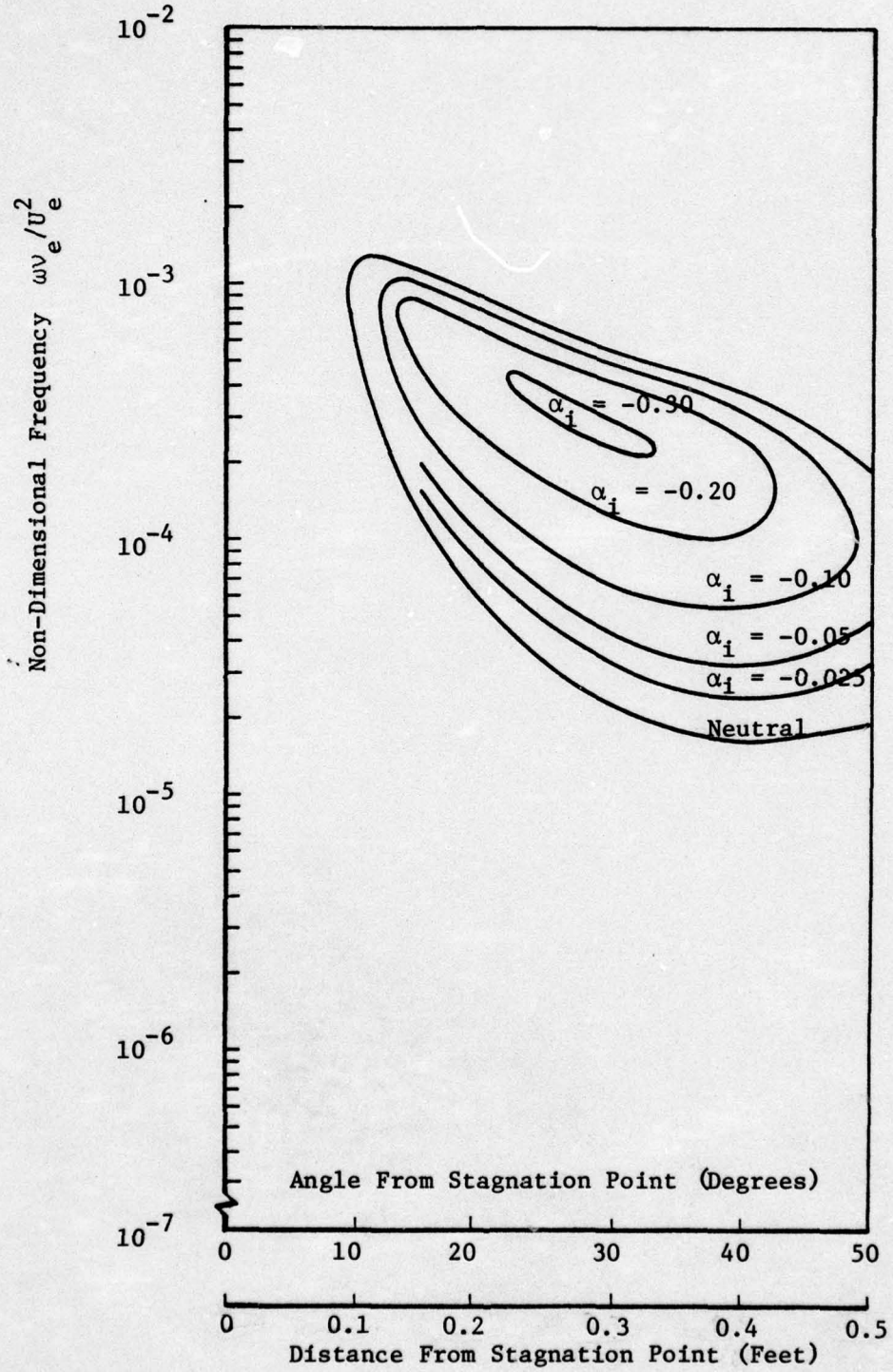


Figure 19 Stability Characteristics of a 7-Inch Sphere; T_w/T_e = 0.6 , k = 2.0 mils , P_c = 30 psia -- Amplification Rates

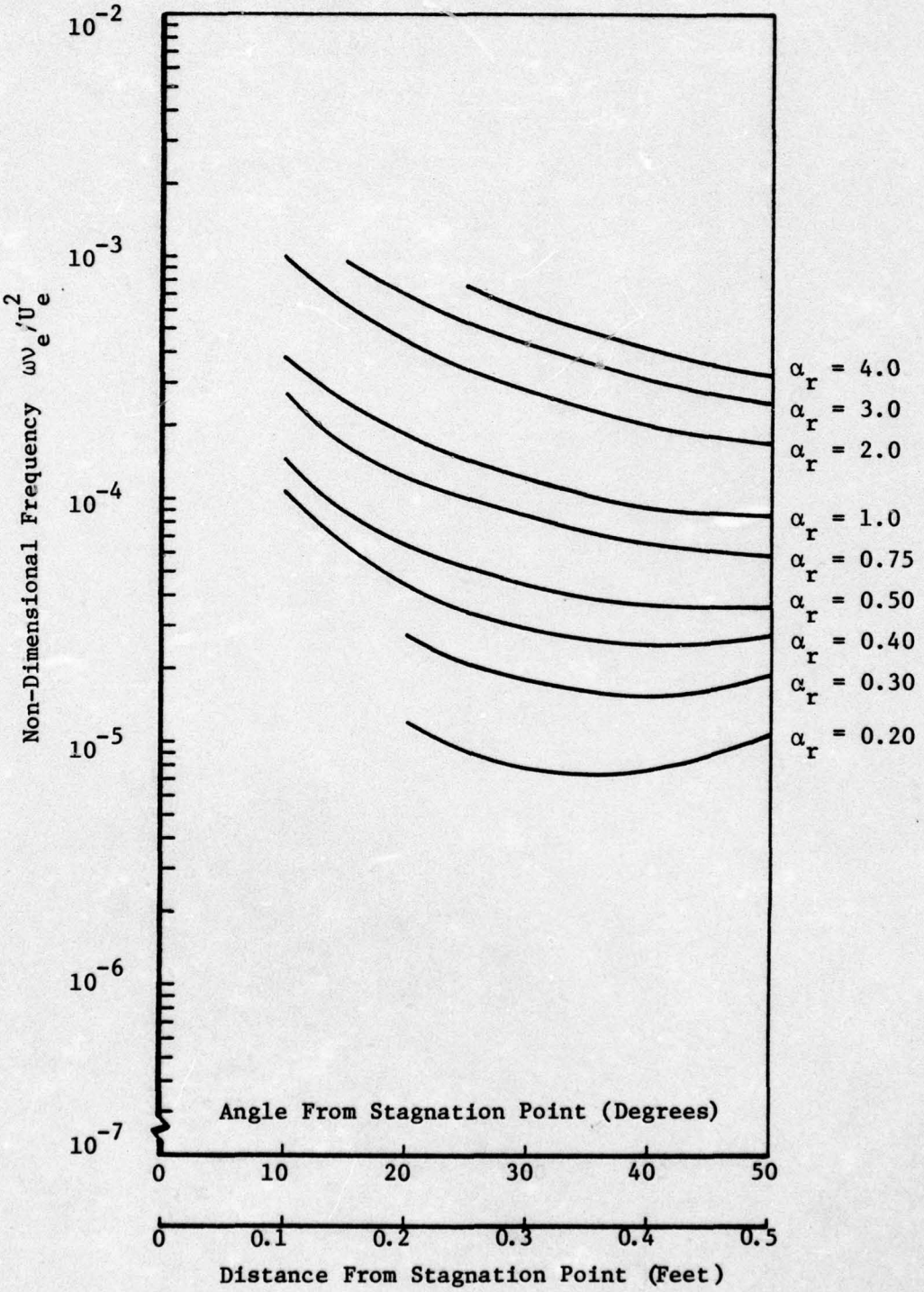


Figure 20 Stability Characteristics of a 7-Inch Sphere; T_w/T_e = 0.6 , k = 2.0 mils , P_c = 30 psia -- Wave Numbers

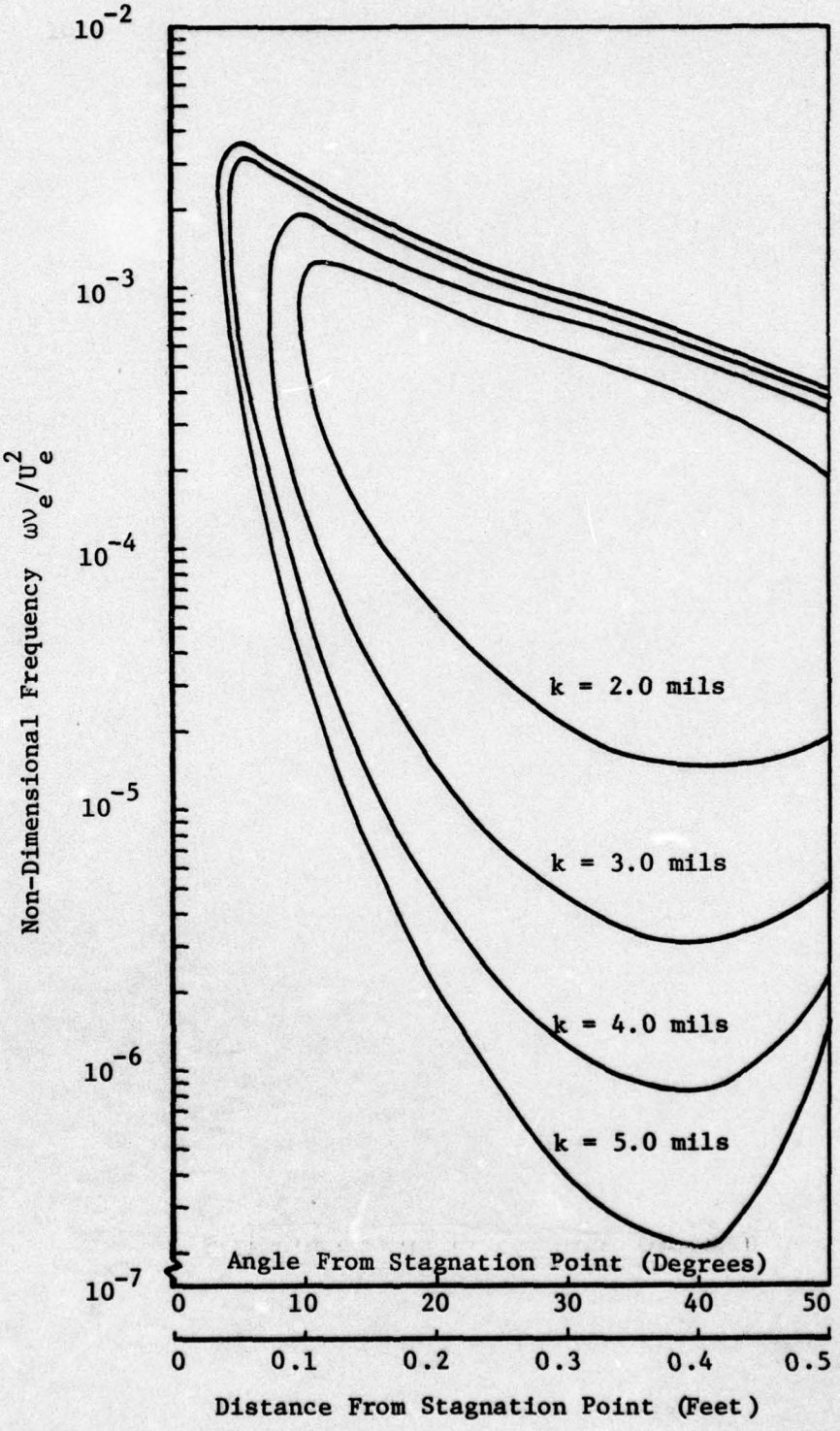


Figure 21 Stability Characteristics of a 7-Inch Sphere; Composite Results Showing Effects of Roughness on Neutral Stability Curves

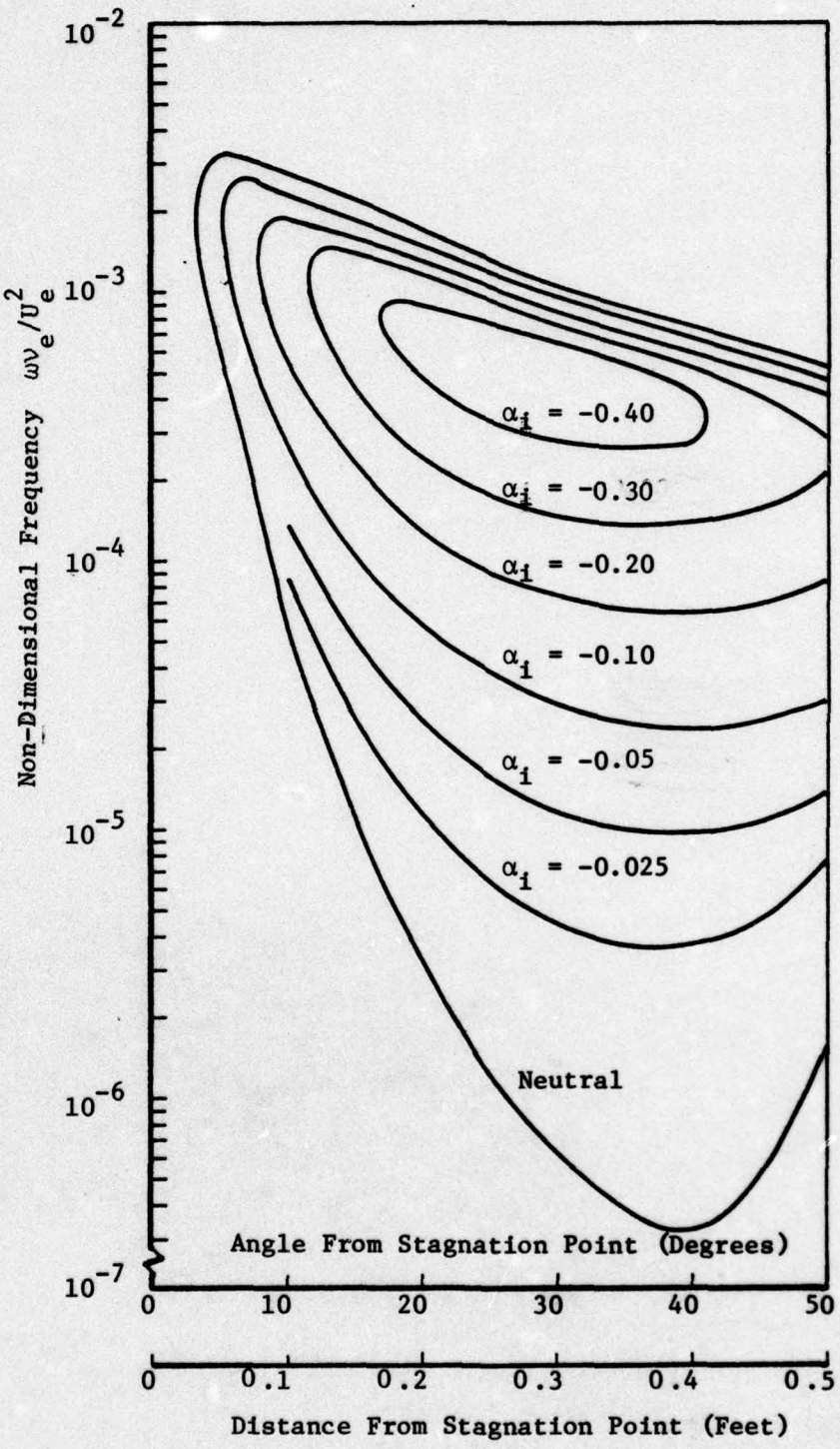


Figure 22 Stability Characteristics of a 7-Inch Sphere; T_w/T_e = 0.6 , k = 5.0 mils , No Surface Mass Addition--Amplification Rates

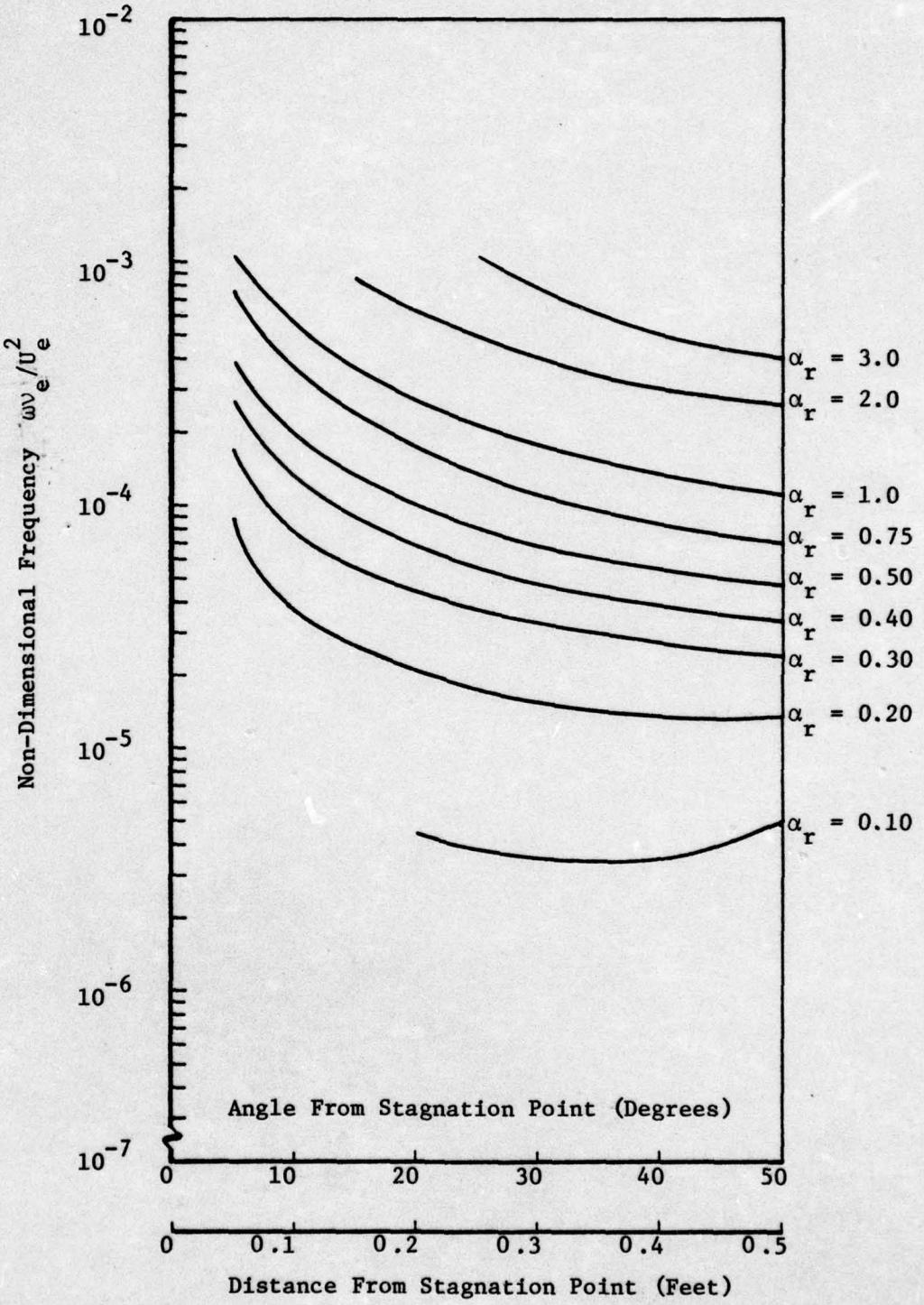


Figure 23 Stability Characteristics of a 7-Inch Sphere; T_w/T_e = 0.6 , k = 5.0 mils, No Surface Mass Addition--Wave Numbers

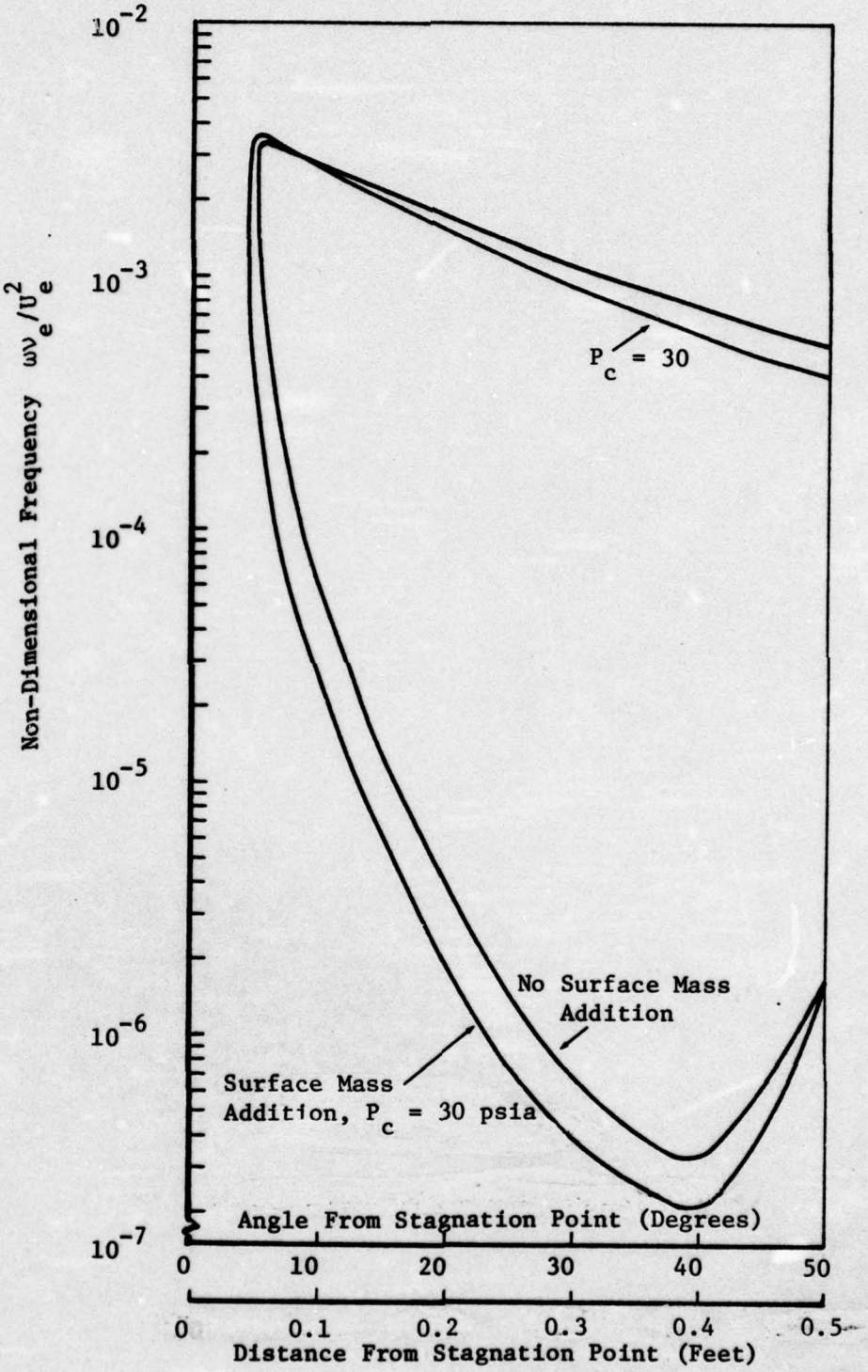


Figure 24 Stability Characteristics of a 7-Inch Sphere; Composite Results Showing Effect of Surface Mass Addition on Neutral Stability Curves in the Presence of Roughness

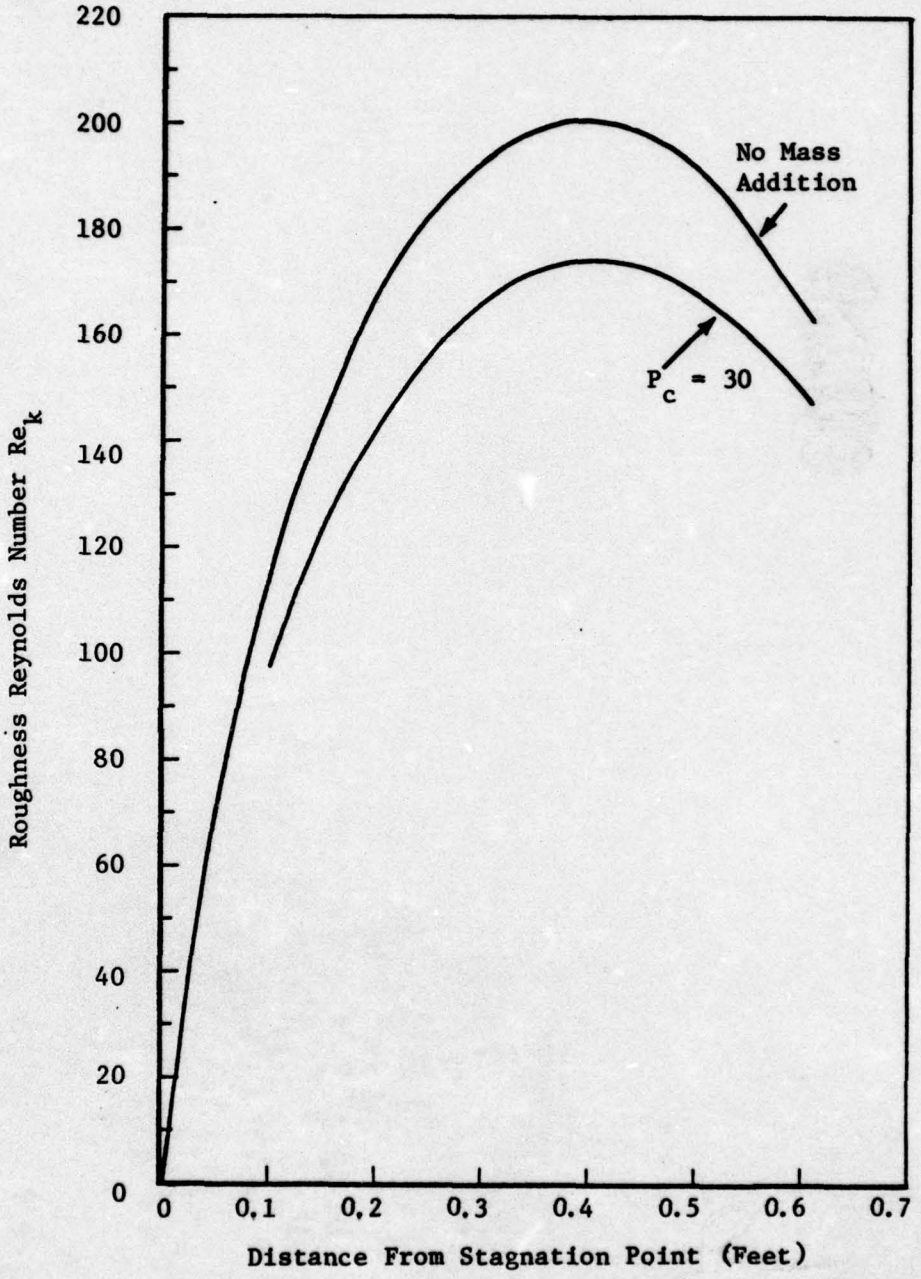


Figure 25 Roughness Reynolds Number of a 7-Inch Sphere in the Presence of and in the Absence of Surface Mass Addition; k = 5.0 mils, T_w/T_e = 0.6

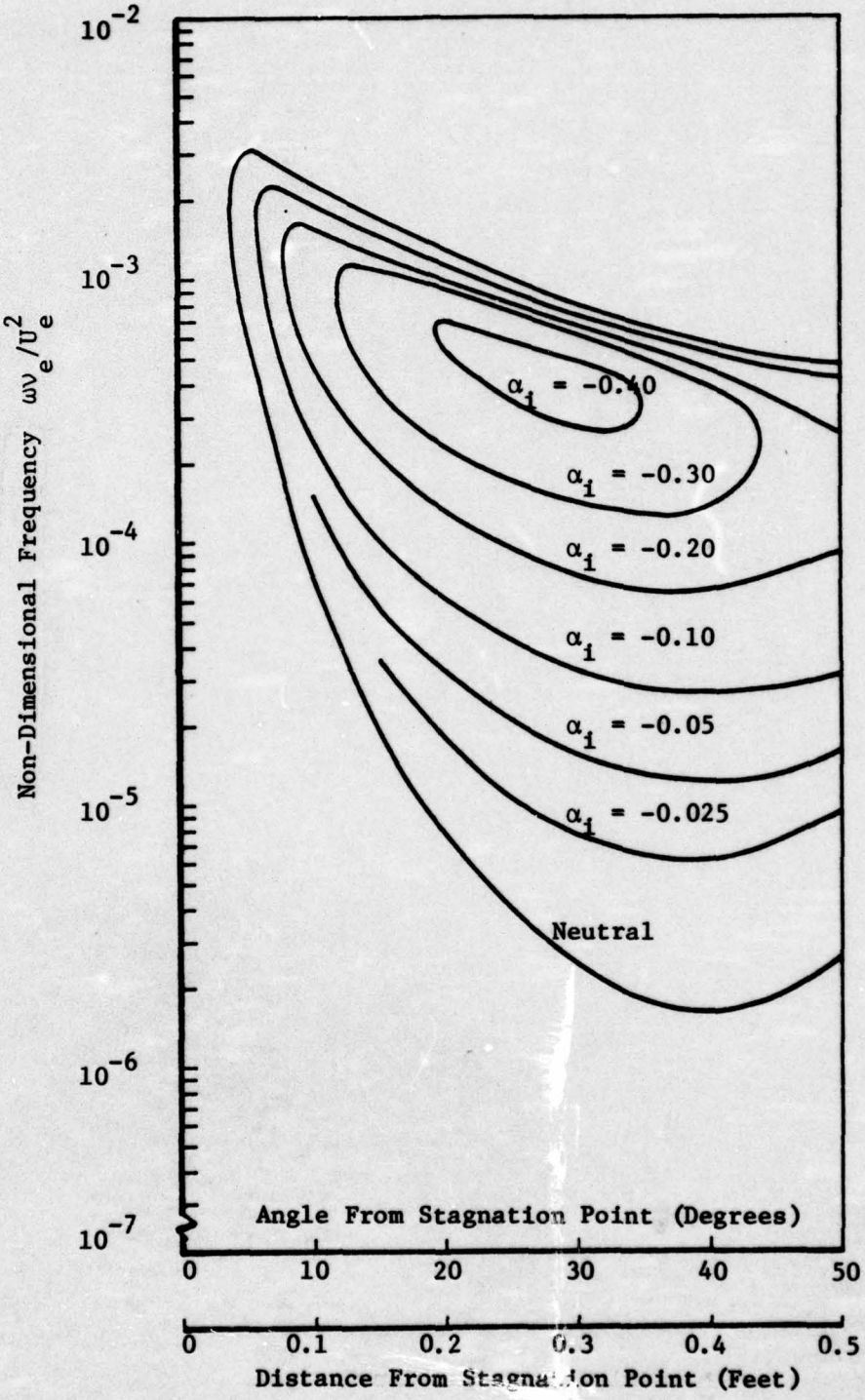


Figure 26 Stability Characteristics of a 7-Inch Sphere; T_w/T_e = 0.8 , k = 5.0 mils , P_c = 30 psia -- Amplification Rates

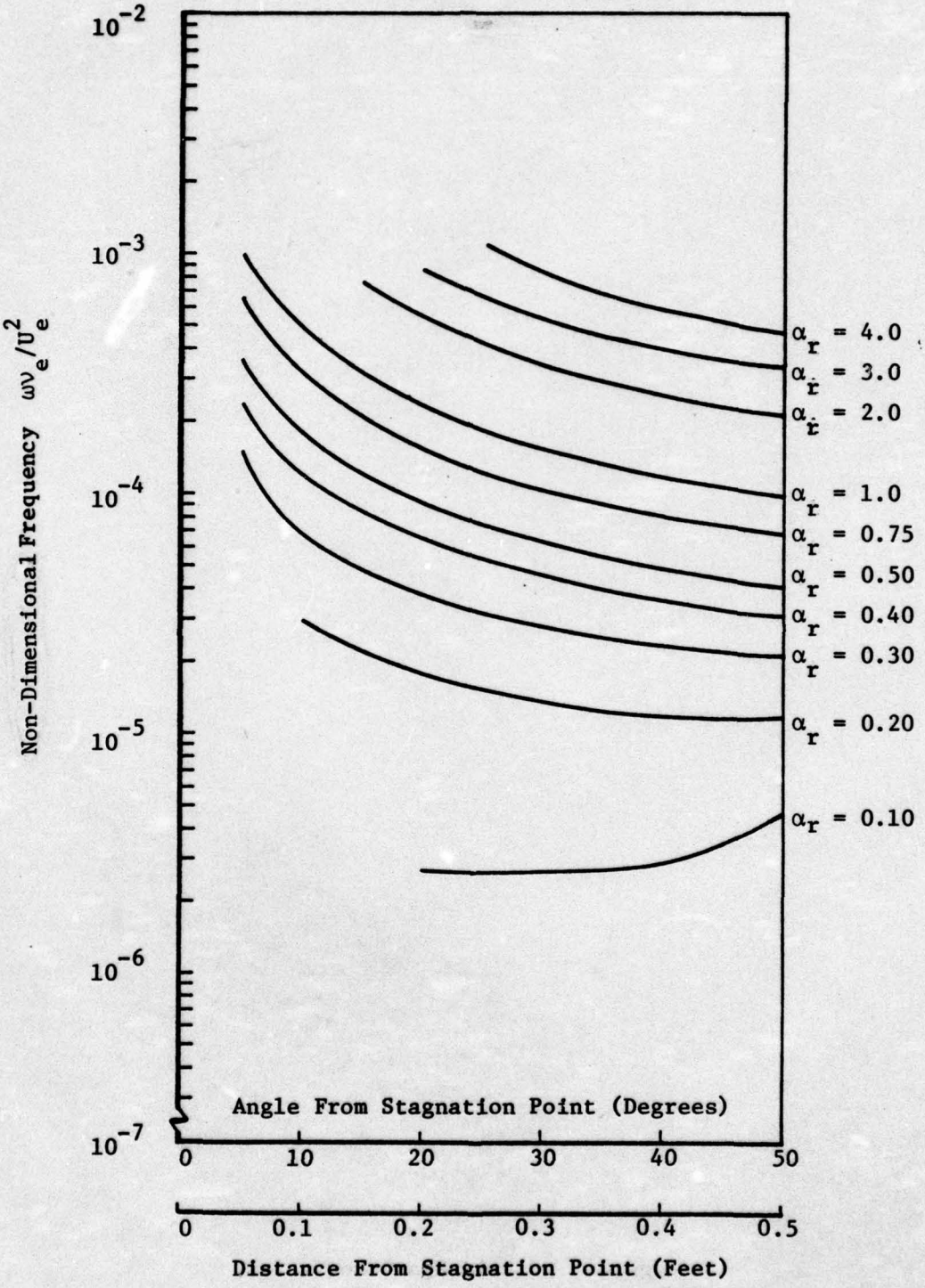


Figure 27 Stability Characteristics of a 7-Inch Sphere; T_w/T_e = 0.8 , k = 5.0 mils , P_c = 30 psia -- Wave Numbers

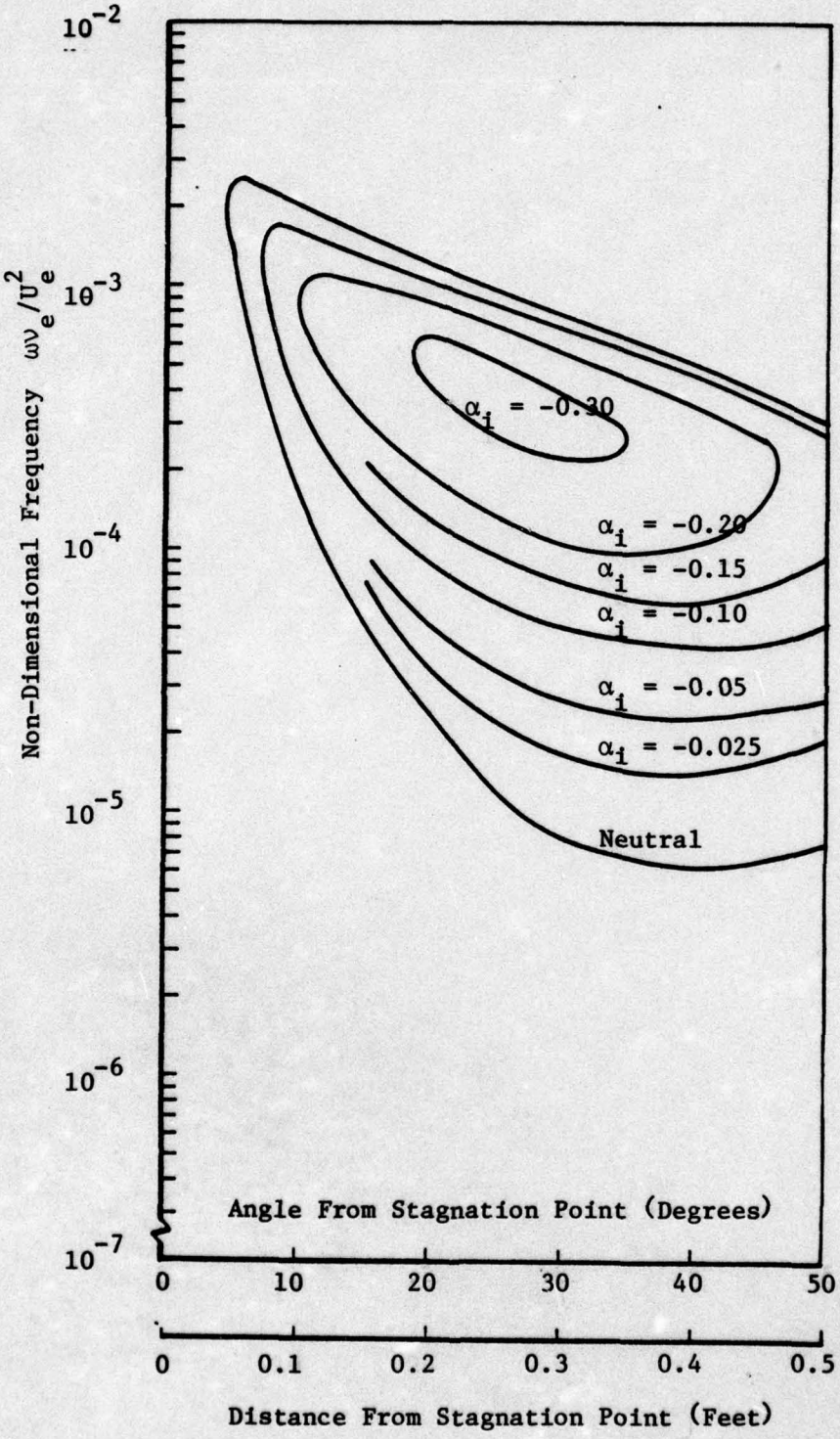


Figure 28 Stability Characteristics of a 7-Inch Sphere; T_w/T_e = 1.0 , k = 5.0 mils , P_c = 30 psia -- Amplification Rates

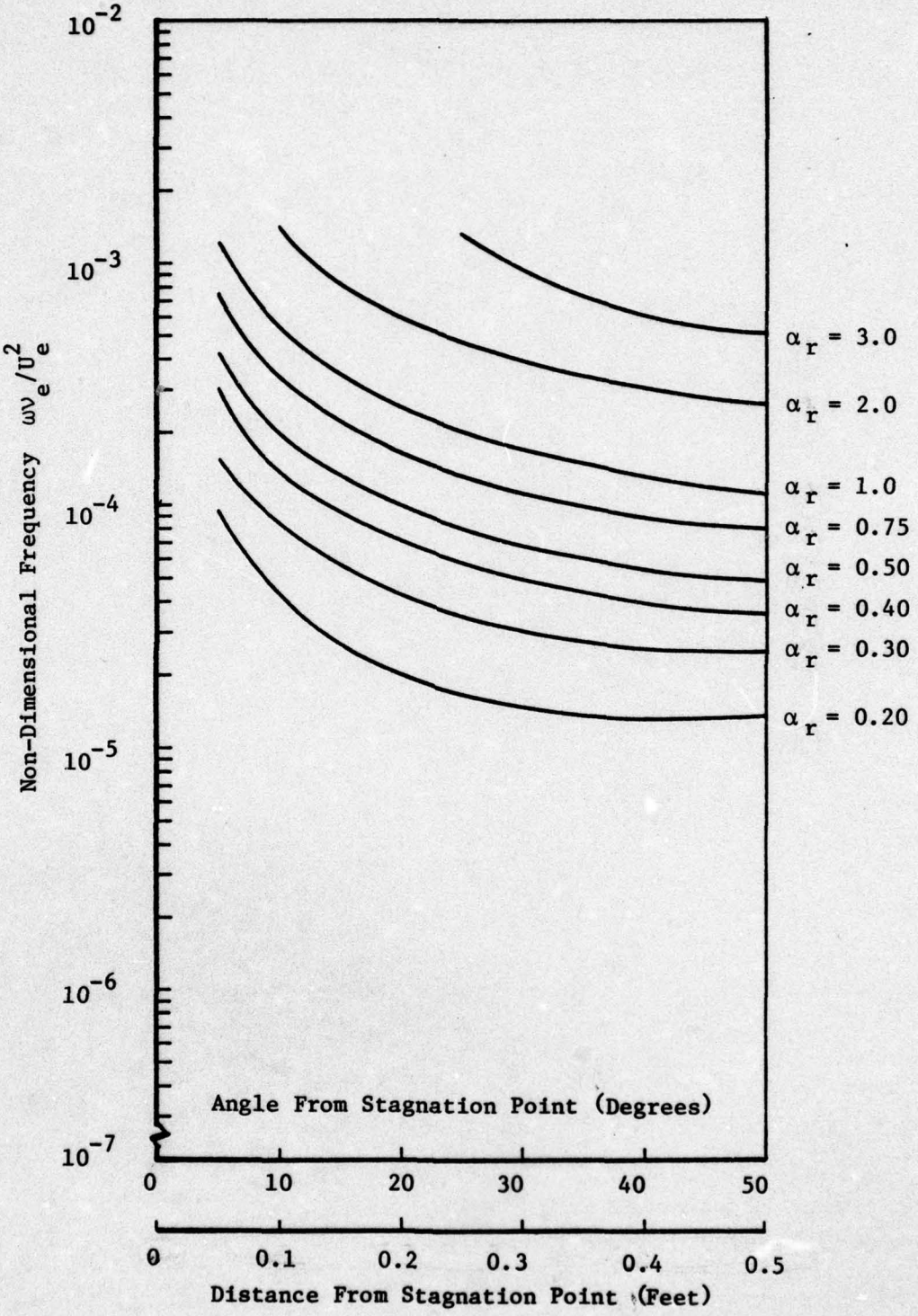


Figure 29 Stability Characteristics of a 7-Inch Sphere; T_w/T_e = 1.0 , k = 5.0 mils , P_c = 30 psia -- Wave Numbers

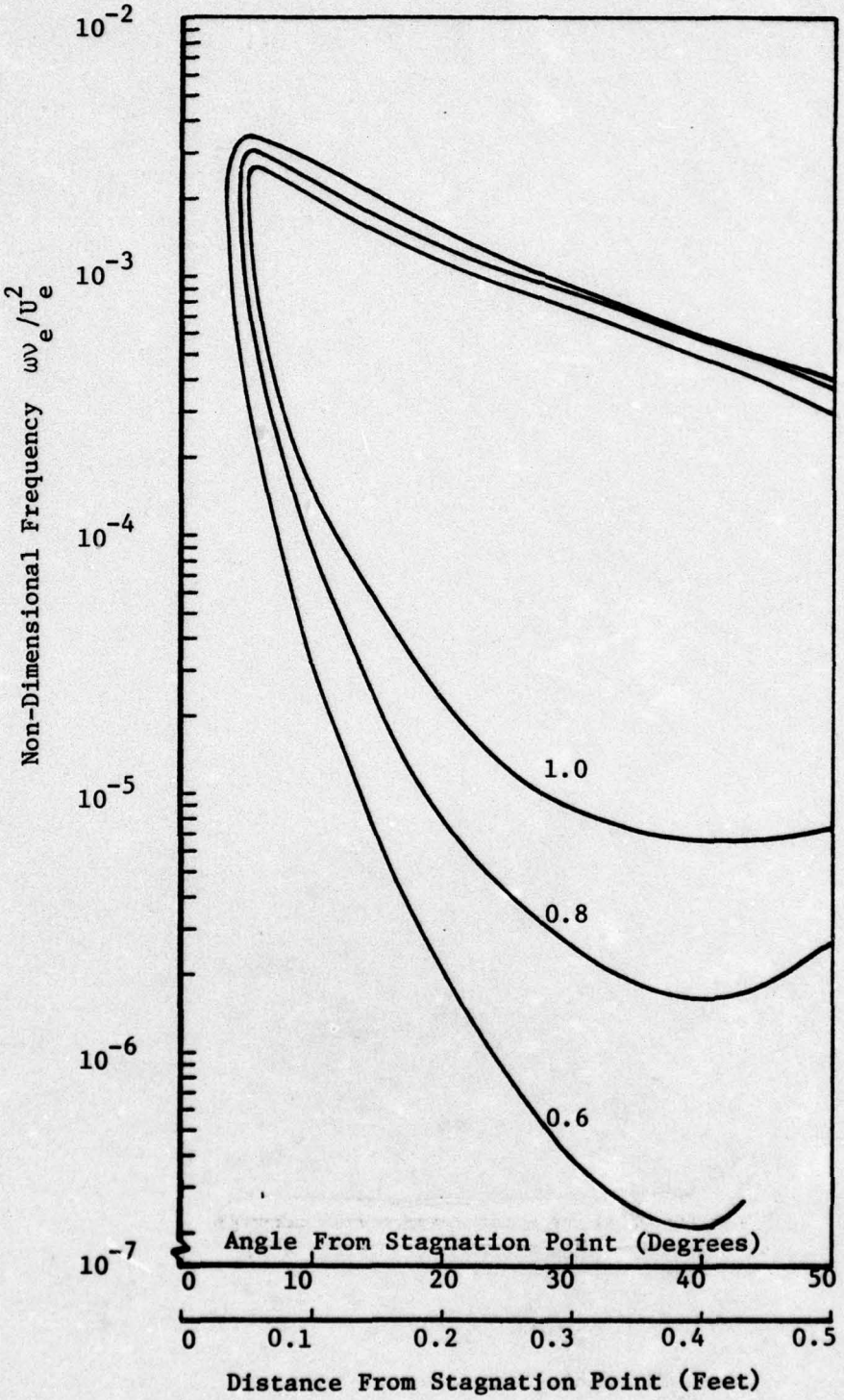


Figure 30 Stability Characteristics of a 7-Inch Sphere; Composite Results Showing Effects of Wall Temperature Ratio on Neutral Stability Curves in the Presence of Wall Roughness and Surface Mass Addition

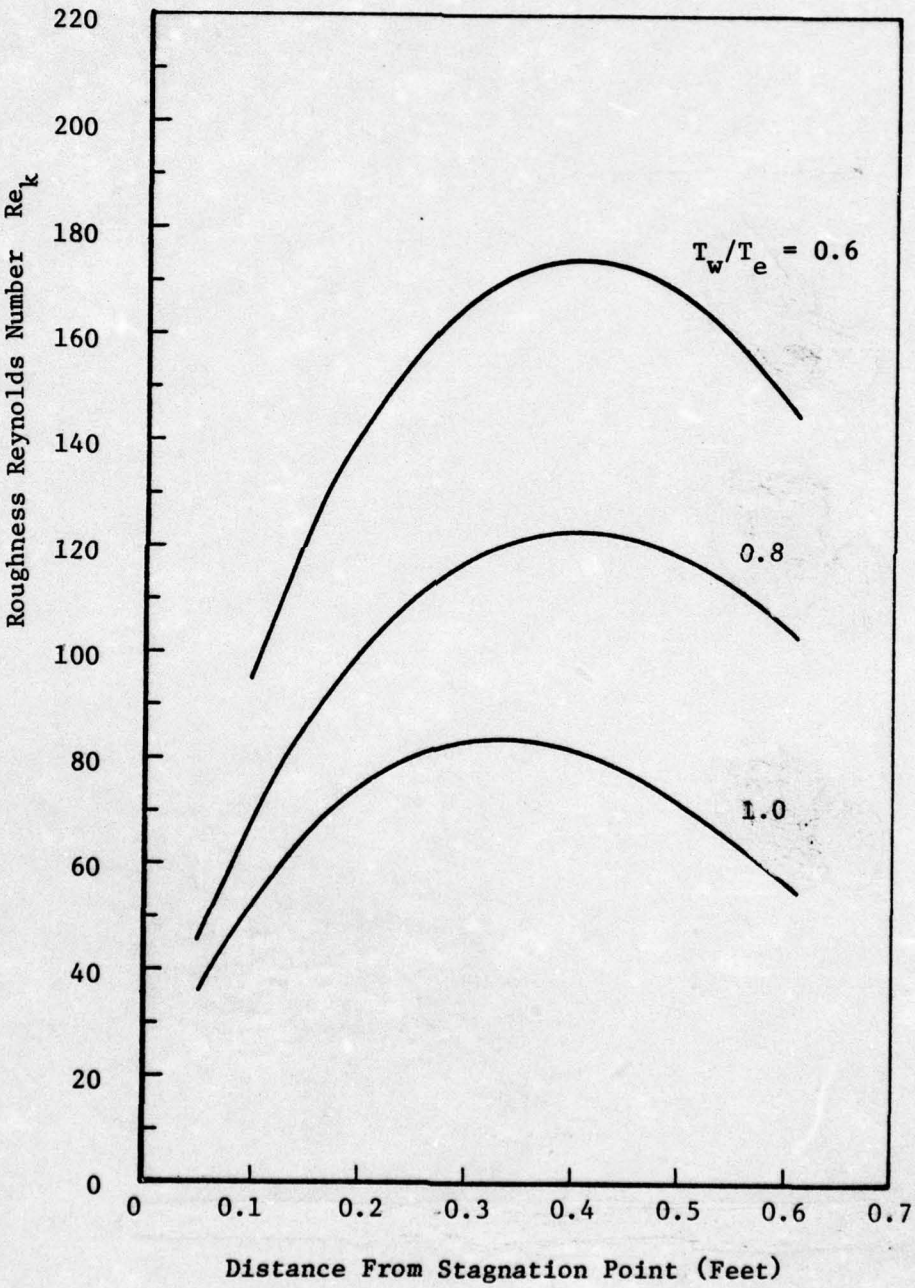


Figure 31 Roughness Reynolds Number of a 7-Inch Sphere; as a Function of the Wall Termperature Ratio; k = 5.0 mils, P_c = 30 psia

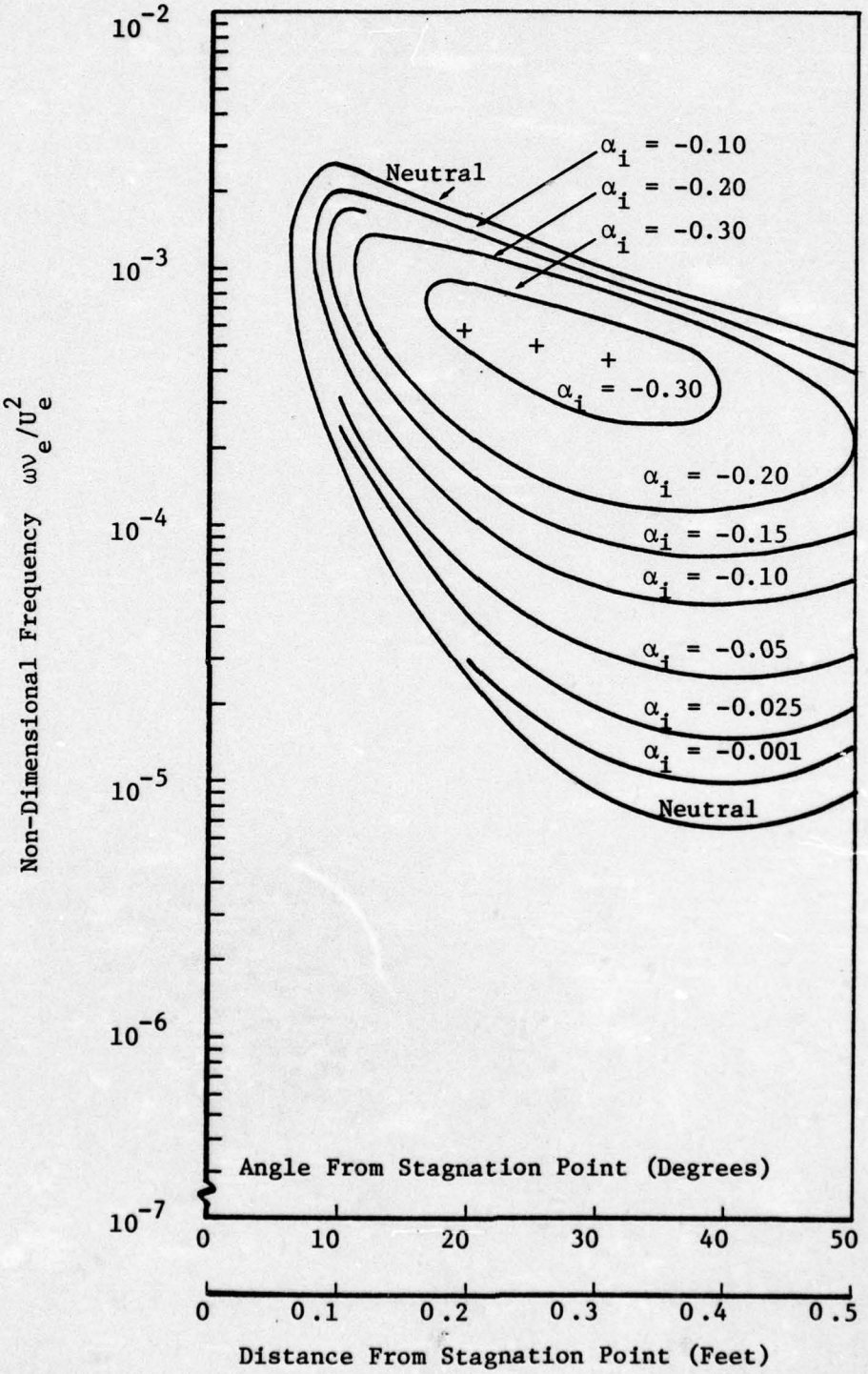


Figure 32 Stability Characteristics of a 7 Inch Sphere; T_w/T_e = 1.0 , k = 5.0 mils , No Surface Mass Addition--Amplification Rates

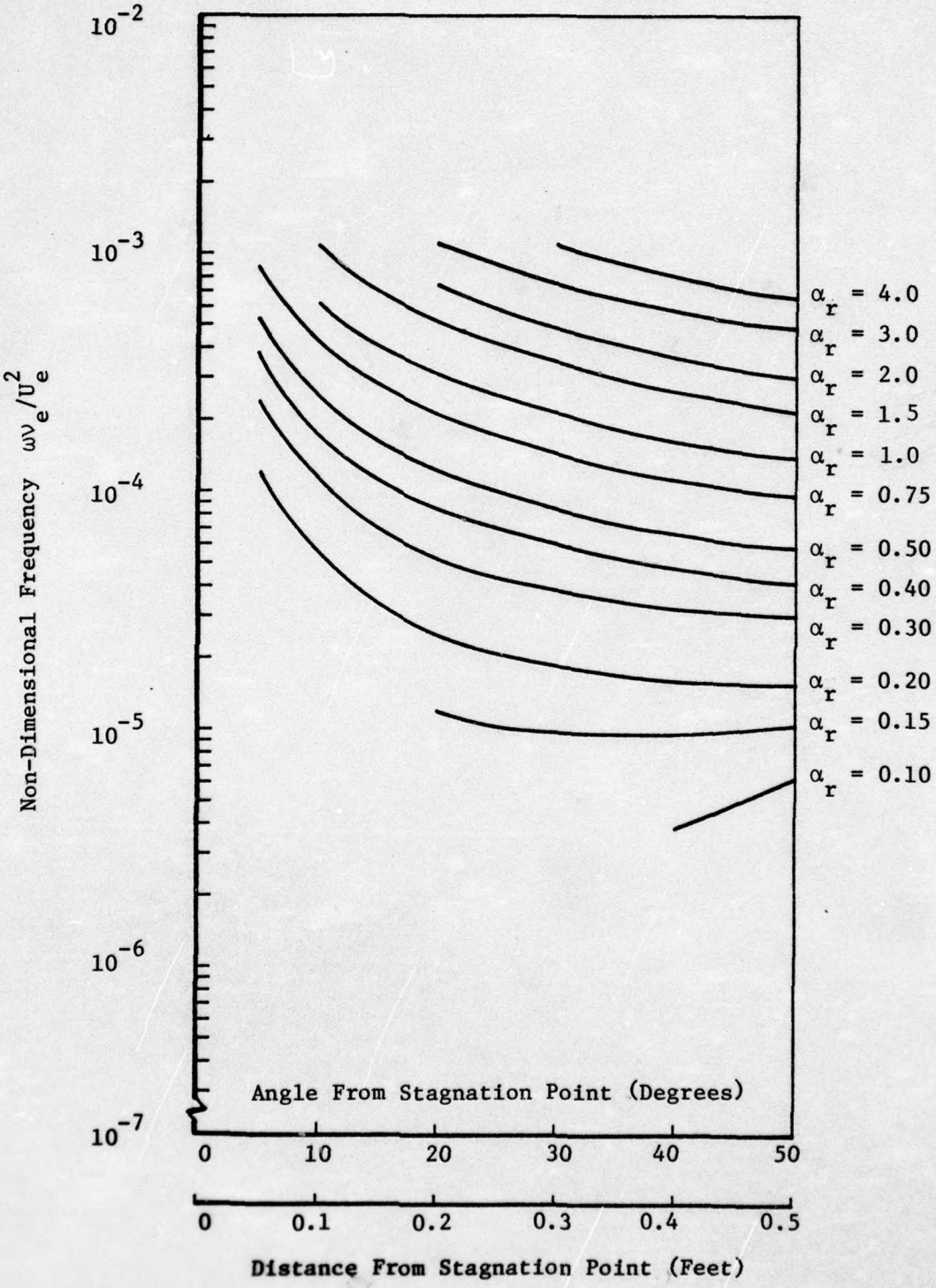


Figure 33 Stability Characteristics of a 7-Inch Sphere; T_w/T_e = 1.0 , k = 5.0 mils , No Surface Mass Addition--Wave Numbers

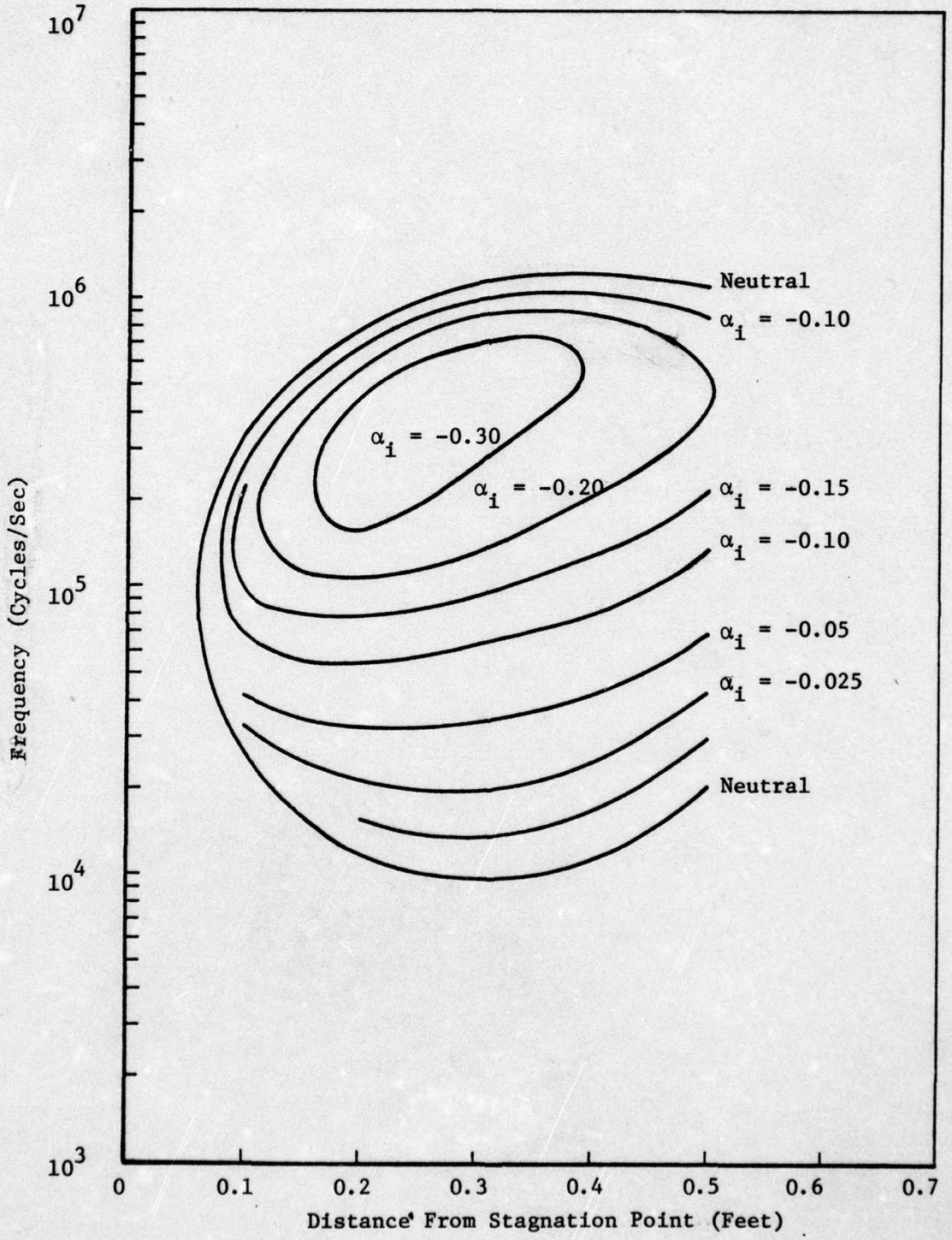


Figure 34 Dimensional Stability Characteristics of a 7-Inch Sphere; T_w/T_e = 1.0 , k = 5.0 mils , No Surface Mass Addition-- Amplification Rates

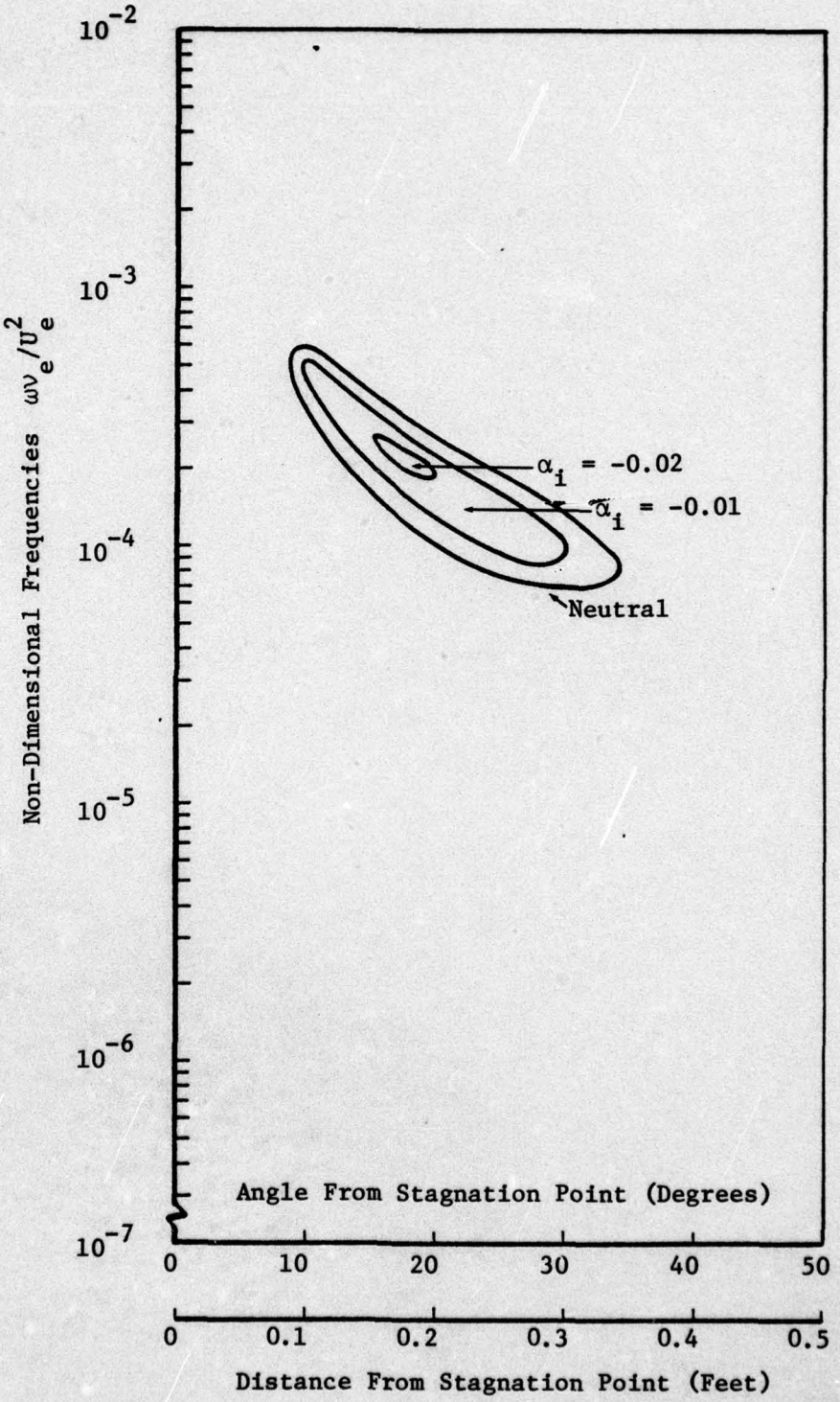


Figure 35 Stability Characteristics of a 7-Inch Sphere; T_w/T_e = 1.0, Smooth Wall, P_c = 45 psia -- Amplification Rates

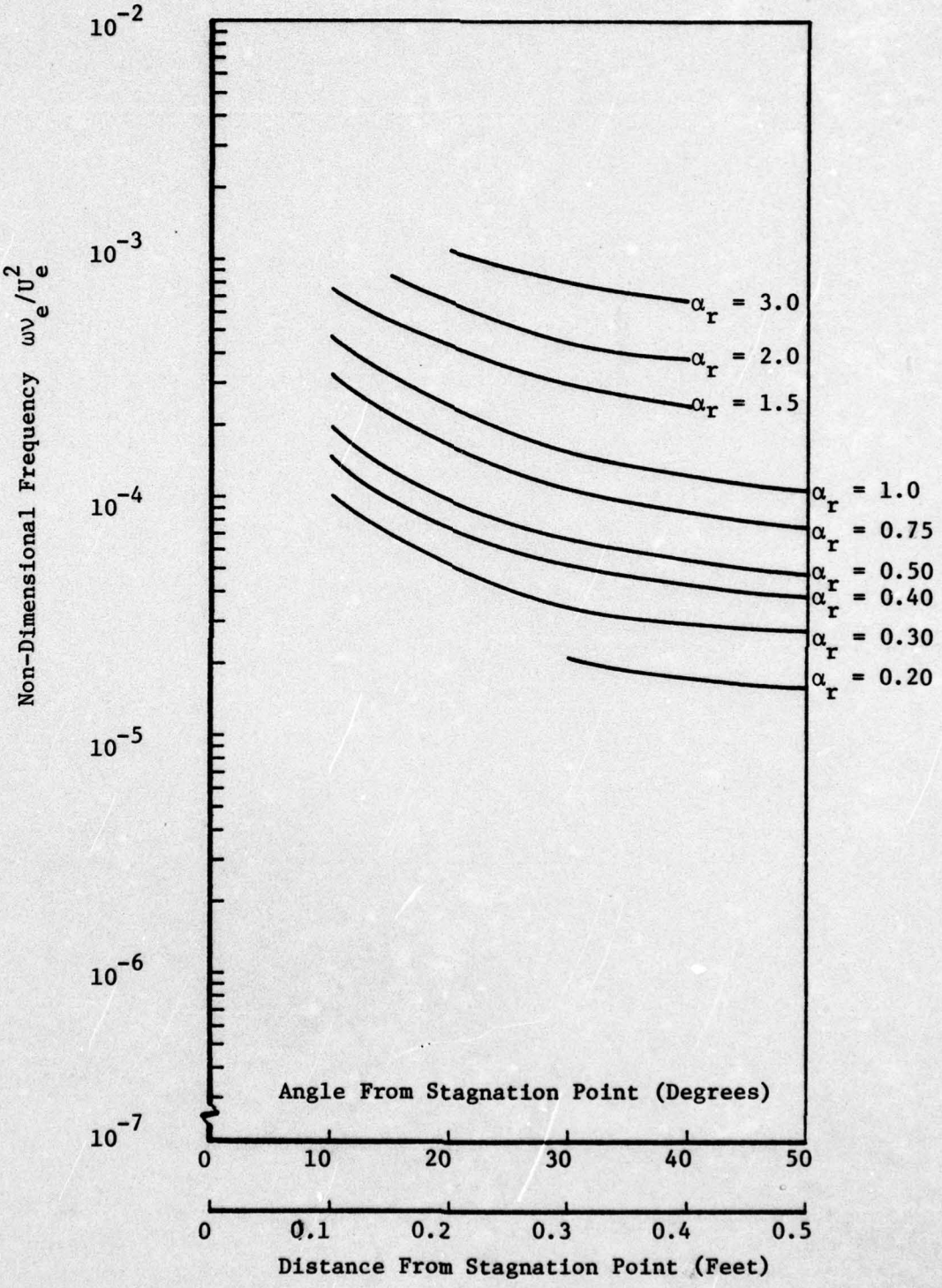


Figure 36 Stability Characteristics of a 7-Inch Sphere; T_w/T_e = 1.0 , Smooth Wall, P_c = 45 psia -- Wave Numbers

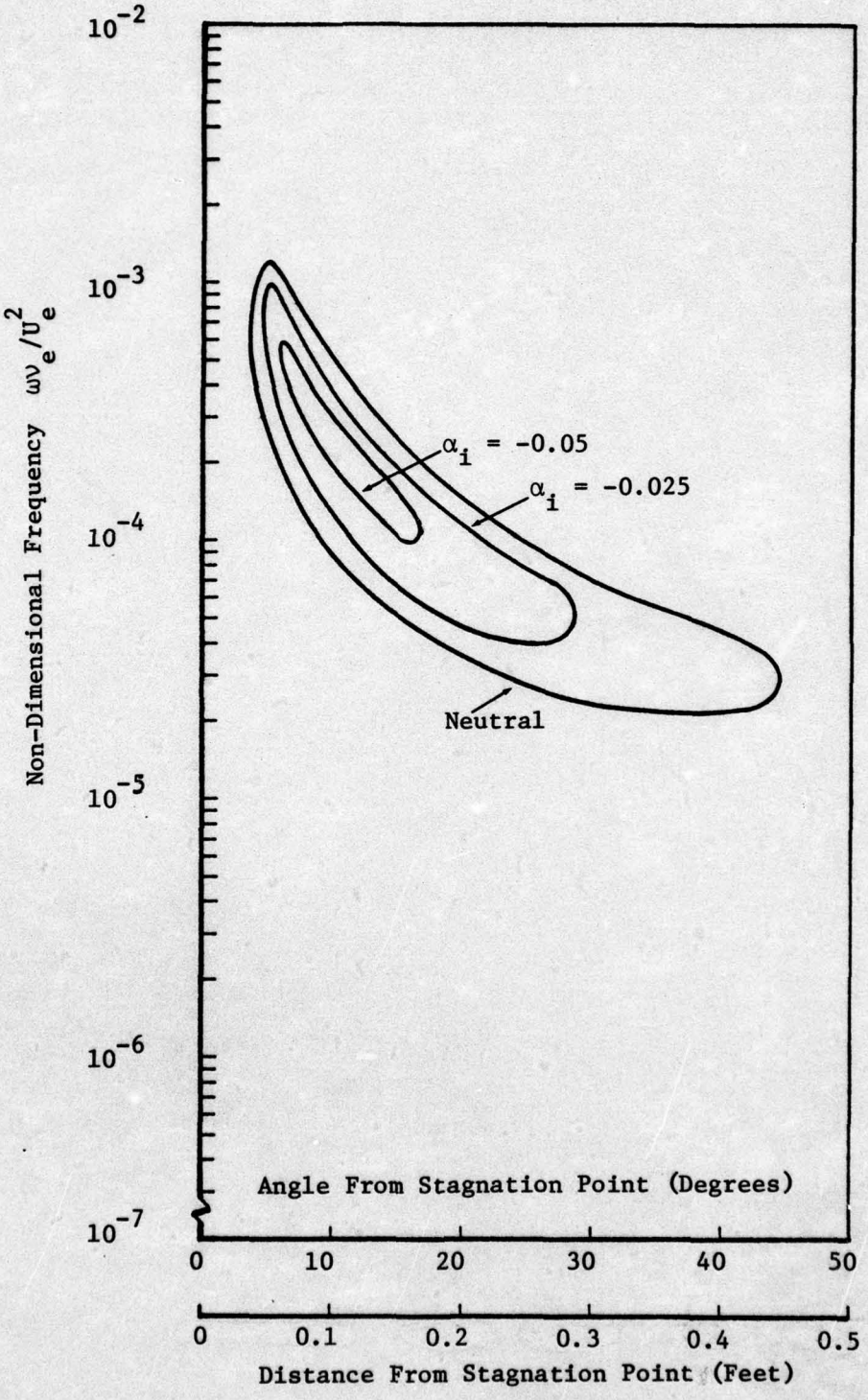


Figure 37 Stability Characteristics of a 7-Inch Sphere; T_w/T_e = 1.0 , Smooth Wall, P_c = 60 psia-- Amplification Rates

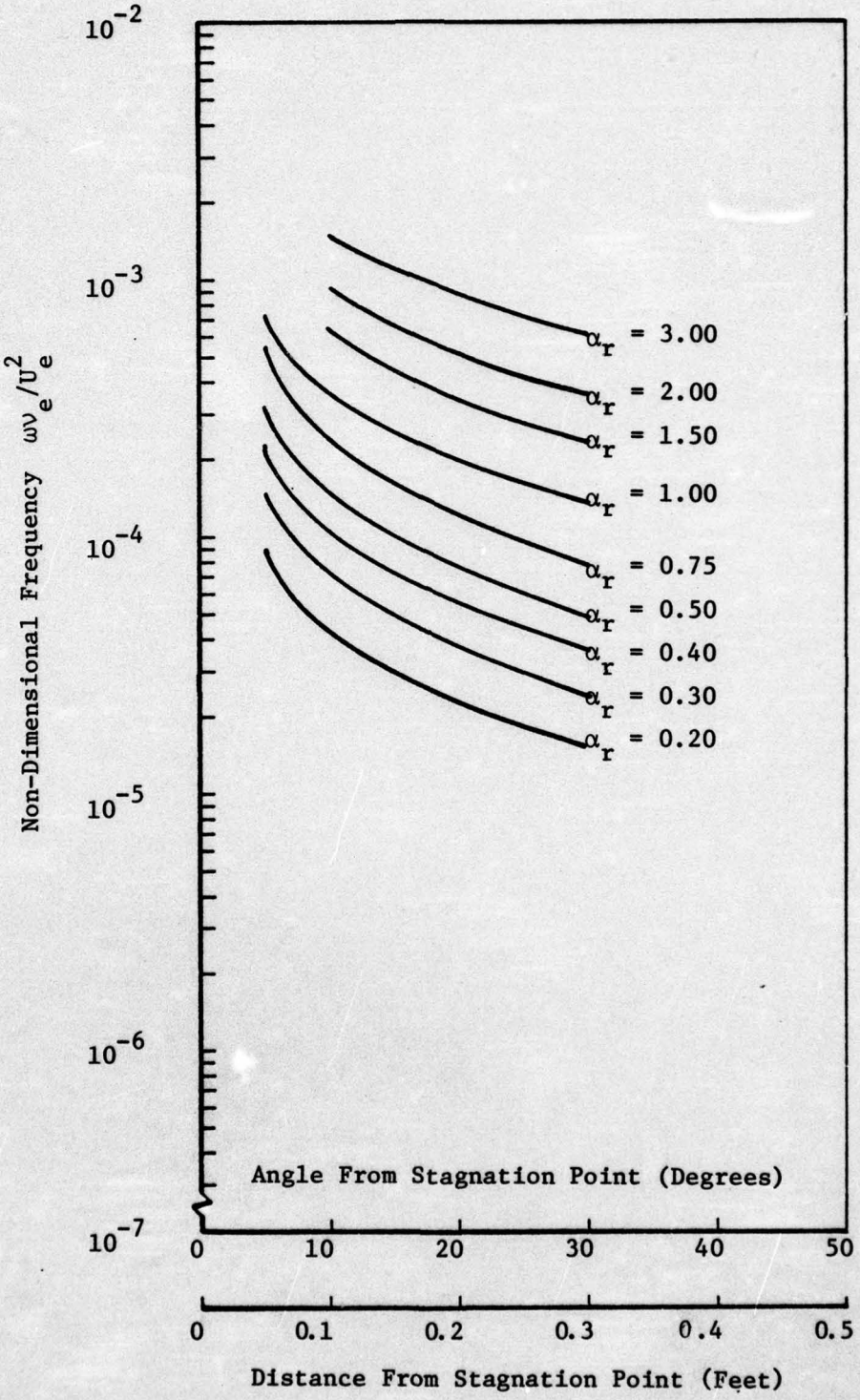


Figure 38 Stability Characteristics of a 7-Inch Sphere; T_w/T_e = 1.0 , Smooth Wall, P_c = 60 psia -- Wave Numbers

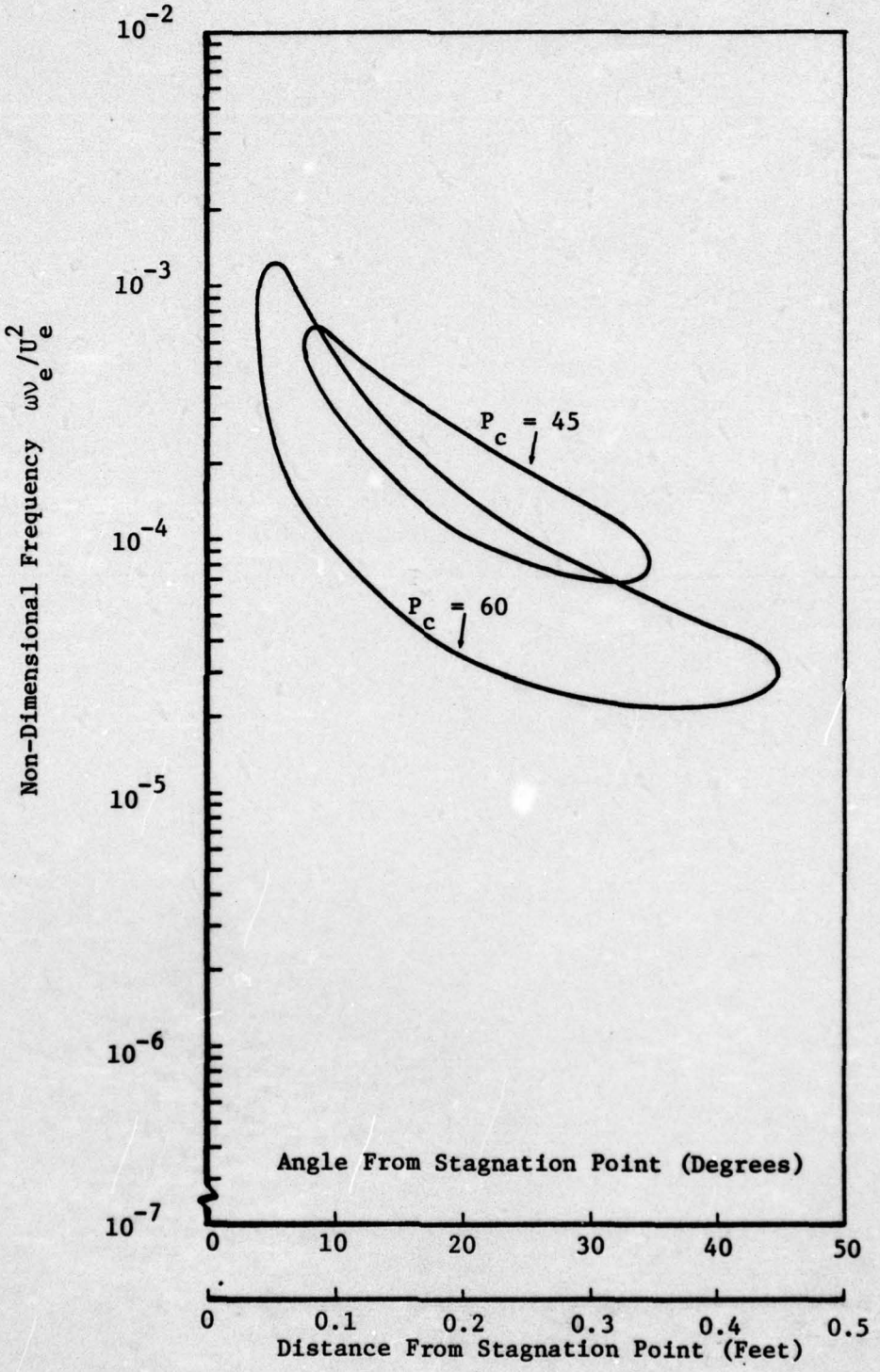


Figure 39 Stability Characteristics of a 7-Inch Sphere; Composite Results Showing Effect of Surface Addition in the Presence of a Smooth Wall

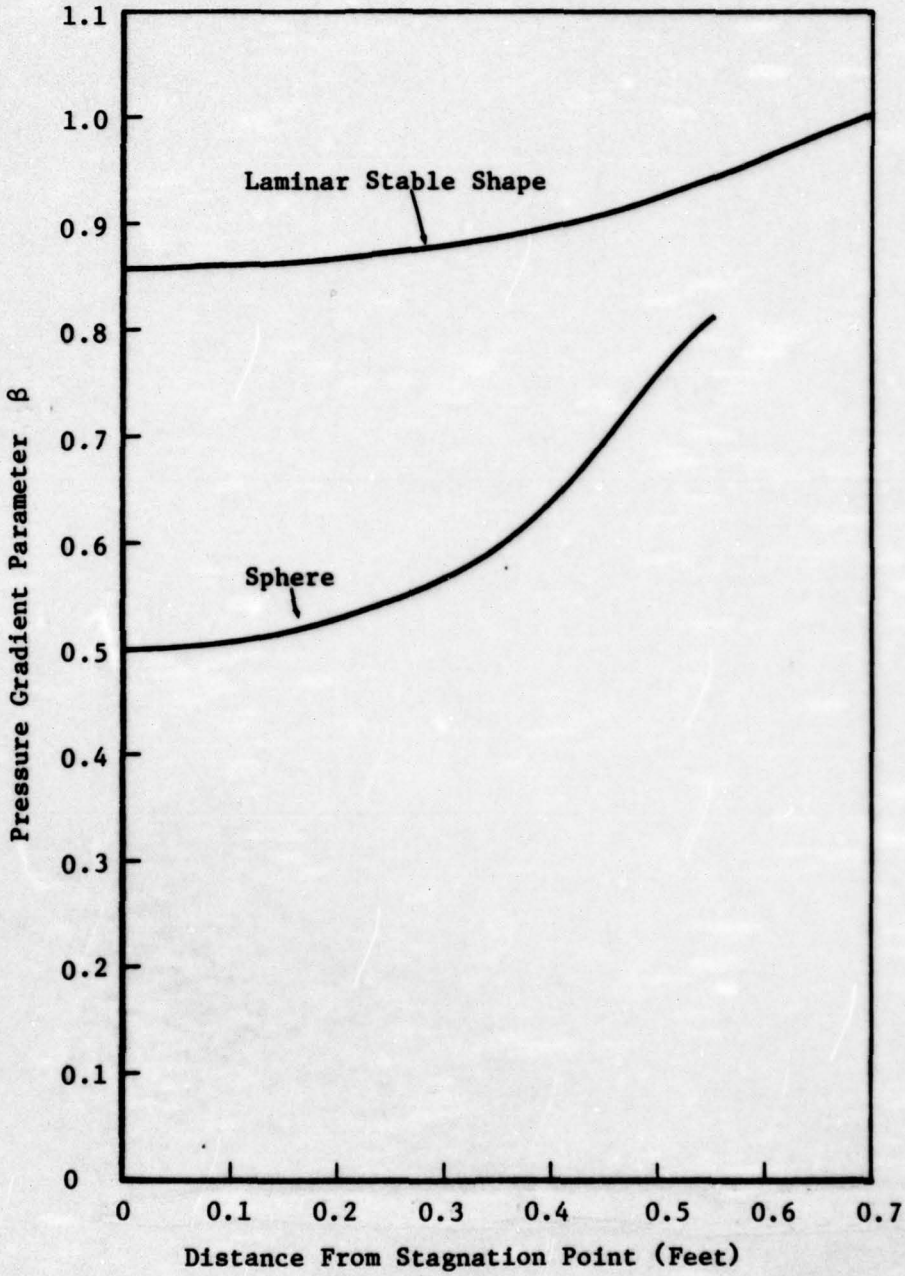


Figure 40 Comparison of the Non-Dimensional Pressure Gradient Parameter For a Laminar Stable Shape and a Spherical Body

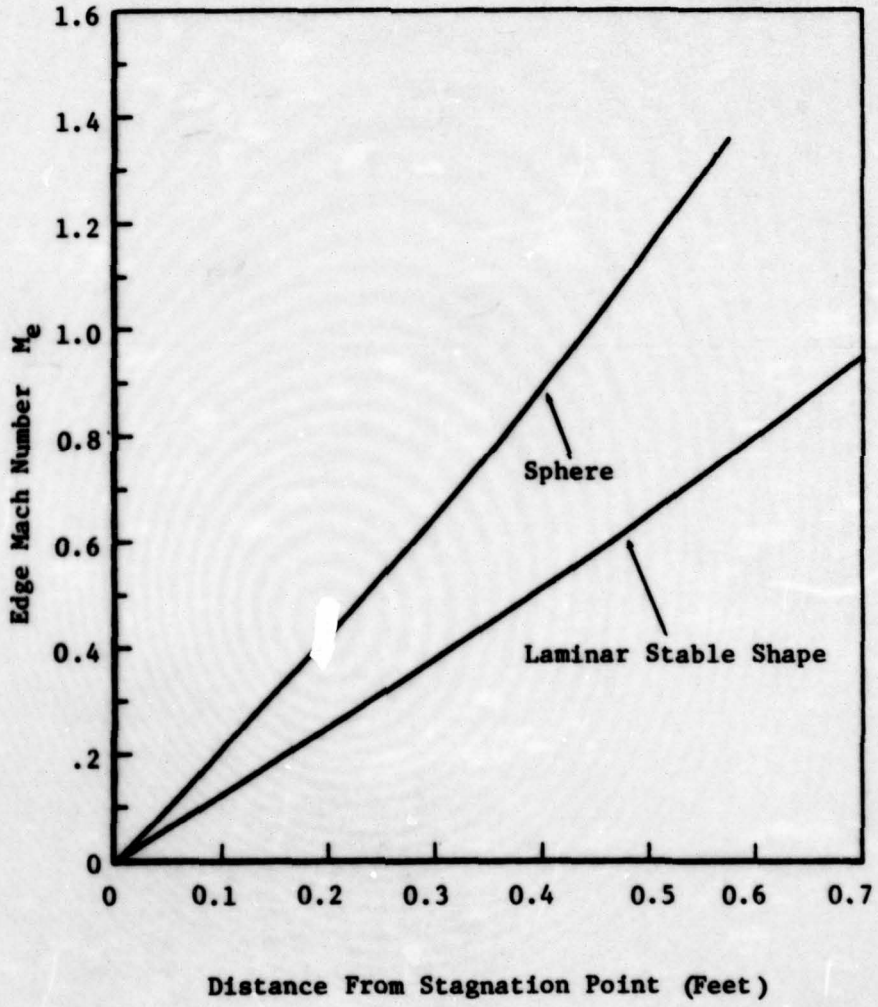


Figure 41 Comparison of the Mach Number Variation of a Laminar Stable Shape and a Spherical Body

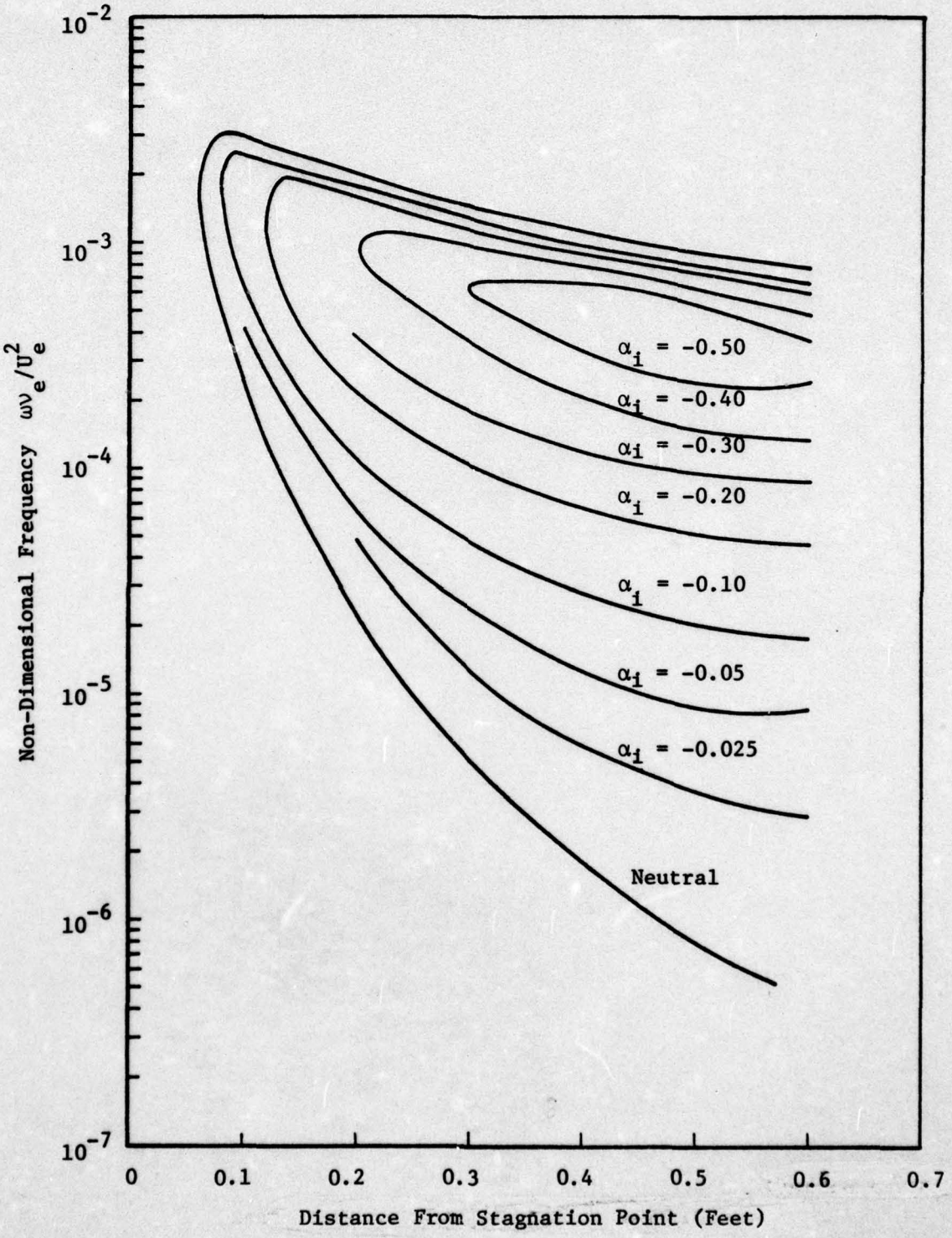


Figure 42 Stability Characteristics of a Laminar Stable Shape; T_w/T_e = 0.6 , k = 5.0 mils , β' = 0.6 --Amplification Rates

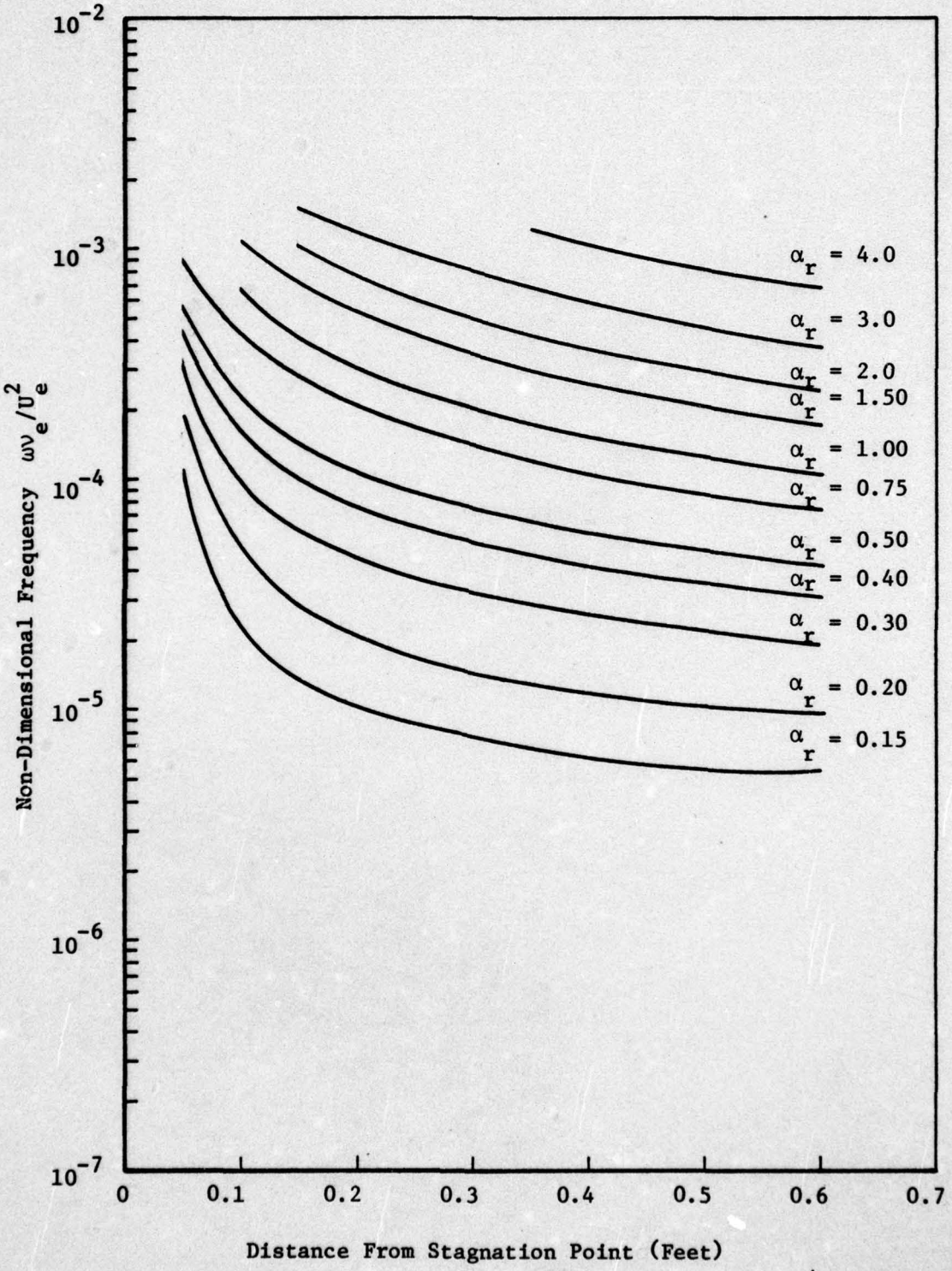


Figure 43 Stability Characteristics of a Laminar Stable Shape; T_w/T_e = 0.6 , k = 5.0 mils , β' = 0.6 --Wave Numbers

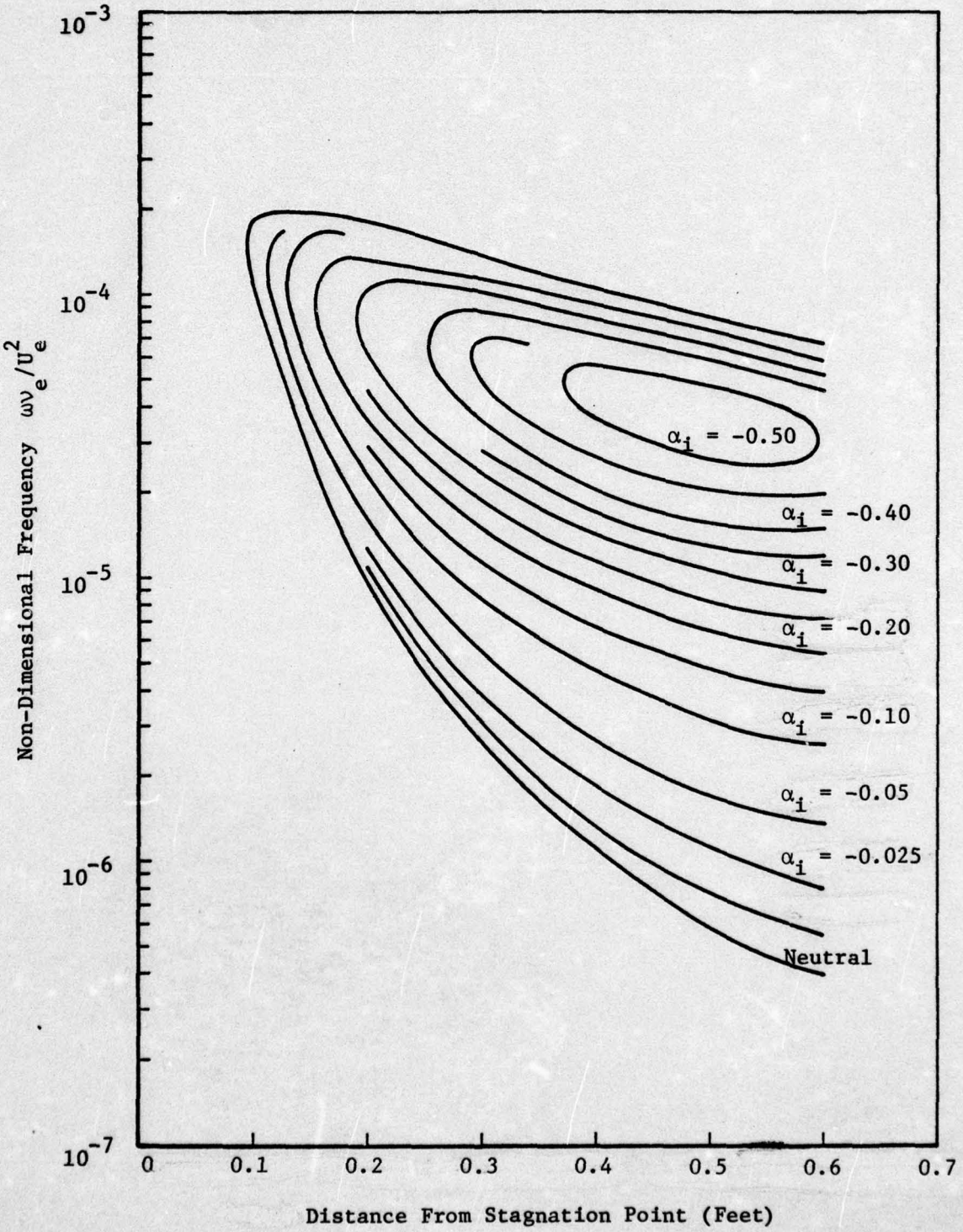


Figure 44 Stability Characteristics of a Laminar Stable Shape; T_w/T_e = 0.6 , k = 3.0 mils , β' = 0.6 --Amplification Rates

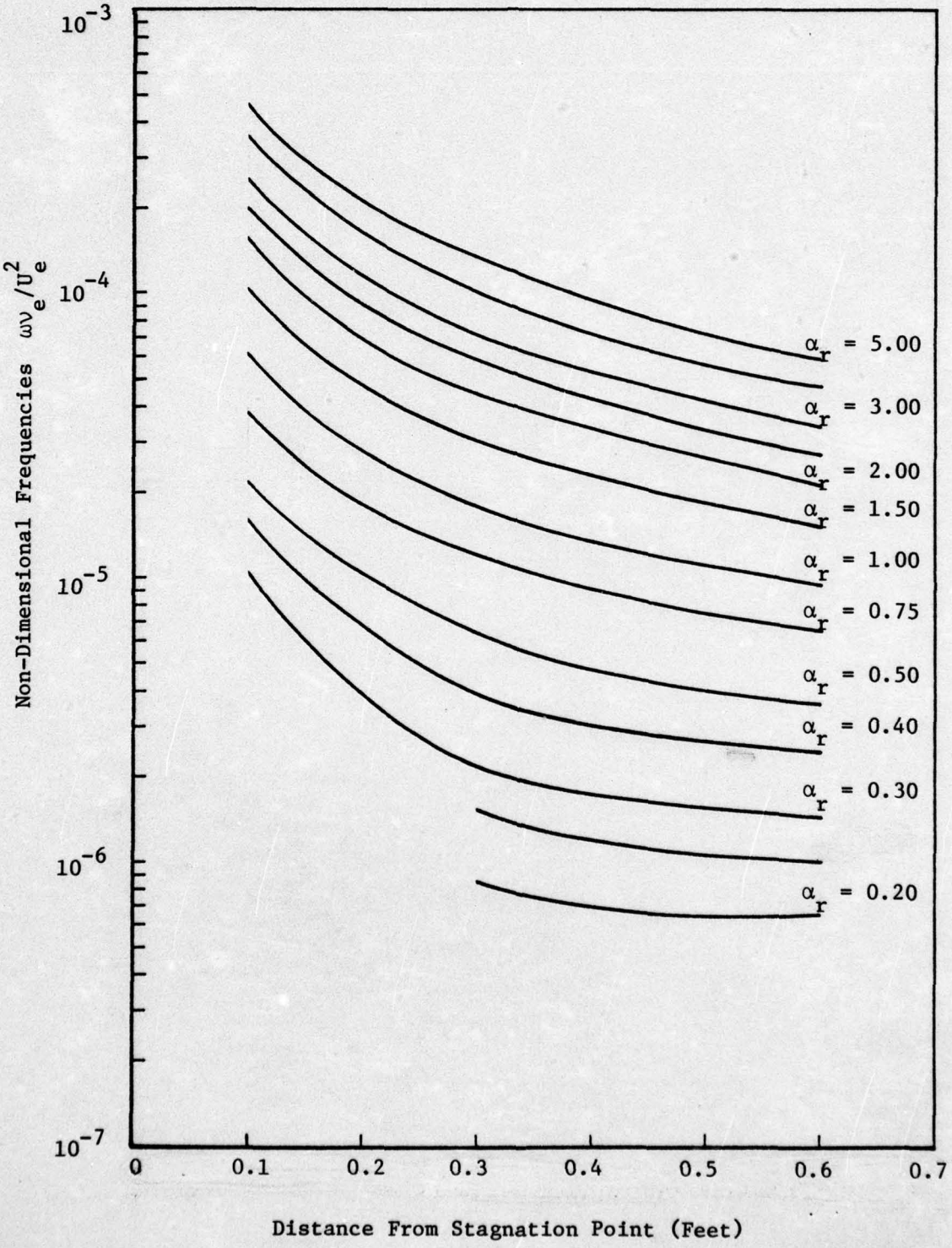


Figure 45 Stability Characteristics of a Laminar Stable Shape; T_w/T_e = 0.6 , k = 3.0 mils , β' = 0.6 --Wave Numbers

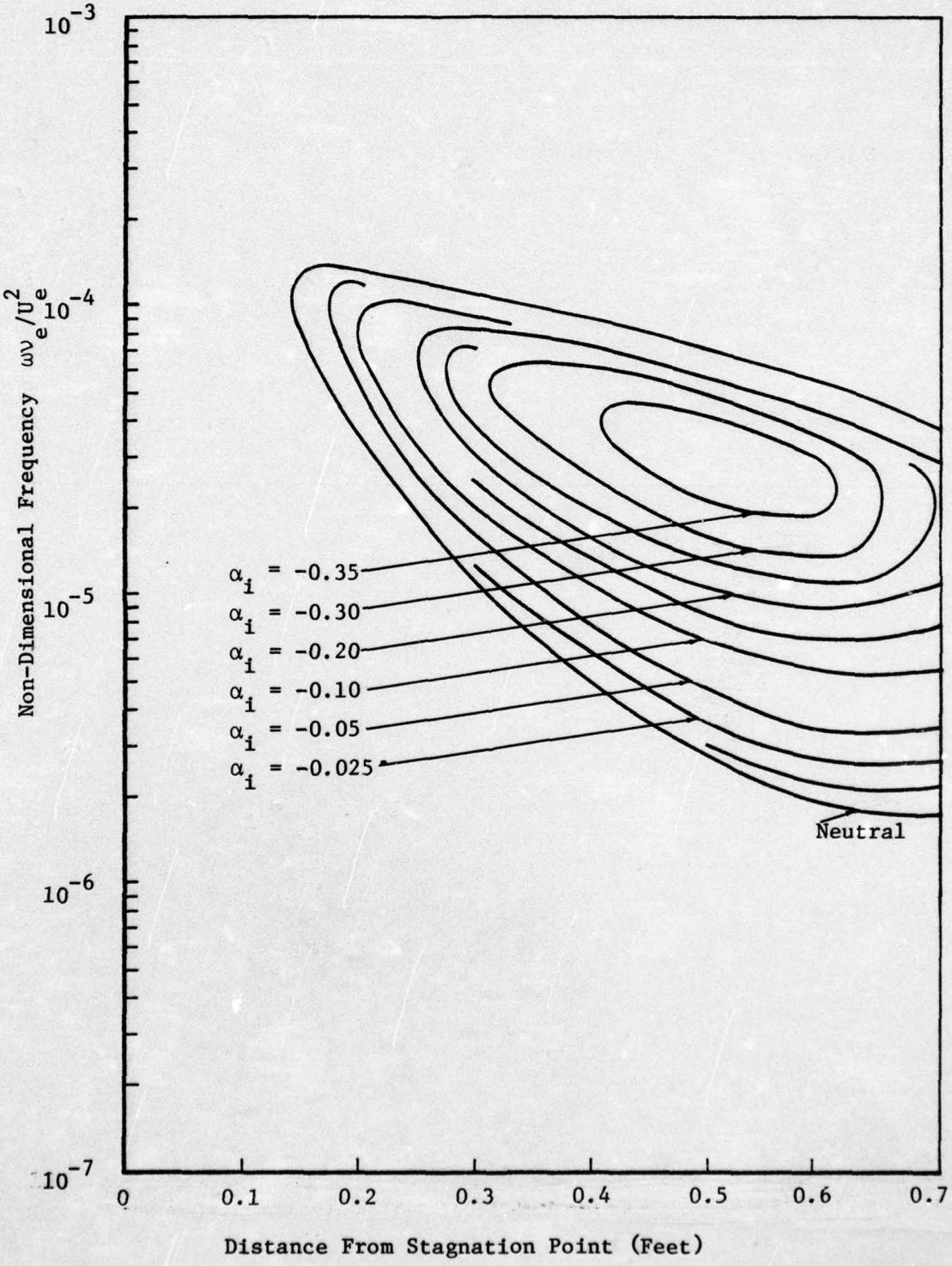
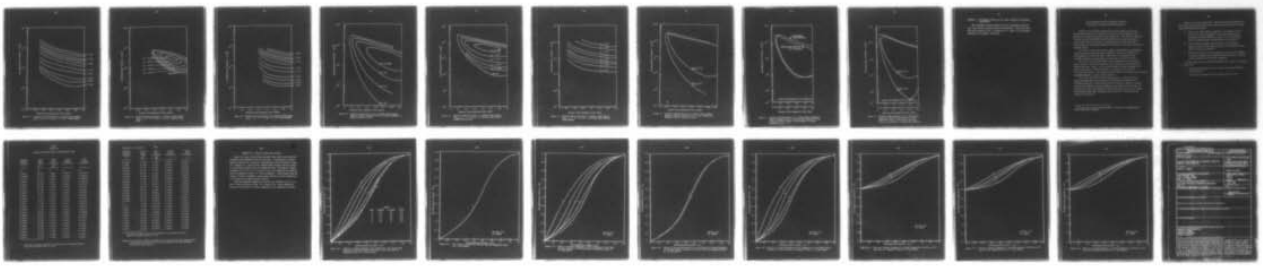


Figure 46 Stability Characteristics of a Laminar Stable Shape; T_w/T_e = 0.6 , k = 2.0 mils , β'=0.6 --Amplification Rates

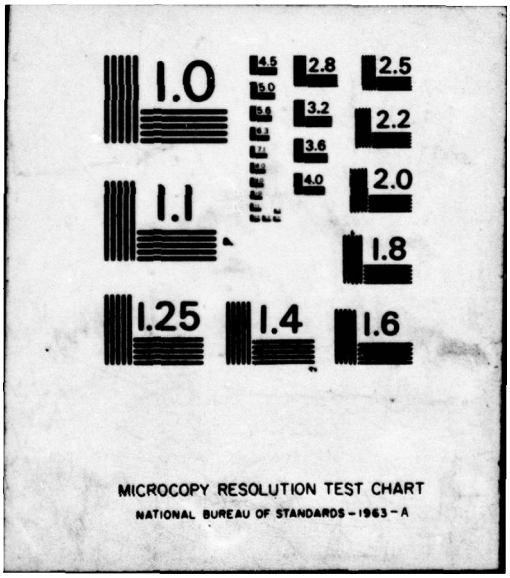
AD-A035 712 FLOW RESEARCH INC KENT WASH F/G 20/4
STABILITY AND TRANSITION IN BOUNDARY LAYERS ON REENTRY VEHICLE --ETC(U)
JUN 76 C L MERKLE F44620-74-C-0049
UNCLASSIFIED FLOW RES-71 AFOSR-TR-76-1107 NL

2 OF 2
AD A035712



END

DATE FILMED
3-77


1.0
1.1
1.25
1.4
1.6
1.8
2.0
2.2
2.5
2.8
3.2
3.6
4.0
4.5
5.0
MICROCOPY RESOLUTION TEST CHART
NATIONAL BUREAU OF STANDARDS - 1963 - A

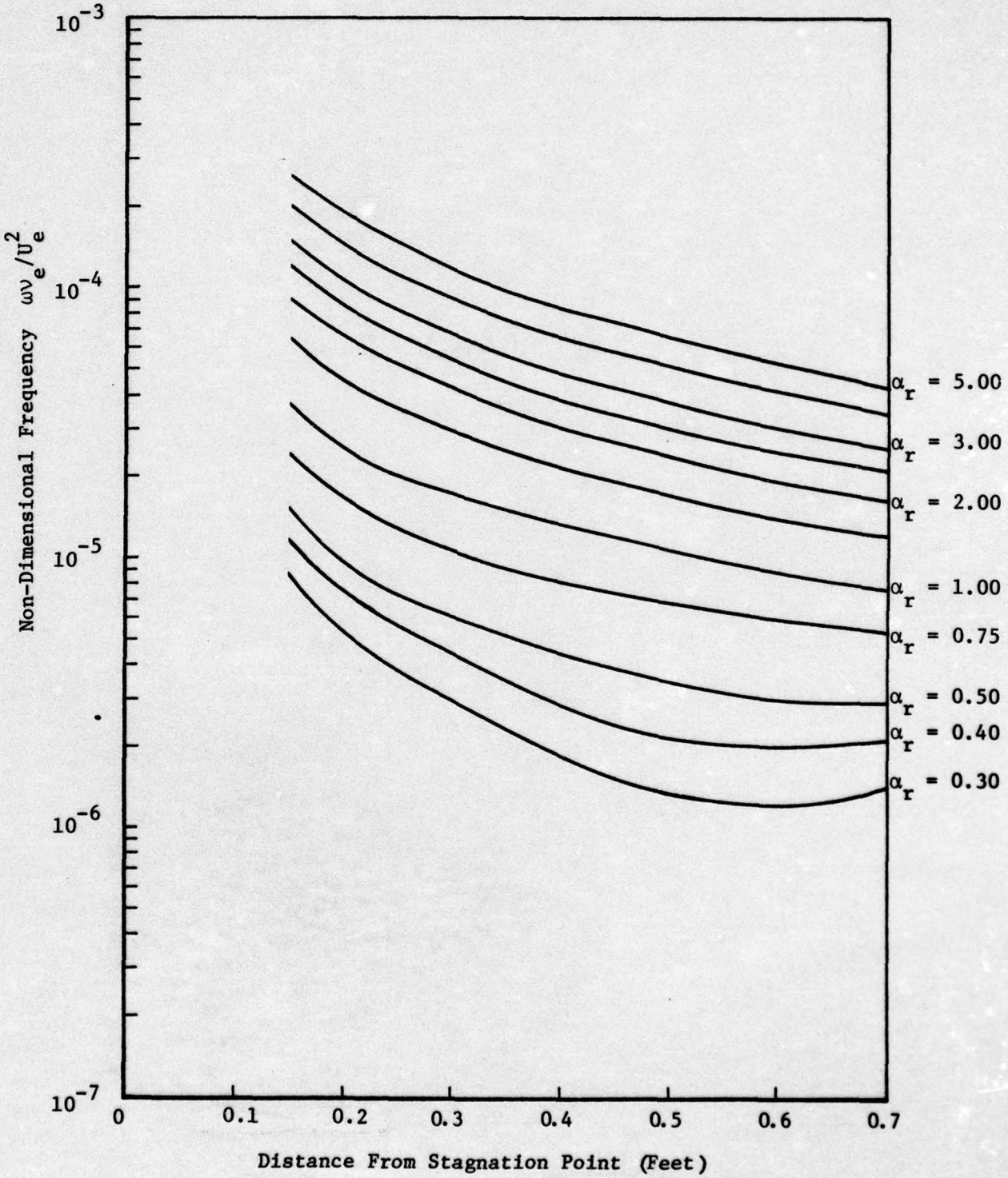


Figure 47 Stability Characteristics of a Laminar Stable Shape; T_w/T_e = 0.6 , k = 2.0 mils , β'= 0.6 --Wave Numbers

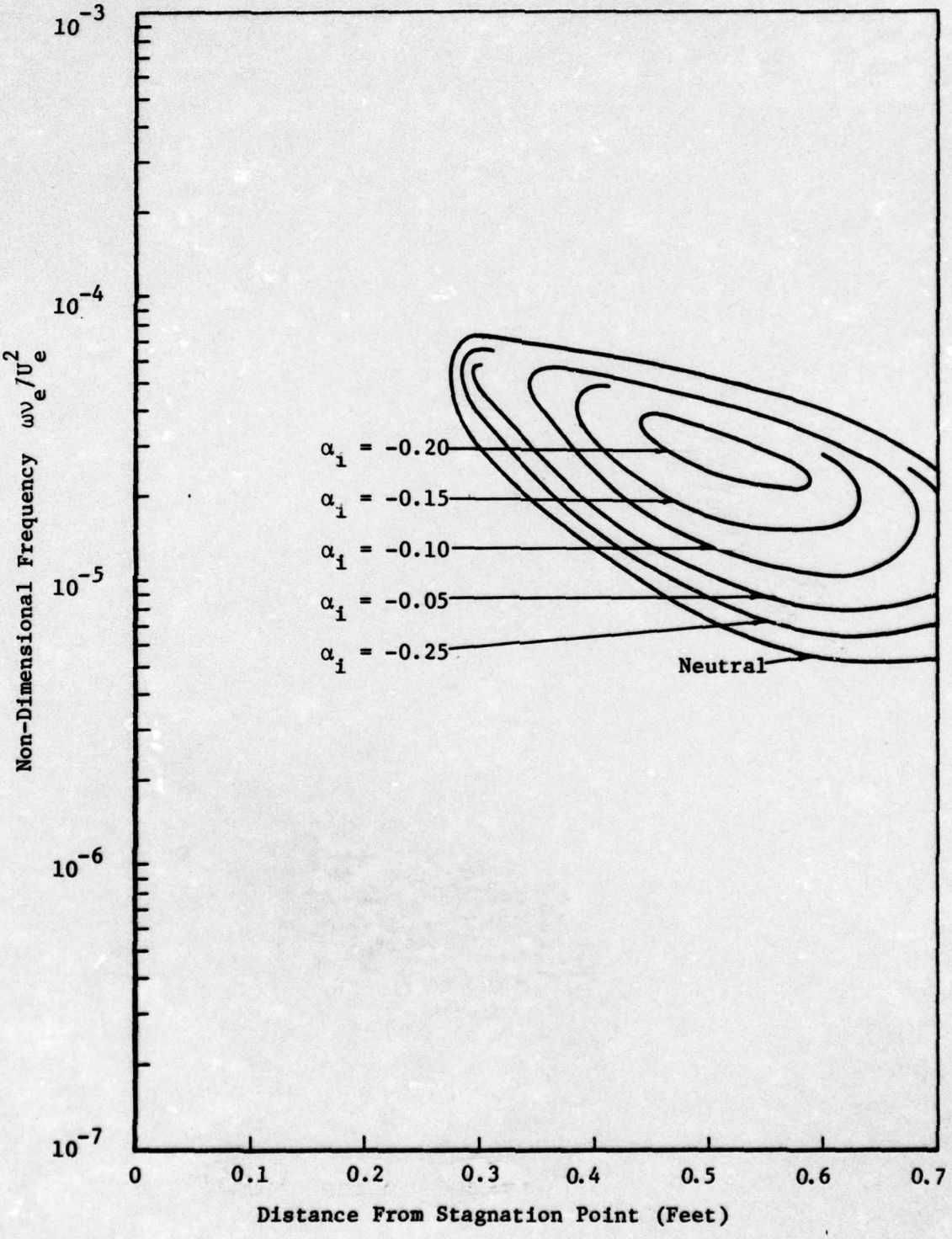


Figure 48 Stability Characteristics of a Laminar Stable Shape; T_w/T_e = 0.6 , k = 1.5 mils , β'= 0.6 --Amplification Rates

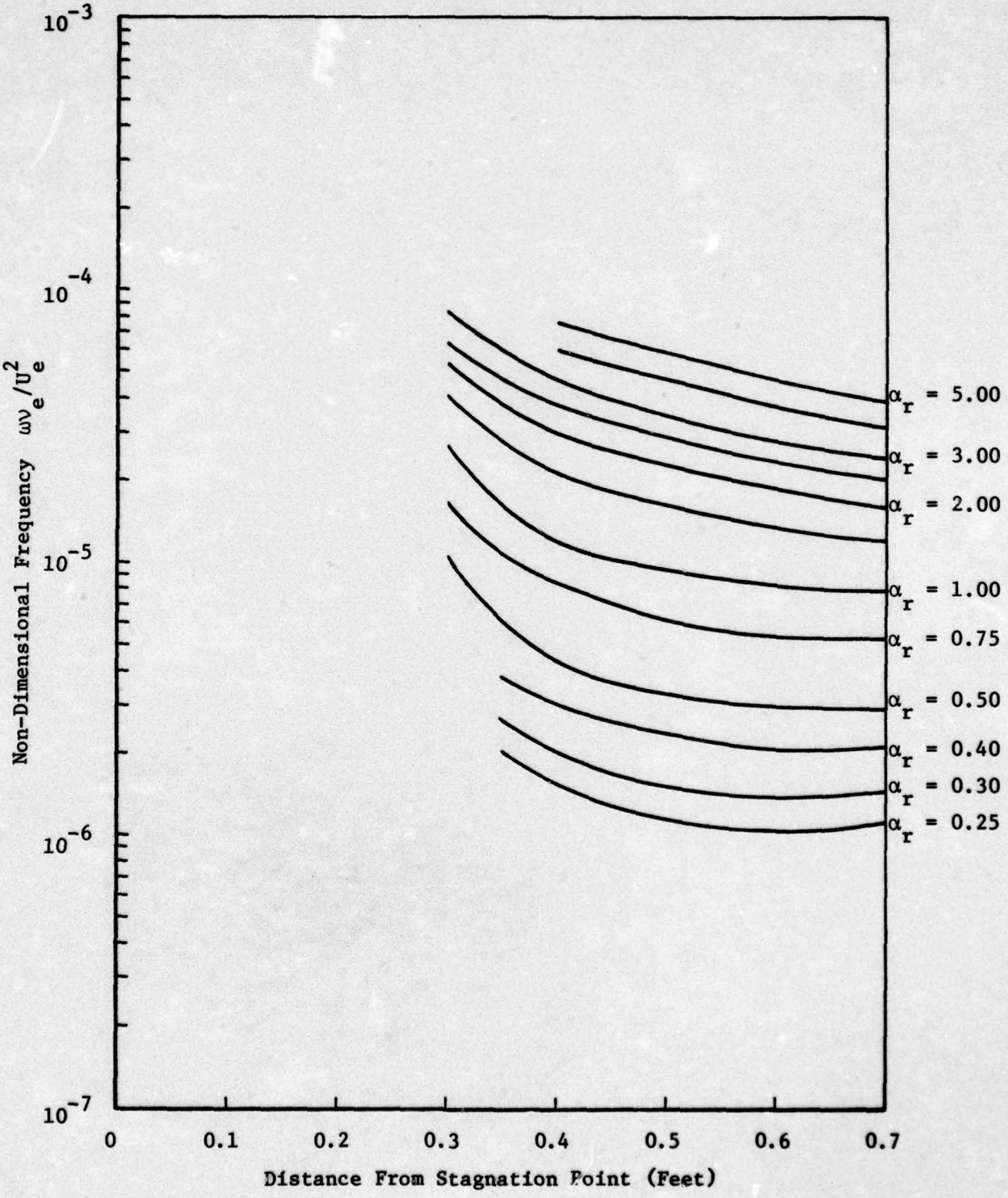


Figure 49 Stability Characteristics of a Laminar Stable Shape; T_w/T_e = 0.6 , k = 1.5 mils, β'= 0.6 --Wave Numbers

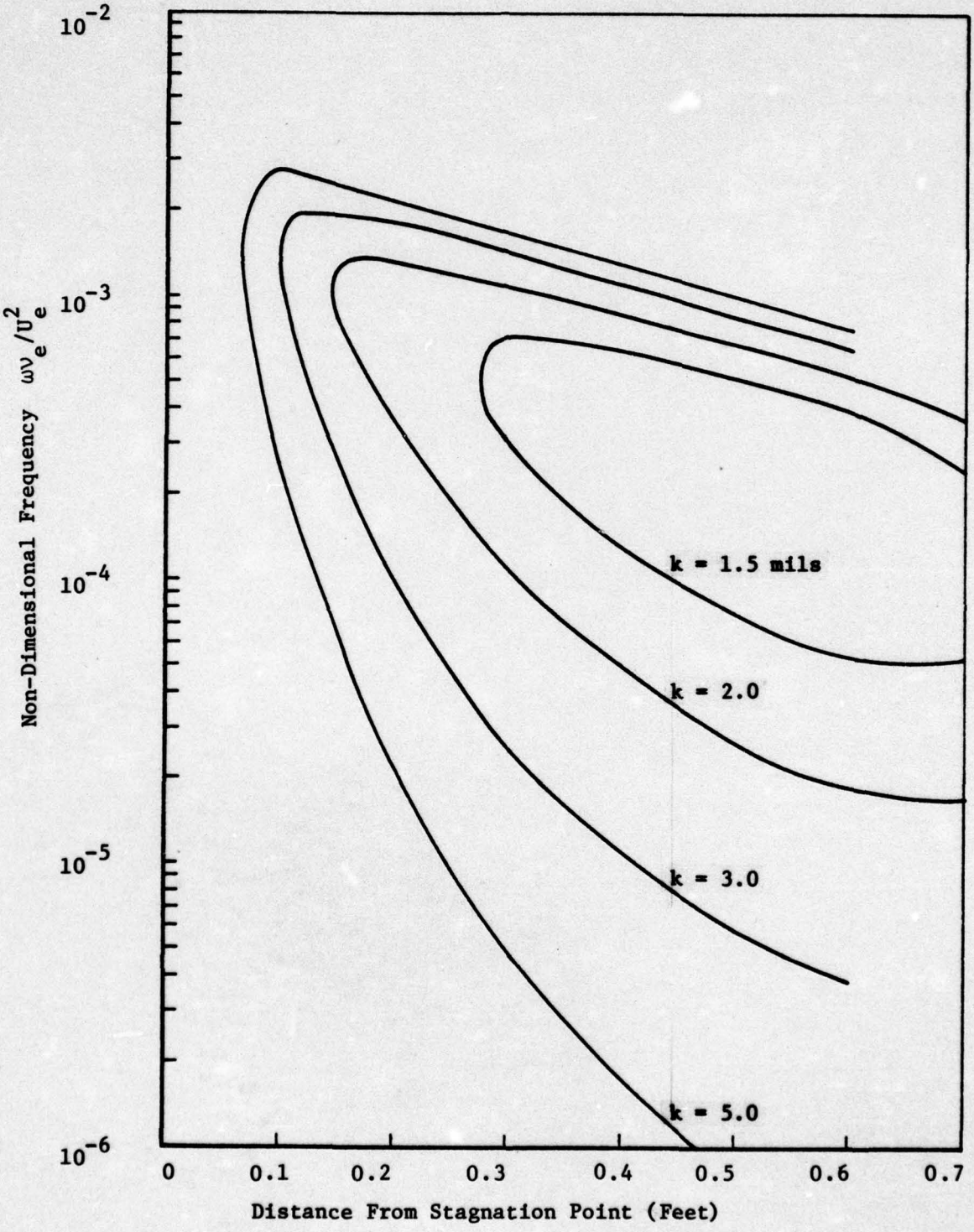


Figure 50 Stability Characteristics of a Laminar Stable Shape; Composite Results Showing Effect of Surface Roughness on Neutral Stability Curves

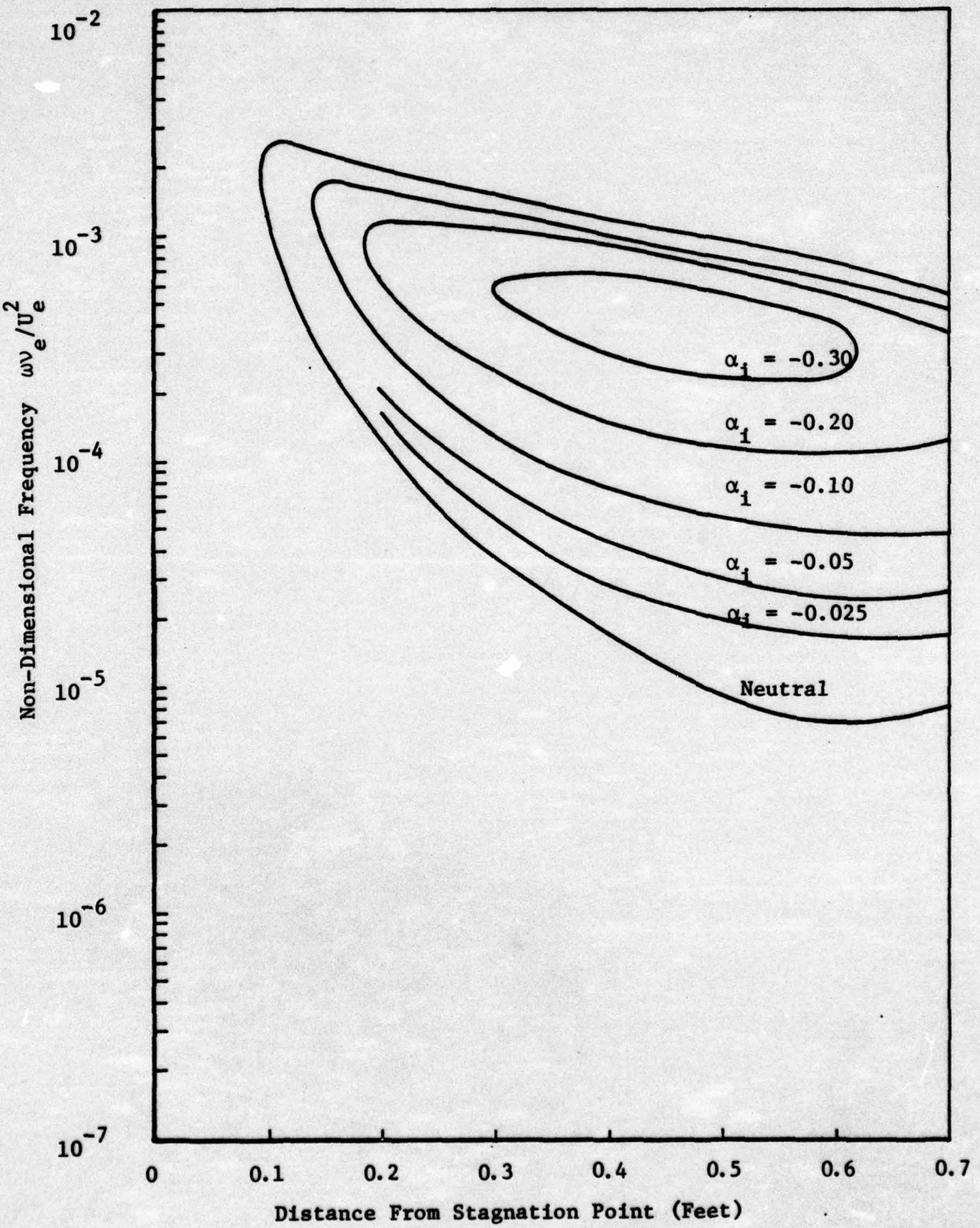


Figure 51 Stability Characteristics of a Laminar Stable Shape; T_w/T_e = 1.0 , k = 5.0 mils , No Surface Mass Addition --Amplification Rates

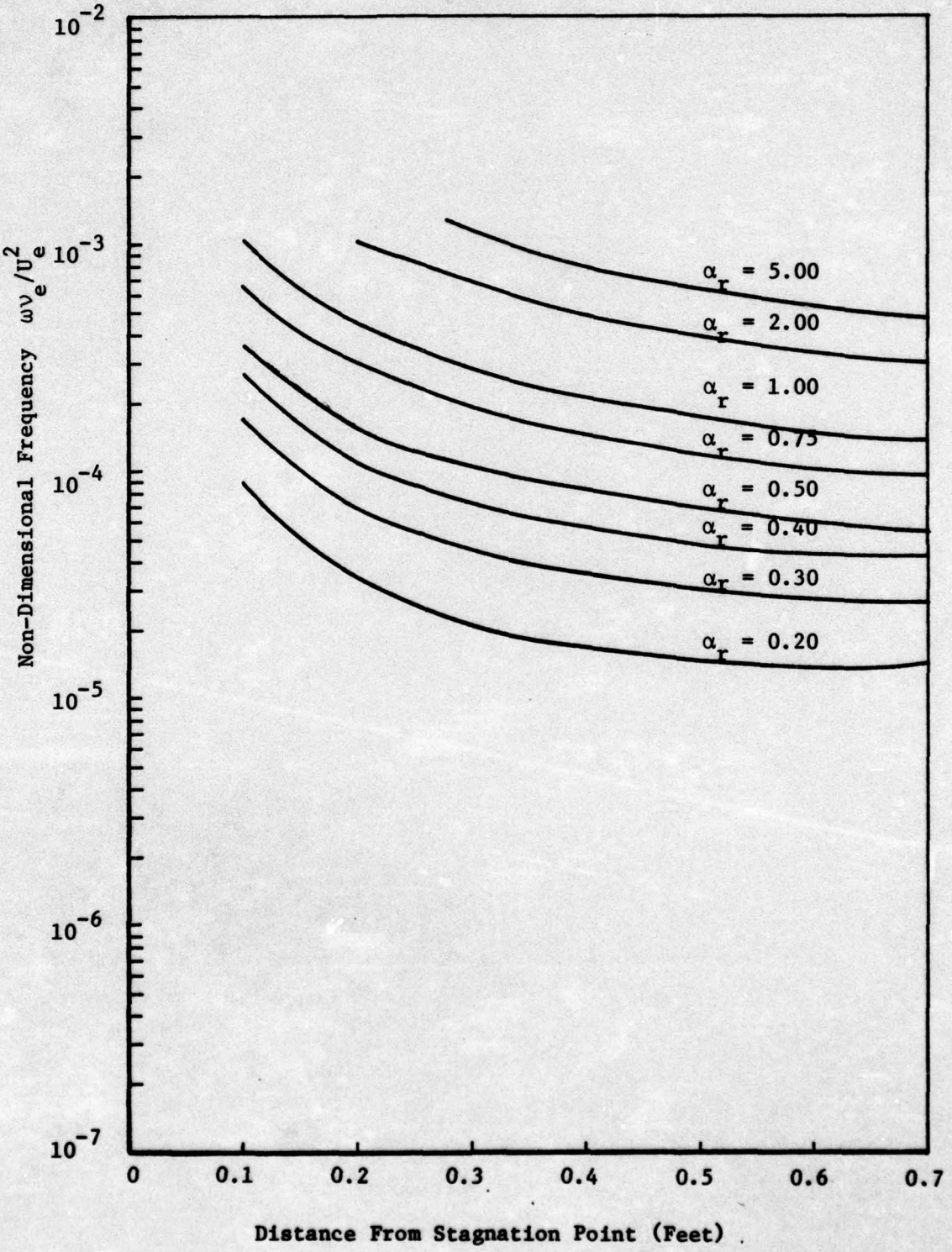


Figure 52 Stability Characteristics of a Laminar Stable Shape; T_w/T_e = 1.0 , k = 5.0 mils , No Surface Mass Addition --Wave Numbers

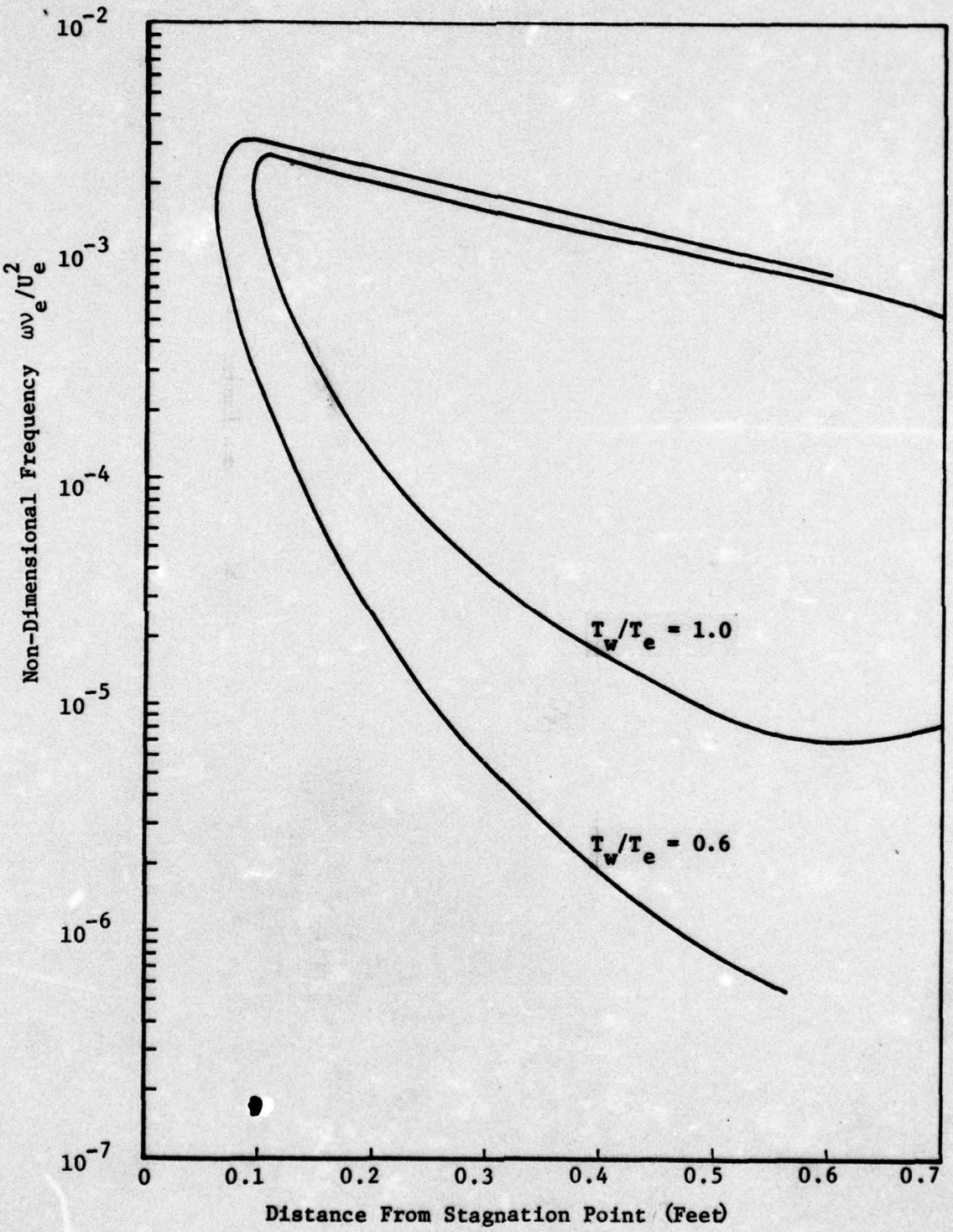


Figure 53 Stability Characteristics of a Laminar Stable Shape; Composite Results Showing Effects of Wall Temperature Changes on Neutral Stability Curves

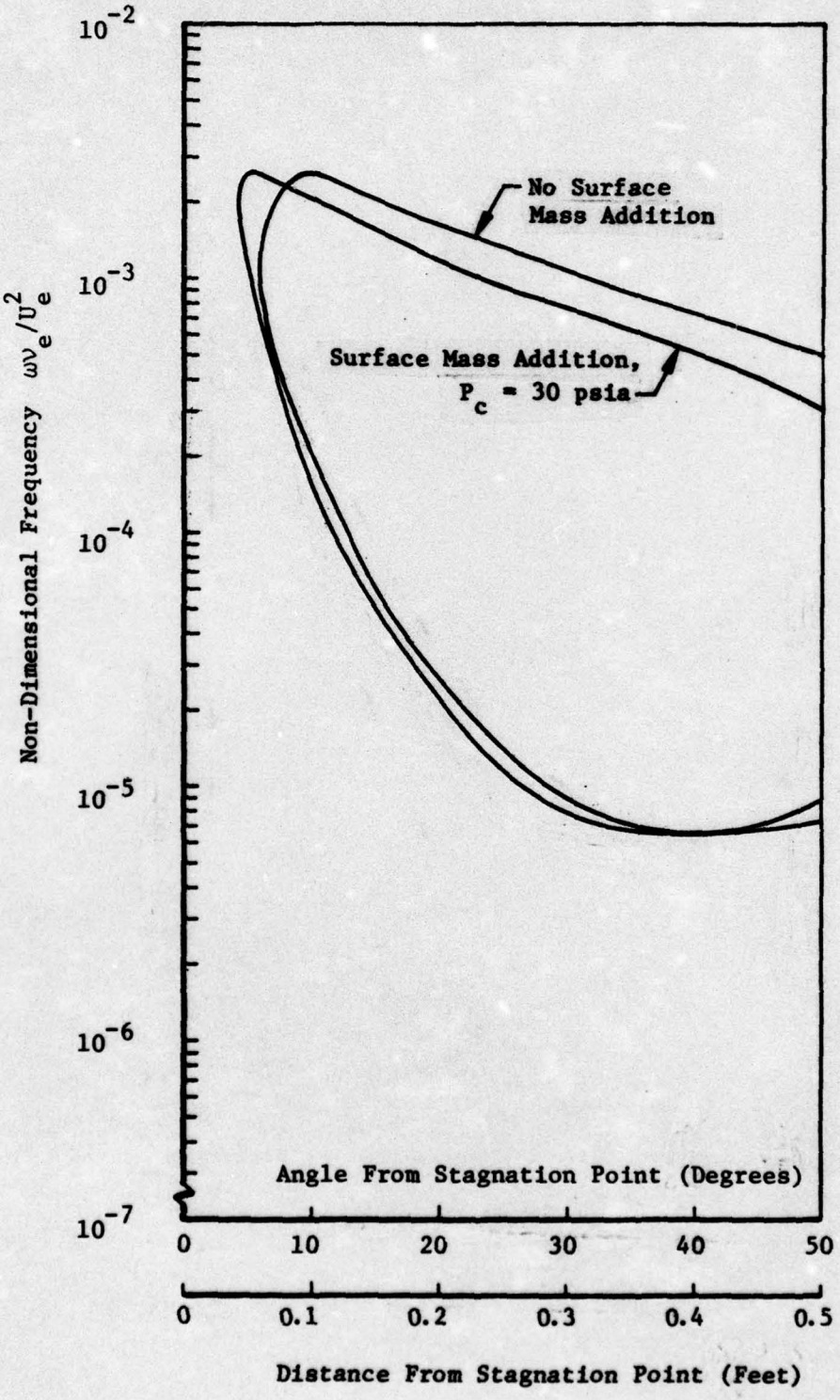


Figure 54 Stability Characteristics of a 7-Inch Sphere; Composite Results Showing Effects of Surface Mass Addition on the Neutral Stability Curves in the Presence of Surface Roughness, T_w/T_e = 1.0

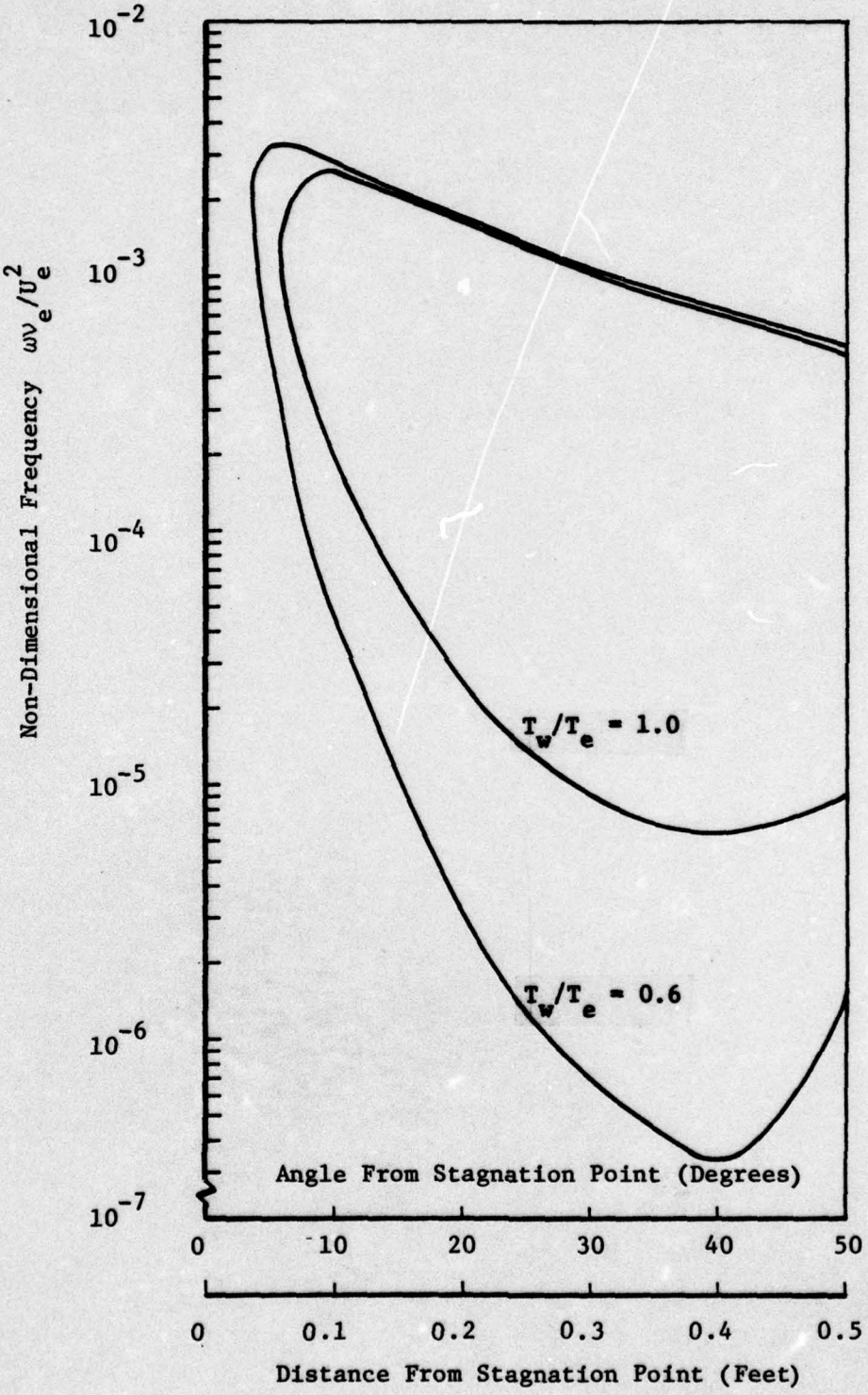


Figure 55 Stability Characteristics of a 7-Inch Sphere; Composite Results Showing Effects of Wall Temperature Ratio on the Neutral Stability Curve in the Absence of Surface Mass Addition

APPENDIX I: Recommended Transition Test Cases (Compiled By Aerospace Corporation)

The following six pages describe the ten recommended transition test cases and the necessary auxiliary information. These test cases have been compiled by Drs. W. Bishop and R. L. Baker of the Aerospace Corporation, El Segundo, California.

Recommended Code Documentation Cases for Blunt Body Transition Prediction Methods

Under Air Force OSR sponsorship, several contractors have for the past three years been attempting to apply analytical methods to the prediction of blunt body boundary layer transition. The efforts at Physical Sciences Incorporated (PSI) and DCW Industries have been based upon a second order closure turbulence modelling approach while the work at Flow Research Incorporated (FRI) has been from the viewpoint of linearized stability theory.

In order to assess the accuracy, general applicability and flexibility of the various transition prediction methods, a set of test conditions has been prepared. Each of the above contractors is requested to make transition prediction calculations for each of the 10 cases in Table I.

As can be seen from the Table, the calculations have been divided into 6 subsets. The overall objective of the cases given in each subset is stated in the first column. In the second column the input conditions for each case are given. Additional input, as required, is given in the accompanying Tables. The roughness values quoted are average peak-to-valley roughness heights, except as noted otherwise.

For each case the contractor should supply a complete list of all input constants and boundary conditions along with the boundary layer transition prediction. In the third column is listed the "primary" variable for each case. After a transition prediction calculation has been made, the amount of increase or decrease in value of this variable in order to change the boundary layer state, holding all other variables and input constant, should be calculated.*

---

*In some cases it may not be possible to "change the boundary layer state" under this constraint

Finally, as a result of the above calculations and the experience of three years of funded research, each contractor should discuss in detail each of the following questions:

1. Over a very wide range of roughness scale heights, what is the effect of surface roughness on nosetip boundary layer transition and what difference, if any, is there between the affect of sandgrain type and distributed type roughness?

2. How does the transition onset behavior for blunt biconic shapes, laminar stable shapes and other non-spherical shapes differ from that on a sphere?

3. What are the effects of wall cooling and surface mass addition on nosetip boundary layer transition both separately, combined and in combination with surface roughness?

To what extent are the conclusions stated in the answers to questions 1-3 "valid" for:

4. Transition data taken in the freestream noise environment of AEDC tunnel B?

5. The range of freestream Mach numbers from 2 to 20?

TABLE I

Recommended Code Documentation Cases *

No.	Objective	Input Conditions	Primary Variable
1.	Combined effects of surface roughness, wall cooling and mass addition	p^o = 220 psia, T^o = 850°R k = .005", B' = 0.6 T_w/T_e = 0.6, R_n = 7.0"	k
2.	Same as 1	Same as 1	B'
3.	Same as 1	Same as 1	T_w/T_e
4.	High Mach number combined effects of surface roughness, wall cooling and mass addition	Flight trajectory in Table II, R_n = 0.75," k = .0004", Altitude = 50 kft	Altitude (B', H_w/H^o & T_w given as functions of altitude in Table II)
5.	Same as 4	Same as 4, except k = .015", ℓ/k = 5, distributed roughness	Same as 4
6.	Freestream noise effects	p^o = 260 psia, T^o = 850°R, k = .005", B' = 0.0 T_w/T_e = 1.0, R_n = 7" Fluctuating shock layer variables as given in Figures 1 and 2	Unsteady shock layer flowfield
7.	Surface mass addition effects	p^o = 220 psia, T^o = 850°R, T_w/T_e = 1.0, k = 0.0 B' = 0.6, R_n = 7.0"	B'
8.	Non-spherical shape	Same as 1, except laminar stable shape as given in Table III	k
9.	Roughness effects for small k/θ	M_∞ = 3.14, R_n = 6.5", k = .0001", Re_∞/ft = 16.5 x 10^6, p^o = 0.7 atm T^o = 495°R, T_w/T_e = 0.6	k
10.	Same as 9	M_∞ = 2.73, R_n = 4.0", k = .0002," Re_∞/ft = 17.0 x 10^6, p^o = 0.77 atm T^o = 517°R, T_w/T_e = 0.75	k

* For each case, a transition prediction calculation is to be made and then the change in the value of the primary variable required to change the transition state, i.e, laminar to turbulent or turbulent to laminar, is to be calculated.

TABLE II

Flight Trajectory Variables for Cases 4 and 5

Altitude (kft)	Velocity (ft/sec)	Stagnation Enthalpy (BTU/lb)	Freestream Density (lb/ft^3)	p_{t_2} (atm)	B'	T_w (^oR)	H_w/H^o
98901	22880	10456	.00105	8.07	.69*	7082	.46
95338	22851	10430	.00130	9.97	.76	7142	.46
91778	22814	10397	.00154	11.8	.71	7191	.47
88222	22771	10357	.00186	14.2	.71	7244	.48
84678	22718	10309	.00221	16.7	.72	7290	.48
81138	22653	10250	.00260	19.6	.72	7335	.48
77611	22573	10178	.00310	23.2	.72	7383	.49
74098	22476	10091	.00368	27.3	.72	7428	.49
70597	22359	9986	.00448	32.9	.72	7480	.50
67119	22213	9856	.00519	37.6	.72	7516	.50
63668	22037	9700	.00611	43.6	.71	7555	.51
60243	21821	9511	.00719	50.3	.70	7591	.52
56857	21550	9276	.00846	57.7	.69	7623	.52
53517	21234	9006	.00986	65.3	.67	7650	.53
50226	20879	8708	.0116	74.3	.65	7676	.54
46998	20485	8382	.0135	83.2	.63	7696	.55
43829	20049	8024	.0157	92.7	.60	7712	.56
40732	19572	7652	.0182	102	.57	7721	.57
37713	19056	7254	.0210	112	.54	7727	.58

*To a good approximation, B' may be considered to be constant over the spherical nosetip at a given altitude

TABLE III

LAMINAR STABLE SHAPE CONFIGURATION

Running Surface Distance, s^*	Local Body Angle, $\alpha(^o)$	Local Body Curvature, $\frac{d\alpha}{ds}$	Local Radial Coordinate, r	Local Axial Coordinate, z
0.0	90.	-1.	0.0	0.0
0.025217	88.555	-1.0002	0.025214	0.0003179
0.050049	87.132	-1.0009	0.050028	0.0012524
0.075137	85.692	-1.0022	0.075066	0.0028224
0.10023	84.250	-1.0039	0.10006	0.0050215
0.12506	82.820	-1.0061	0.12473	0.0078172
0.15015	81.372	-1.0089	0.14958	0.011267
0.17523	79.920	-1.0123	0.17433	0.015344
0.20007	78.477	-1.0162	0.19872	0.019998
0.22515	77.013	-1.0209	0.22324	0.025323
0.25024	75.541	-1.0263	0.24761	0.031274
0.27507	74.077	-1.0323	0.27158	0.037780
0.30016	72.588	-1.0393	0.29561	0.044975
0.32525	71.089	-1.0473	0.31945	0.052795
0.35008	69.592	-1.0562	0.34283	0.061148
0.37517	68.067	-1.0665	0.36622	0.070208
0.40000	66.541	-1.0780	0.38913	0.079788
0.42535	64.967	-1.0915	0.41224	0.090195
0.45043	63.387	-1.1067	0.43482	0.10112
0.47501	61.817	-1.1238	0.45664	0.11243
0.50010	60.188	-1.1439	0.47859	0.12459
0.52519	58.527	-1.1674	0.50017	0.13738
0.55027	56.830	-1.1950	0.52137	0.15079
0.57690	54.980	-1.2303	0.54342	0.16571
0.60147	53.221	-1.2698	0.56333	0.18012

* All length variables have been normalized by the stagnation point radius of curvature which is 7.68"

TABLE III - concluded

Running Surface Distance, s^*	Local Body Angle, $\alpha(^o)$	Local Body Curvature, $\frac{d\alpha}{ds}$	Local Radial Coordinate, r	Local Axial Coordinate, z
0.62605	51.400	-1.3182	0.58278	0.19514
0.65063	49.502	-1.3794	0.60173	0.21079
0.67520	47.505	-1.4591	0.62014	0.22707
0.70183	45.191	-1.5791	0.63940	0.24544
0.72538	42.959	-1.7359	0.65579	0.26235
0.75098	40.220	-2.0227	0.67279	0.28149
0.77504	37.085	-2.6103	0.68784	0.30026
0.80000	31.955	-4.4794	0.70209	0.32074
0.82503	27.348	-2.2723	0.71437	0.34254
0.85005	24.777	-1.4293	0.72532	0.36504
0.87501	23.047	-1.0306	0.73542	0.38786
0.90003	21.746	-0.80111	0.74494	0.41100
0.92506	20.710	-0.65297	0.75400	0.43433
0.95002	19.854	-0.54986	0.76264	0.45775
0.97504	19.123	-0.47370	0.77099	0.48134
1.0	18.488	-0.41545	0.77903	0.50497
1.0250	17.927	-0.36928	0.78685	0.52874
1.0501	17.424	-0.33179	0.79446	0.55264
1.0751	16.972	-0.30098	0.80184	0.57649
1.1000	16.560	-0.27511	0.80904	0.60039
1.1251	16.181	-0 25297	0.81611	0.62446
1.1501	15.833	-0.23401	0.82299	0.64845
1.1750	15.511	-0.21751	0.82973	0.67248
1.2000	15.210	-0.20303	0.83634	0.69655
1.2251	14.928	-0.19016	0.84287	0.72078

* All length variables have been normalized by the stagnation point radius of curvature which is 7.68"

NOTE: A non-similar laminar boundary layer calculation for this configuration and the environment of Case No. 8 is available from The Aerospace Corporation upon request.

APPENDIX II: Details of Mean Flow Profiles

Some of the mean flow profiles that have been used in this study are presented here in graphical form for reference. In particular, the mean velocity profiles for a number of representative cases are given in Figs. II-1 through II-5. Each of these figures shows the mean velocity profile at a particular distance form the stagnation point, including arc length distances of 0.1, 0.2, 0.3, 0.4, and 0.5 feet (all distances are measured from the stagnation point on a 7-inch hemisphere). These figures show the effects of surface roughness, surface mass addition, and wall temperature on the slope of the mean velocity profiles.

Some corresponding temperature profiles (for distances of 0.1, 0.3, and 0.5 feet) are given in Figs. II-6 through II-8. These temperature plots show the effects of surface roughness on the temperature profiles.

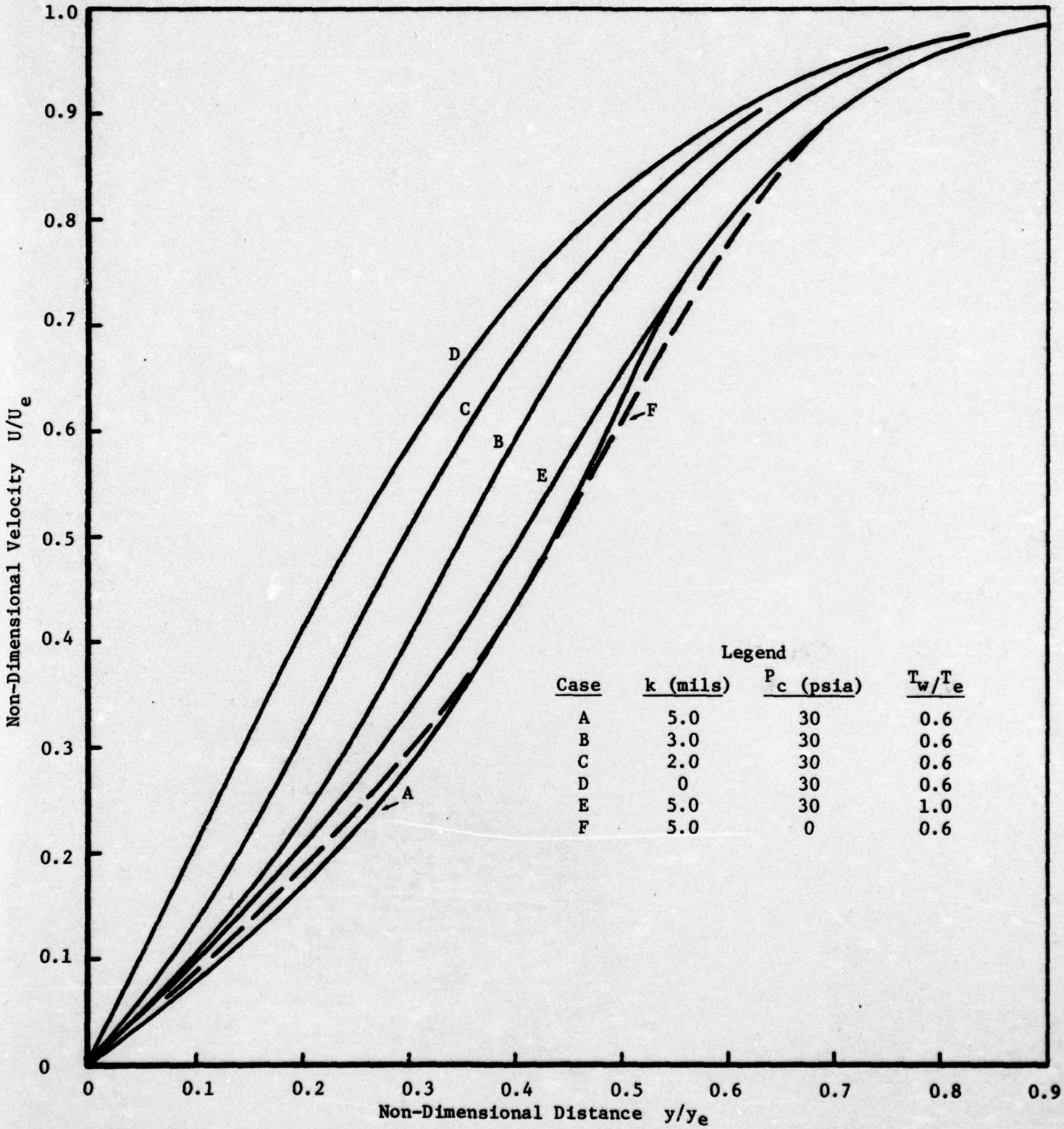


Figure II-1. Effects of Surface Roughness, Wall Temperature, and Surface Mass Addition on the Mean Velocity Profiles at 0.10 Feet From the Stagnation Point on a 7-Inch Sphere.

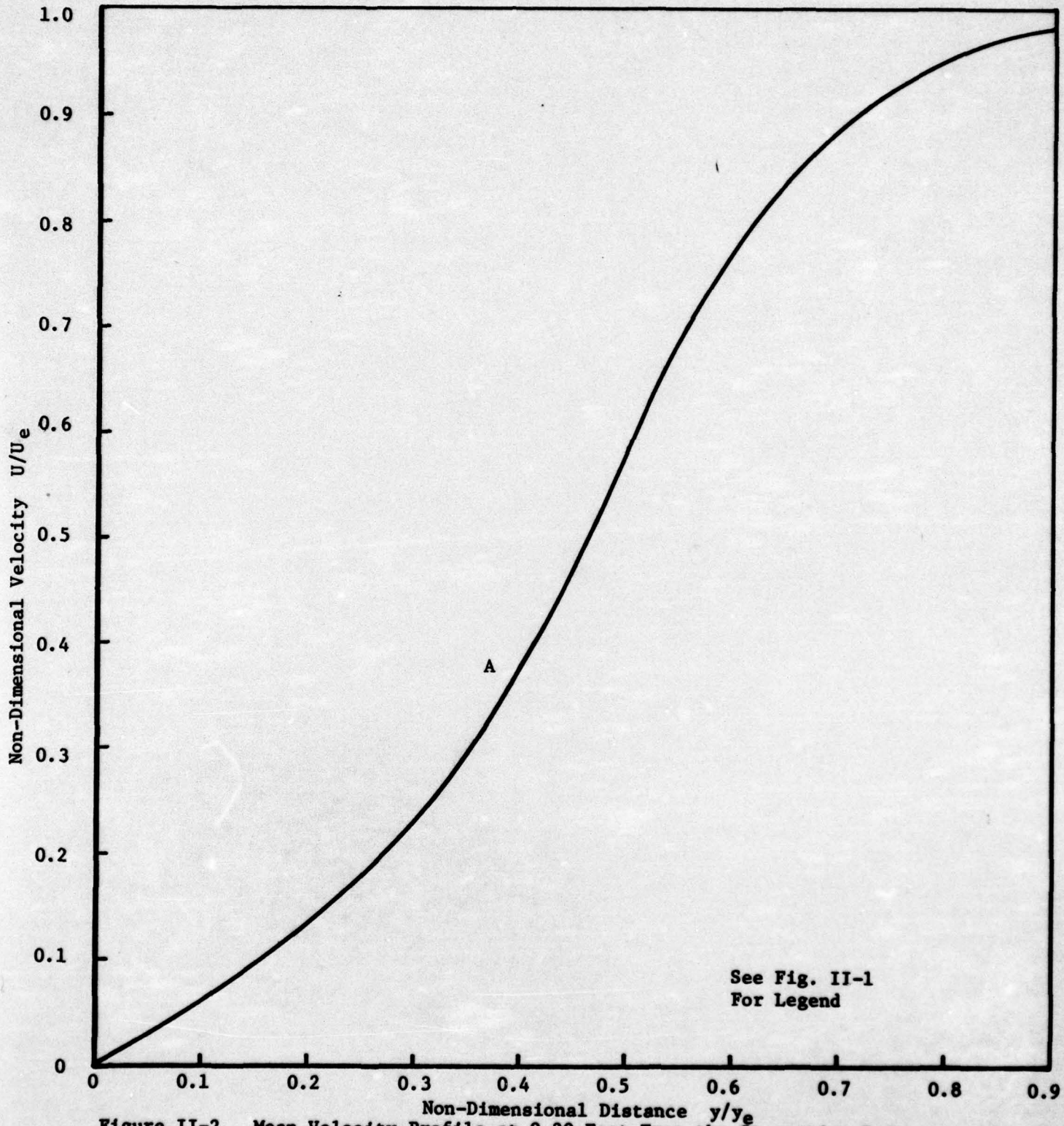


Figure II-2. Mean Velocity Profile at 0.20 Feet From the Stagnation Point on a 7-Inch Sphere.

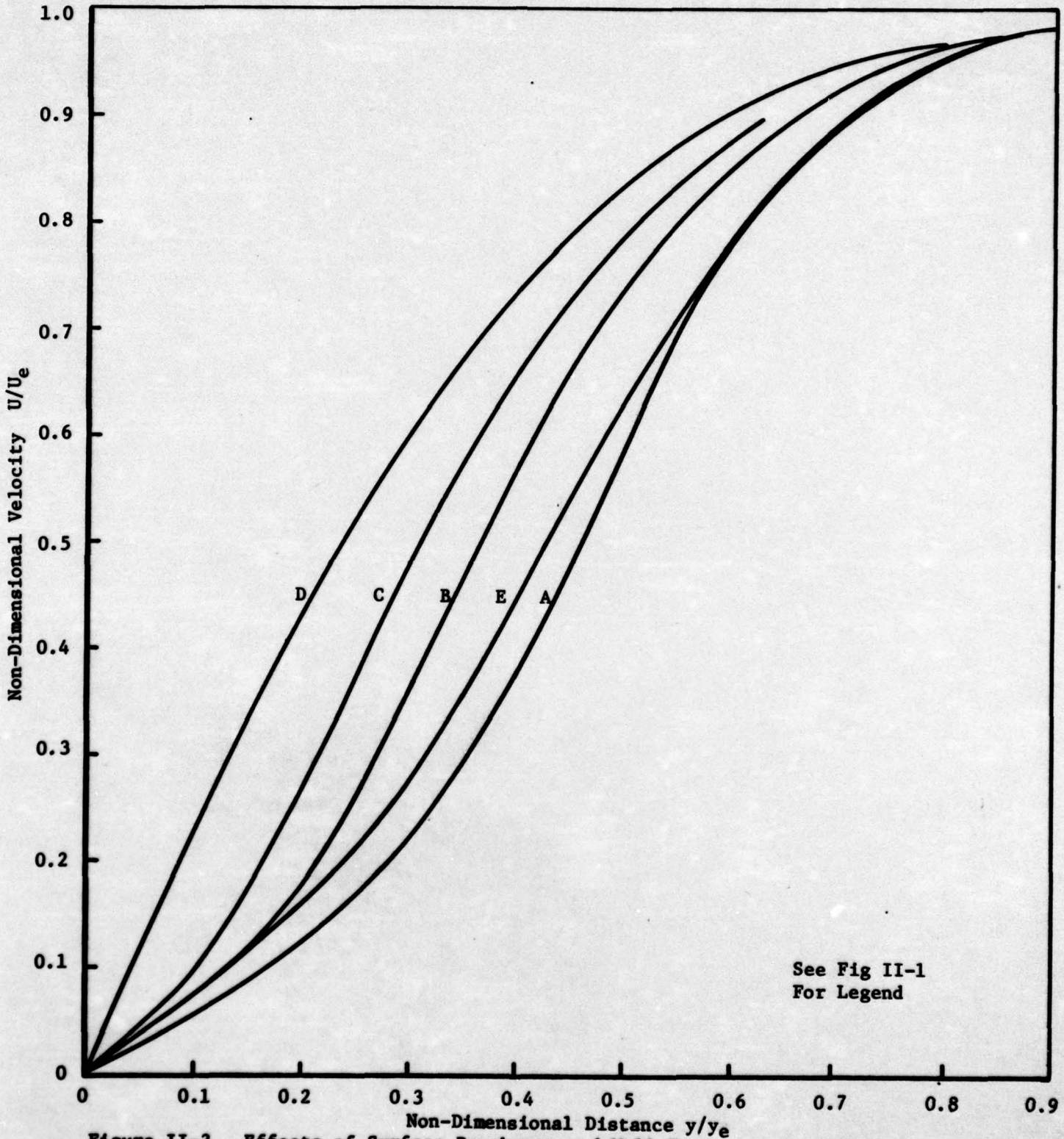


Figure II-3. Effects of Surface Roughness and Wall Temperature on the Mean Velocity Profiles at 0.30 Feet From the Stagnation Point on a 7-Inch Sphere.

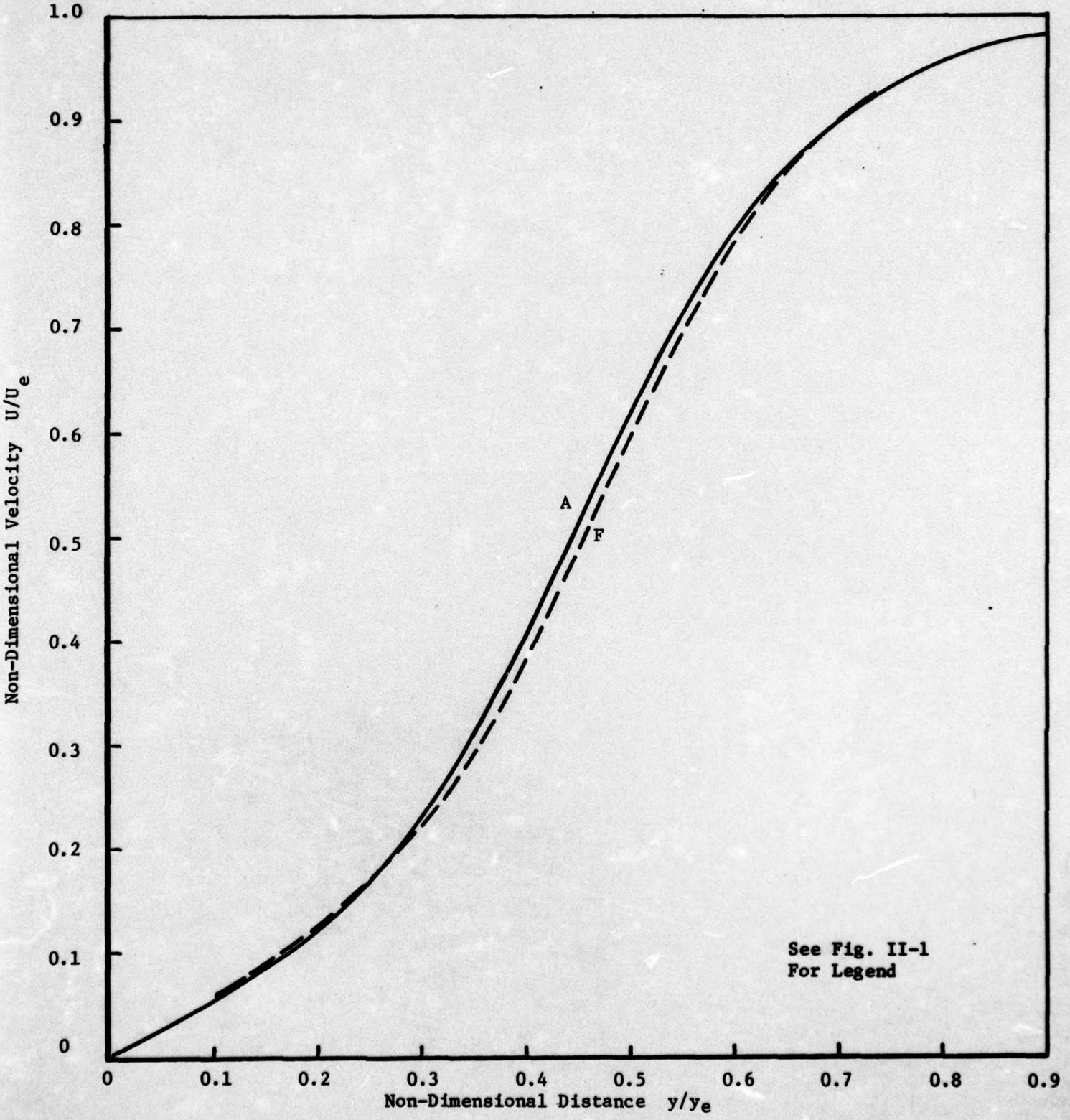


Figure II-4. Effects of Surface Mass Addition in the Presence of Surface Roughness on the Mean Velocity Profiles at 0.40 Feet From the Stagnation Point on a 7-Inch Sphere.

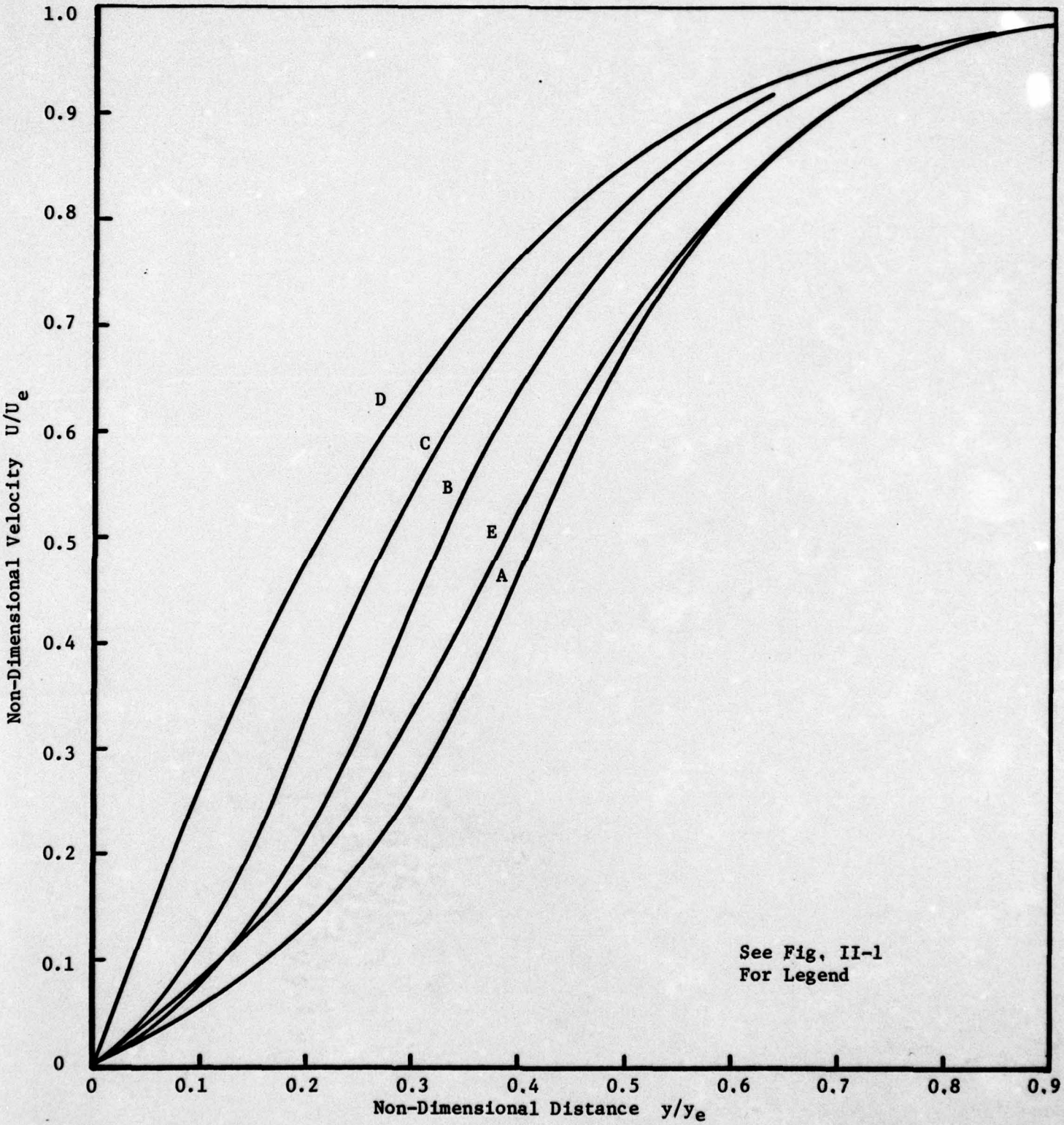


Figure II-5 Effects of Surface Roughness and Wall Temperature on the Mean Velocity Profiles at 0.50 Feet From the Stagnation Point on a 7-Inch Sphere.

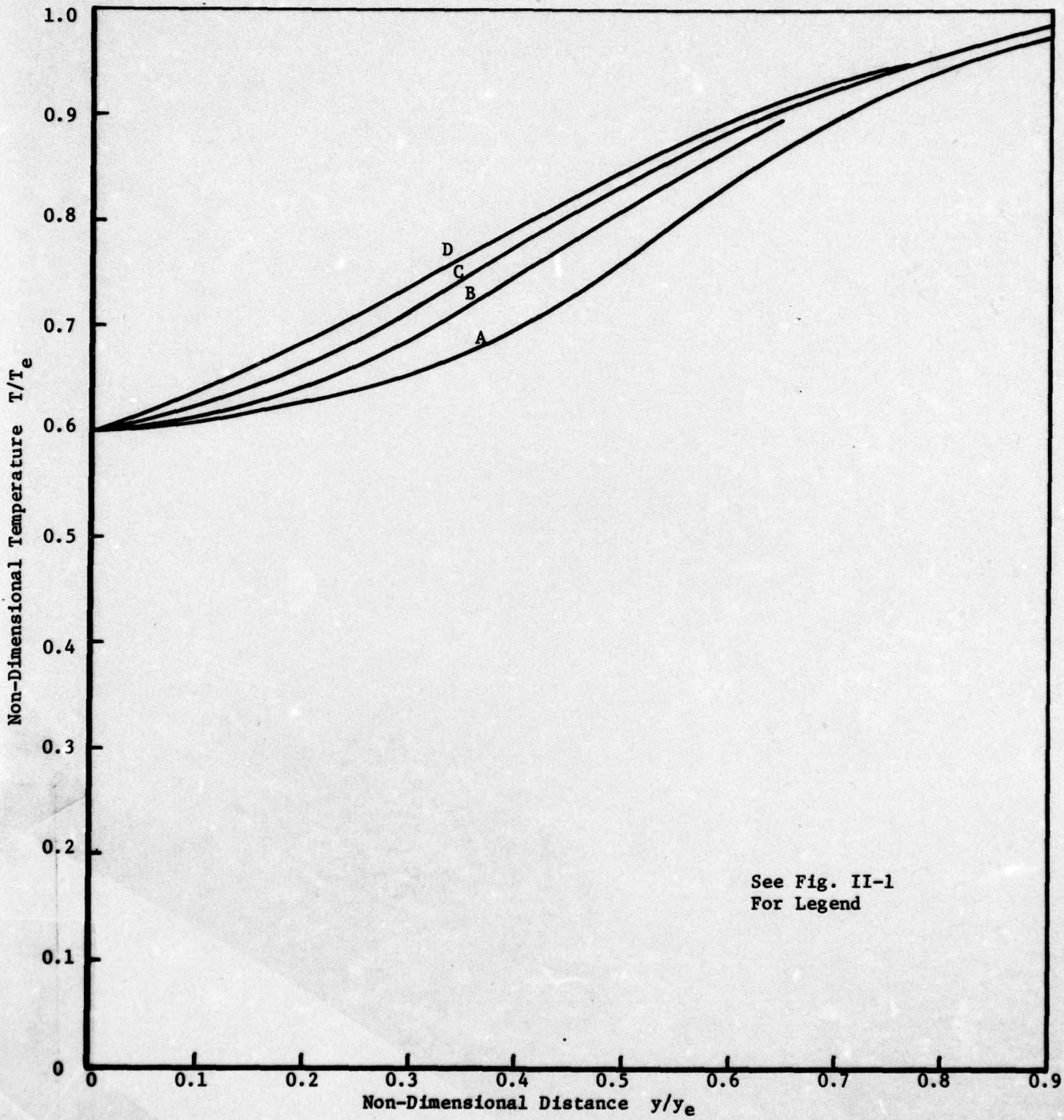


Figure II-6. Effects of Surface Roughness on the Mean Temperature Profiles at 0.10 Feet From the Stagnation Point on a 7-Inch Sphere.

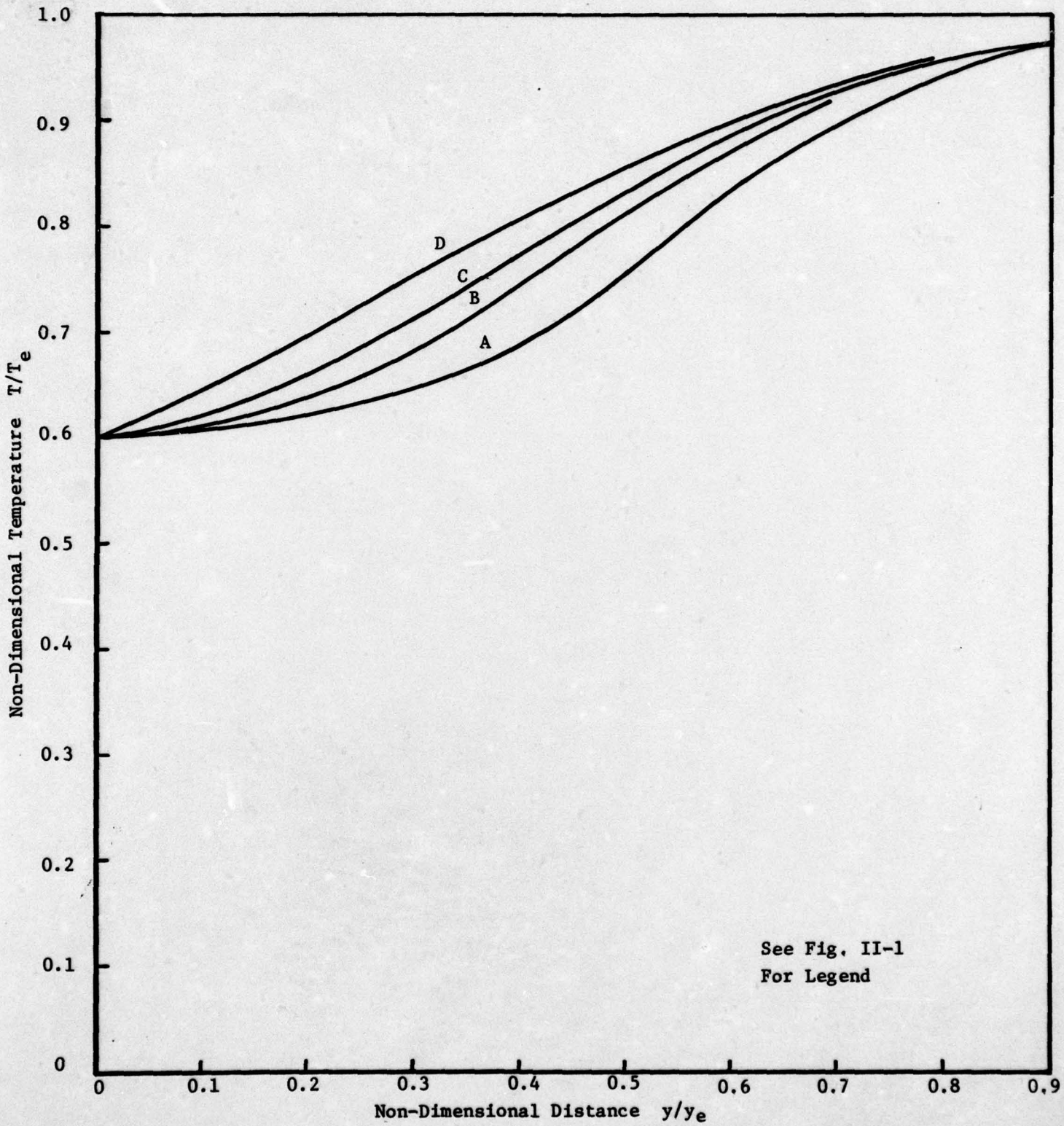


Figure II-7. Effects of Surface Roughness on the Mean Temperature Profiles at 0.30 Feet From the Stagnation Point on a 7-Inch Sphere.

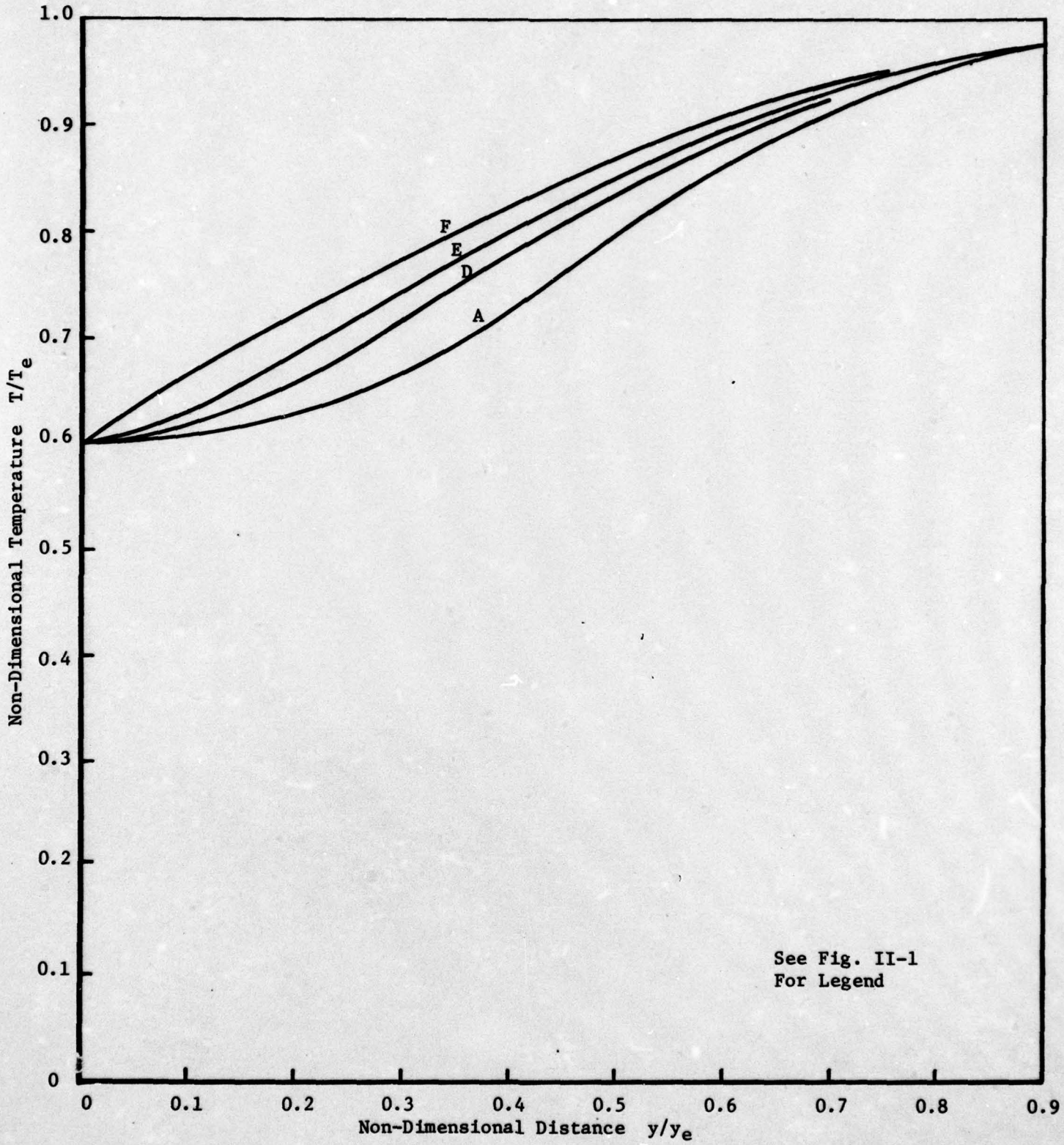


Figure II-8. Effects of Surface Roughness on the Mean Temperature Profiles at 0.50 Feet From the Stagnation Point on a 7-Inch Sphere.

UNCLASSIFIED

SECURITY CLASSIFICATION OF THIS PAGE (When Data Entered)

REPORT DOCUMENTATION PAGE		READ INSTRUCTIONS BEFORE COMPLETING FORM
1. REPORT NUMBER AFOSR-TR-76-1107	2. GOVT ACCESSION NO.	3. RECIPIENT'S CATALOG NUMBER
4. TITLE (and Subtitle) STABILITY AND TRANSITION IN BOUNDARY LAYERS ON REENTRY VEHICLE NOSETIPS		5. TYPE OF REPORT & PERIOD COVERED FINAL 16 July 1975-15 July 1976
		6. PERFORMING ORG. REPORT NUMBER Flow Research Report No 71
7. AUTHOR(s) CHARLES L MERKLE		8. CONTRACT OR GRANT NUMBER(s) F44620-74-C-0049
9. PERFORMING ORGANIZATION NAME AND ADDRESS FLOW RESEARCH, INC 1819 S CENTRAL AVENUE KENT, WA 98031		10. PROGRAM ELEMENT, PROJECT, TASK AREA & WORK UNIT NUMBERS 681307 9781-02 61102F SAMSO:63311F
11. CONTROLLING OFFICE NAME AND ADDRESS AIR FORCE OFFICE OF SCIENTIFIC RESEARCH/NA BLDG 410 BOLLING AIR FORCE BASE, D C 20332		12. REPORT DATE June 1976 13. NUMBER OF PAGES 115
14. MONITORING AGENCY NAME & ADDRESS(if different from Controlling Office)		15. SECURITY CLASS. (of this report) UNCLASSIFIED 15a. DECLASSIFICATION/DOWNGRADING SCHEDULE

16. DISTRIBUTION STATEMENT (of this Report)

Approved for public release; distribution unlimited.

17. DISTRIBUTION STATEMENT (of the abstract entered in Block 20, if different from Report)

18. SUPPLEMENTARY NOTES

19. KEY WORDS (Continue on reverse side if necessary and identify by block number)

BOUNDARY LAYER TRANSITION
STABILITY THEORY
NOSETIP TRANSITION
REENTRY VEHICLES

20. ABSTRACT (Continue on reverse side if necessary and identify by block number)

The stability characteristics of the boundary layer on the nosetip of a reentry vehicle have been investigated for a wide range of conditions. Results based upon classical parallel-flow stability theory indicate that boundary layers on smooth-walled nosetips are stable by a wide margin at realistic Reynolds numbers. The addition of nonparallel effects, including the axisymmetric vortex stretching that is encountered as the boundary layer is swept over the nosetip, moves the neutral stability curve to lower Reynolds numbers, but by only negligible amounts, indicating that the parallel-flow analysis is more than adequate for the present

DD FORM 1 JAN 73 1473 EDITION OF 1 NOV 65 IS OBSOLETE

UNCLASSIFIED

problem. The stability results for rough-surfaced nosetips, which are based on a phenomenological model for the effects of roughness on the mean flow profiles, yield completely different conclusions. The presence of roughness can produce large, strongly unstable regions on the nosetip. In particular, the interaction between roughness and other parameters is especially important. The results indicate that in the presence of roughness, wall cooling is strongly destabilizing, whereas the effects of the pressure gradient are very weak. Both of these predictions are completely different from smooth-wall stability results but are in agreement with numerous experimental transition results. The calculations also indicate that surface mass addition is destabilizing in the presence of smooth walls (but by much smaller amounts than indicated in the experiments of Demetriades), while it has very small effects in the presence of wall roughness. A general observation based on these results is that boundary layer transition on nosetips occurs because of the simultaneous effects of surface roughness, strong favorable pressure gradients, and wall cooling.